AN ANALYSIS OF RESIDUAL STRESSES IN THE BASIC CUTTING PROCESS

by

Upamaka Ramakrishna Rao, M.Sc.

A thesis presented in the University of London
for the award of the Degree of
Doctor of Philosophy.

Department of Mechanical Engineering,
Imperial College of Science and Technology,
University of London.

February, 1971.

TO MY FATHER

Abstract

The present state of knowledge of residual stresses due to machining is critically reviewed and the need for a better understanding of the influence of mechanical factors on the formation of residual stresses is indicated.

It is assumed that the action of a cutting tool in generating the residual stresses is equivalent to that of the 'ploughing force'. An analytical approach is presented for determining the residual-stress distributions in orthogonal cutting, employing a numerical-integration process. A strain-hardening material is assumed, with stress-strain behaviour of the type $\sigma = k\epsilon^n$. A computer programme is developed, based on the model, and the computation performed for a range of the parameters involved.

For rapid and accurate experimental determination of residual-stress distributions, a new technique is developed, involving continuous monitoring of the bending deflection with continuous layer removal. The experimental data is processed by computer to obtain Calcomp plots of the stress distributions.

The results obtained in plain turning of steel XC-45 show the influence of cutting speed, depth of cut, rake-angle, the cutting-edge angle and the wear of the tool, on the residual-stress distributions. High tensile stresses of the order of 1.5 times the initial yield strength of the material are revealed, thereby indicating that the residual stresses generated are of practical importance.

A comparison of the experimental and analytical results shows that the model may be successfully employed to predict the influence of the cutting conditions and the work-material properties on residual-stress distributions.

Acknowledgements

It is with feelings of profound thankfulness and gratitude that I acknowledge the guidance and encouragement rendered to me by Dr. J. R. Crookall, at every stage during the course of this work.

My grateful thanks are due to the staff of the department, especially Mr. A. Christie, for assistance in the workshop and laboratory.

Thanks are also due to my friends for their kind help and my wife for typing the thesis.

U. R. K. Rao.

Contents

List of symbols

A	Area of the anode
E	Young's modulus
G	Modulus of rigidity
G_1, G_2	Stresses from strain-gauge readings for strip segment
H'	Gradient of the equivalent stress plastic strain curve
I	Current
I_d	Current density
K	Strength coefficient in the stress-strain relationship $S_s = KE_s^n$
P	Ploughing force
Q	Rake-face force
R	Initial radius to centre line of tube wall before removing a layer
R_A	Reaction stresses in the ring segment
R_B	Reaction stresses in the strip segment
R_o	Mean radius of tube wall before slitting
R_1	Mean radius of tube wall after slitting
R'	Radius to centre line of tube wall after removing a layer
R_f	Resultant force
S	Circumferential length over which a layer is removed
U	Volume of the metal removed
V	Voltage
a	Thickness of layer removed
b	Thickness of specimen after the removal of a layer
b_o	Original thickness of tube wall
f_A	Residual stresses in the ring specimen
f_B	Residual stresses in the strip specimen
g_1	Spacing between scribed lines on the ring before slitting

g_2	Spacing between scribed lines on the ring after slitting
h	Distance from the neutral axis in bending
k	Strength coefficint in the stress-strain relationship $\sigma = k\epsilon^n$
ℓ	Length of tube
n	Strain-hardening index
q	Quantity of charge
s	Bending stress in removed layer
t	Time of electropolishing
w	Width of specimen
x,y,z	Cartesian coordinates
α	A constant
β	Angle of inclination of the ploughing force with the normal to the surface
δ	A constant; also, prefix to indicate the error in a quantity
γ	Shear strain
γ_{xy} etc.	Cartesian components of shear strain
$\gamma_{\theta z}$ etc.	Polar components of shear strain
$(\gamma_{xy})_r$ etc.	Residual shear strains
ϵ	True strain
ϵ_m	Mean strain $(\epsilon_x + \epsilon_y + \epsilon_z)/3$
$\epsilon_x, \epsilon_y, \epsilon_z$	Normal true strains
$\bar{\epsilon}$	Effective strain
$\bar{\epsilon}^p$	Effective plastic strain
$\epsilon'_x, \epsilon'_y, \epsilon'_z$	Deviatoric strains
$(\epsilon_x)_r$ etc.	Residual strains
θ, r, z	Cylindrical coordinates
λ	Semi-angle of the wedge
ν	Poisson's ratio
σ	True stress
$\bar{\sigma}$	Effective stress
σ_b	Bending-stress component added when a layer is removed
σ_d	Direct-stress component added when a layer is removed

σ_m	Mean stress $(\sigma_x + \sigma_y + \sigma_z)/3$
σ_u	Average stress in a removed layer
$\sigma_x, \sigma_y, \sigma_z$	Normal stresses in cartesian coordinates
$\sigma'_x, \sigma'_y, \sigma'_z$	Deviatoric stresses
$(\sigma_x)_r$, etc.	Residual stresses
$\sigma_\theta, \sigma_r, \sigma_z$	Normal stresses in polar coordinates
τ	Shear stress
τ_{xy} etc.	Cartesian components of shear stress
$\tau_{\theta z}$ etc.	Polar components of shear stress
$(\tau_{xy})_r$ etc.	Residual shear stresses

Other symbols are explained in the text.

1. Introduction

The need for greater reliability of machine elements is growing with the recent advances in engineering in general and aero-space technology in particular. Often, it is the surface of a stressed component that suffers the most severe operating conditions and hence it is the surface quality that determines its operating life. Thus the concept of 'surface integrity'[1*], defined as the extent to which the physical and mechanical characteristics of the surface layers of a component match those of the bulk material, has come to be generally accepted. Consequently, investigations leading to the determination of the operating ranges for process variables to yield the maximum surface integrity are assuming prominence in metal-processing research.

Residual stress in the surface layers is one of the main characteristics in determining the surface integrity. Residual stresses are defined as the stresses existing in a body in the absence of any externally applied load. They are produced when there is a non-uniform plastic deformation such as occurring due to mechanical, chemical, thermal, or other origin. It is usual to distinguish between micro- and macro-residual stresses. The former arise when there are microstructural inhomogeneities and they are distributed over areas of the order of the

---

* Numbers in superscript represent the serial numbers of references.

individual grain size. The latter can arise even in a homogeneous body and are distributed over much larger areas. Residual macrostresses are important in determining the fatigue strength and corrosion resistance of components. In this investigation only macrostresses are considered.

It has been demonstrated that residual tensile stresses at the surface are detrimental to the fatigue strength[2-7] and stress-corrosion resistance[8-10]. Residual stresses can cause warping and distortion on machining, and consequently difficulty in obtaining the desired dimensions on a precision component. The problem of 'dishing' of thin compressor rotors during machining is well known. Beneficial effects have been obtained by introducing controlled compressive residual stresses by the methods of mechanical prestressing like strain-strengthening, shot-peening and tumbling. These methods have been capitalised upon by the automotive, aircraft and other industries[6].

It is to be expected that the nature and distribution of the residual stresses induced by a process are dependent on the process variables. Hence by a proper choice of these variables it should be possible to obtain the most beneficial, or the least harmful, residual-stress configuration in the component. For this it is necessary to have a clear knowledge of the influence of the process variables on the residual stresses produced.

Since a considerable proportion of engineering

components are finished by conventional machining, it is appropriate that this should be the earliest to receive attention. In the present investigation, it was proposed that the residual stresses induced in the basic cutting process be studied. With a view to evaluating the existing knowledge on the subject of residual stresses due to machining, literature review was undertaken and is given in some detail in chapter 2.

From the review it appeared that research in this field was experimental and was mainly concerned with stresses due to grinding. Owing to the dissimilar conditions under which the various investigations were performed and to the author, some doubts on the accuracy of the methods employed for residual-stress determination, it did not seem possible to draw general conclusions. Research into thick-chip processes like turning and milling was limited. Henriksen who had much experimental work in this sphere to his credit reported all his data in terms of 'resultant stress' which represented the load carried per inch width of a 'stressed layer' of unspecified thickness. Thus, although his results were useful in revealing the stress-inducing effect of the process on the surface, they did not indicate the actual value of stress at the surface or the peak value of stress in the stressed layer. Nevertheless these are important from the point of view of the fatigue strength and resistance to corrosion. Russian investigators have produced some useful experimental data on stresses in turning and

milling. However, apparent controversies still exist, and the need for an analytical basis for explaining the mechanism of stress formation is evident.

The formation of residual stresses during machining is associated with the plastic deformation due to mechanical working, the thermal expansion and contraction effects, and the volume changes due to microstructural transformations. A theoretical analysis of the complete problem of predicting the residual-stress distributions due to machining, given the conditions of machining and the material behaviour, poses considerable difficulties. The contributions of Weck[11], Gurney[12] and Merwin and Johnson[13] were concerned with the theoretical predictions of residual stresses induced in welding, flame heating and rolling respectively.

An attempt has been made in this investigation to solve a part of the residual-stress problem in the basic cutting process using a simplified model which takes into account only the plastic deformation due to mechanical working. The modifying effects oftemperature and structural transformations are to be inferred qualitatively. The details of the theoretical analysis are given in chapter 3. It was not expected that the theoretical model would yield precise values for the residual stresses. Apart from the other idealisations used for the model, the difficulty in taking into exact account the complex strain-rate field prevailing in the cutting zone during cutting, and the difficulty of obtaining experimental

data pertaining to the material behaviour at the high strain rates, are the factors which prevent precise quantitative prediction of residual stresses from being made. Hence, it was only hoped that the model would clearly demonstrate the influence of the cutting variables on the nature of the residual-stress distribution.

For the purpose of obtaining more precise information which could be used to test the theoretical model, it was proposed to obtain experimentally residual-stress distributions due to plain turning. In view of the fact that experimental determinations of residual-stress distributions are very time-consuming, it was necessary to make a careful choice of the range of parameters for study. From a review of the existing data given in chapter 2, it appeared that a useful contribution to the information available could be made by investigating the effect of cutting speed. The effect of other parameters namely the rake angle, depth of cut and tool wear have been briefly investigated to provide the background against which the predictions of the theoretical model could be checked. The plain-turning operation was chosen for experimental investigation for two reasons. Firstly, it produced an axisymmetric component which was convenient for residual-stress analysis. Secondly, it was quite easy to vary the cutting speed and other parameters over a wide range. Thus although orthogonal cutting (e.g. in a lathe) might provide data which would facilitate direct comparison with the theoretical model, the difficulty of

obtaining suitable specimens for residual-stress analysis with chatter-free surfaces necessitated the use of plain turning.

The expected steep gradients of stress, confined to thin surface layers, called for a special method of measurement of residual stresses. The available destructive and nondestructive methods were reviewed and are examined in some detail in chapter 2. It was felt that a bending-deflection technique using thinwalled tubular specimens, having the diameter-to-thickness ratio greater than ten, would be the most suitable for the proposed investigation. The tube was machined on the outer surface under the test conditions and sections of the tube wall were then removed for residual stress analysis. Basically, this involved removing material from the stressed surface electro-chemically, whilst continuously monitoring the change in curvature of the specimen, using a sensitive measuring technique.

Initially, a modification of the method developed by Denton[14] was employed. Denton used a discontinuous technique, in which layer removal and measurement of change of curvature were carried out alternately and on separate pieces of equipment. These modifications consisted in

(a) stress-free and uniform removal of stressed layers by electropolishing

and (b) more precise measurement of deflections by an interferometric method. The method enabled direct

measurement in terms of wavelengths of light to be made and obviated the need for reliance on the calibration of mechanical measuring devices. Some residual-stress distributions were successfully measured using this technique. However it sufferred from two disadvantages on account of the step-by-step nature of the layer removal. Firstly, it introduced errors in repositioning of the specimen. Secondly, it was time-consuming.

In view of these drawbacks, a new technique was subsequently developed, involving continuous measurement of specimen deflection as the stressed layers were continuously removed. A detailed account of the technique is given in chapter 4. The technique enabled the stress distributions in the axial and circumferential directions to be determined more accurately and in a shorter time. The experimental data were processed on a digital computer. A computer programme was developed for making the necessary corrections for the re-distribution of stress arising from surface-layer removal. In chapter 5, the results of the experimental investigation and those of the theoretical model employing a step-by-step numerical solution on the computer are examined.

The work of the present investigation may be summarised as follows:

(a) Existing literature in the field of residual stresses due to machining was critically reviewed and the areas which requiredfurther investigation were pointed out.

(b) An analytical model was proposed, which serves to indicate the influence of the cutting variables on the nature of the residual-stress distribution induced in the work-piece.

(c) A technique which enables rapid and accurate measurement of residual-stress distributions in machining to be made, was developed.

(d) The influence of some cutting variables on residual-stress distribution in plain turning was investigated, primarily that of the cutting speed. The influence of rake angle, depth of cut and tool wear was also briefly studied. The results were examined in the light of the proposed model.

2. Review of literature

2.1. Residual stresses due to machining

This section comprises a review of work on residual stresses due to conventional machining operations like grinding, turning and milling, in which material removal is purely by means of the mechanical action of a cutting tool. The object was to find out from the existing experimental data, areas which required further attention, and also to evaluate the theories advanced for explaining the observed residual-stress results.

2.1.1. Stresses due to grinding

A large proportion of the work on residual stresses due to machining has been concerned with the grinding process, and the techniques used have all been experimental.

Grinding stresses were studied by Glikman and Stepanov[16], Frisch and Thomsen[17], Marshal and Shaw[18], Letner[19,20], Colwell, Sinnot and Tobin[21], Field and Kahles[22] and others. Notable contributions were also made by Russian investigators[23,24].

Glikman and Stepanov[16] employed layer removal by acid etching to determine stresses in low-carbon steel. They reported tensile stresses of the order of 25,000 psi (172 MN/m.sq.) on ground surfaces in their experiments using 'heavy cuts that caused severe heating to be developed'. Frisch and Thomsen[17] found tensile stresses as high as 50,000 psi (344 MN/m.sq.) in SAE 1020 annealed

steel, due to surface grinding with a depth of cut of only 0.0003 in. (0.0076 mm). They too employed acid etching for layer removal.

Shaw[25] argued, referring to Lilh's work using X-ray technique, that etching did seem to introduce compressive stresses in hardened steel to the extent of about 10,000 to 20,000 psi (68.8 to 137.6 MN/m.sq.) and hence this must be accounted for in residual-stress determination.

Letner[19,20] investigated the residual stresses in hardened steels using a variety of grinding wheels and grinding fluids. He too employed acid etching and measured deflections using a comparator based on differential-transformer principle. His results indicated that there was no significant difference in the stresses due to the use of different grades of grinding wheel. Water-based grinding fluids did not appear to have any influence either, but certain grinding oils appeared to reduce the magnitude of peak tensile stresses. Fig. 2.1. shows some results obtained by Letner, and indicates the existence of both tensile and compressive stresses in ground surfaces.

Recent investigations by Field and Kahles[22] showed that the important variables in grinding were wheel grade, wheel speed, depth of cut and cutting fluid. Field[26] stated that 'gentle grinding' conditions employing 'soft friable wheels, low wheel speeds, active oils as cutting fluids and low-stress (ie. light) down feed',

resulted in low values of residual stress.

Work by Russian investigators[23,24] indicated that the general picture could be much more complex than this. They found, for instance, that residual compressive stresses could be created at very high wheel speeds. Behaviour with respect to the depth of grinding was different for commercially pure iron and annealed carbon steel U8 (R)*. The former showed compressive stresses for depths of grinding of the order of 0.005 mm. At depths of cut of 0.025 mm the stresses were found to be tensile and at higher depths of cut compressive stresses were generated again. However, results obtained in grinding annealed carbon steel U8 (R) showed that increase in depth of cut caused progressive increase in the tensile residual stresses. Tests on hardened U8 (R) carbon steel showed that the residual stress patterns were closely related to the microstructural changes taking place in the surface and the subsurface layers, which were in turn controlled by the prevailing temperature cycles. The magnitude of residual stresses in the grinding of annealed and hardened U8 (R) carbon steel under similar conditions, was found to be approximately the same, but the depth of their distribution was much greater in the case of hardened steel. Further details of the Russian work can be found in references 23 and 24.

---

* The letter R enclosed within brackets will be used to indicate Russian specification.

The overall picture from the foregoing is that the residual stress formation in grinding is strongly influenced by the metallurgical state of the metal, its specific heat and thermal conductivity, besides, of course, the variables of the grinding process itself (wheel speed, wheel grade, depth of cut and cutting fluid). Although the factors influencing the residual stresses have been found, there appear to be controversies as regards the effect of even the main factors, namely the depth of cut and the wheel speed. From the existing data, it does not seem possible to make generalised conclusions which enable prediction of the nature of residual stresses induced in a given grinding situation; experimental determination appears to be necessary.

2.1.2. Stresses due to turning

Work in this area is limited, and apart from some Russian contribution, most of it is due to Henriksen[27-30]. Earlier investigations took the form of determining the depth of workhardened layer under machined surfaces by hardness and X-ray measurements.

Herbert[31] (1926) and Digges[32] (1932) performed hardness surveys on turned surfaces. Their results indicated an increase in the depth of hardening with an increase in the size of cut and a decrease in the positive rake angle. Thomassen and McCutcheon[33] employed X-ray methods for determining the depth of workhardened layer in turning and milling of leaded brass. They reported that the depth affected increased with feed and depth of

cut, feed having greater effect. In milling, a 'dull cutter' produced about 300% increase in the depth of layer as compared to a 'sharp' cutter.

These results are useful in assessing the severity of a machining operation in terms of the extent of the workhardened layer and the degree of hardening. However they do not give any indication of the magnitude and sign of the residual stresses induced.

Attempts at residual stress measurement in thick-chip machining began with Henriksen and Ruttman[30]. Henriksen[27-30] investigated the stress produced by single-point cutting tools in orthogonal cutting, plain turning and planing. His results were all reported, as mentioned earlier, in terms of 'resultant stresses' representing the load carried per inch width of the stressed layer. It is not clear as to the nature of the existing stress distribution, nor as to the depth of the stressed layer. Thus, it is possible to find stress distributions like those reported by Field and Zlatin[34] for milling, for which the 'resultant stress' is compressive while the actual stress at the surface is tensile. Hence these results are of limited use, other than for indicating the overall stress-inducing effect of the process. Fig. 2.2 and 2.3 show the results of Henriksen's work in orthogonal cutting of plain-carbon steels. They indicate that the 'resultant stress' increased with an increase in depth of cut, or a decrease in rake angle, or carbon content. Similar tests by Henriksen[29] using

side-cutting tools indicated that the depth of cut was not a significant factor except when low (< 0.016 in.). The 'stress' increased with a decrease in nose radius or an increase in end-cutting edge angle. Side-cutting edge angle did not appear to have any effect.

Colwell[35] used single-point tools on magnesium and aluminium, and obtained estimates of the 'dominant stress' produced, without going into any actual stress measurement. He conjectured that the nature and magnitude of the stress would depend primarily on the geometry and wear condition of the tool and also on cutting speed, size of cut, and the effectiveness of lubrication between the tool flank and the cut surface. His studies on reaming were reported to have indicated that the stresses in the circumferential direction were dominant, when cutting was performed dry, in the presence of a built-up edge (BUE)*. The use of carbon tetrachloride eliminated BUE and resulted in an increase in the dominant compressive stresses. At larger values of feed the dominant stress became tensile.

Russian investigators took a good deal of interest in the basic principles[36-45] and techniques of measurement[46-52] of residual stresses as well as in determining residual-stress distributions due to various production processes[23,24,53-56]. It is felt that any research work

---

* For brevity, Built-up edge will hereafter be referred to as BUE.

in residual stresses due to processing will profit from a detailed study of the published Russian work.

Matalin[23] reviewed (1956) much of the work done in the Soviet Union on residual stresses due to machining. He pointed out that the factors that influenced the formation of residual stresses in turning were cutting speed, feed, cutting fluid, geometry of the tool and properties and microstructure of work-material. The following summary of results may be drawn from his report:

(a) Cutting speed - Steel 45 (R) showed only tensile stresses under low (150 m/min.), as well as high, cutting speeds, with positive rake angles. Steel KhMA (R) showed compressive stresses at high speeds. As the speed increased, the stresses tended to become more compressive. Similar behaviour was observed in the case of steel 30ХГС (R).

(b) Feed - Increase in feed increased the magnitude of residual compressive stresses and the depth over which they were distributed in turning steel 20 (R), as well as steel 50 (R).

(c) Rake angle - The magnitude and sign of residual stresses and the depth of their distribution was primarily determined by the rake angle. Fig. 2.4 summarises the results obtained.

(d) Tool wear and cutting-edge radius - Increase in the effective cutting-edge radius and increase in tool wear caused, in a nonhardenable work-material, an increase in tensile residual stresses. With alloy steels

which exhibited hardening, bluntness or wear resulted in compressive stresses to be generated.

Matalin's report contains further details and qualitative reasoning to explain some of the observed results.

Investigations by Kravchenko[53] threw much light on the general pattern of residual stresses due to turning. His work was concerned with the influence of cooling on residual stresses induced in alloy steel KhN77TYUR (R), steel 45 (R) and steel E1827 (R), using tool tips of hard alloy VK8 (R). Fig. 2.5 shows some typical results. Tests on all materials showed the same essential features for the stress distributions due to turning. The stresses were confined to thin layers, less than about 125 μm, and were mainly tensile at the surface. The application of the cutting fluid resulted in an increase of 15% to 130% in the peak tangential stresses.

In a recent (1967) Russian book[24], some detailed Russian investigations of residual stresses were included. A typical stress distribution due to turning is given in Fig. 2.6. This shows the existence of high compressive stresses in a thin (2-3 μm) surface layer, sharply changing to high tensile stresses between 0.02 - 0.04 mm from the surface and then again to low compressive stresses in deeper layers. The distributions given by Matalin and Kravchenko did not exhibit the first compressive layer. It was stated[24] that in the finish-machining range, an increase in the cutting speed tended

to slightly increase the tensile stresses in the second layer.

Flank wear primarily affected the value and spread of the stresses in the tensile layer. Increase in the carbon content decreased the depth of the stressed zone. Increase in the content of carbides of tungsten increased the depth of the tensile layer. Cutting fluids sulphofrezol and emulsion were found to reduce the value and depth of spread of the tensile stresses. The last-mentioned result appears to contradict the general trends shown by Kravchenko's results.

2.1.3. Stresses due to milling

Stresses due to end, face, and side milling were investigated by Field and Zlatin[34]. They employed end-milling and slab-milling cutters on AISI E4340 steel heat treated to 300 Brinnel, and measured the stress distributions under the surface to a depth of 0.007 in. (0.178 mm) in the direction of feed. A typical result is shown in Fig. 2.7. At higher speeds, the peak tensile stresses were found to be lower than at the lower speeds. Zlatin et al[57] subsequently obtained residual-stress distributions while investigating the effects of tool wear and cutting fluid, in the face milling of a range of materials.

Matalin[23] cited some Russian work in the face milling of steel 45 (R) while stating that at speeds upto 210 m/min. tensile stresses upto 950 MN/m.sq. were produced. With a further increase in the cutting speed

(490-610 m/min.) compressive stresses were developed in the surface layer.

Mitryaev[54] carried out a detailed investigation on the hardening and residual stresses in the face milling of heat-resistant, and titanium, alloys. He drew the conclusion that the amount of hardening and residual stressing could be controlled within limits through speed, feed and geometry of the cutter. Low ductility titanium alloys VT6 (R) and OT4 (R) showed only a slight degree (8 to 20%) of hardening on the work surface and the depth of hardening varied from .050 - .150 mm. The residual stresses on the work surface were mainly compressive and of magnitude 700 to 900 MN/m.sq. Ductile materials (steel 1Kh18N9T (R) and alloy EI766 (R)) were subjected to much greater hardening (20-50%), spread over 0.150 - 0.400 mm. Mainly tensile stresses were found on the work surface. Tool wear and low feed rates (< 0.03 mm/tooth) contributed to a considerable increase in hardening and compressive residual stresses.

Itkin[58] studied the hardening and residual stresses in form-milling a heat-resistant alloy E1617 (R). He reported that an increase in axial rake, and the cutting speed, reduced the depth of work-hardening. He found that tensile stresses were predominant, and that the ratio between the depth of residual stresses and the work-hardened layer decreased with increase in feed rate.

2.1.4. Mechanism of formation of residual stresses

Tentative explanations for the observed changes in the residual stresses with cutting conditions were advanced by several investigators.

Glikman and Stepanov[16] tried to explain the stresses in grinding by considering the thermal factor alone. Although this factor appears to play a significant role, it cannot be the only one. Compressive stresses observed by Letner[20] in the absence of any apparent microstructural changes cannot be explained by taking only the thermal factor.

The view taken by Christenson and Littman[59] that both mechanical and thermal effects could be significant, appears to be reasonable. They argued that grinding temperatures could be high enough to produce sufficient nonuniform expansion in the work to cause compressive yielding of the material just beneath the ground surface, thus generating residual tensile stress; if the heating was insufficient to cause yielding, the cold work of the surface in chip formation might produce compressive stress.

Russian investigators[24] explained the appearance of compressive residual surface stress in grinding (in a material which did not exhibit any phase transformations) by postulating that plastic deformation due to mechanical forces predominated over that due to thermal effects. Where tensile stresses appeared, thermal effects were considered to have had the greater influence. In a

material where phase transformations could occur, the additional factor of volume changes accompanying phase transformations was employed to explain the observed behaviour.

Henriksen[29] attempted to explain the stresses due to thick-chip machining by taking only the mechanical effects into account. He assumed that at moderate speeds the temperature was small enough so that its effect could be ignored. He further reasoned[30] that the pattern of grain flow on the finished surface indicated the presence of tensile residual stresses. It is observed at this point, that often the residual stresses due to plastic deformation are opposite in sign to those that have caused the plastic flow.

Colwell[35] held the view that stresses due to mechanical sources might be tensile or compressive depending upon the conditions of cut and the work-material. Referring to Baldwin's work, he stated that compressive stresses might be due to a surface type of rolling action taking place between the tool and the work. He cited some photo-elastic studies of the stressed zone near the cutting tool as the possible means of explaining the tensile residual stresses.

Matalin[23] considered the results of experimental data in turning, milling and grinding, in formulating the following qualitative picture for the mechanism:

There are four principal factors controlling the residual-stress distribution.

(1) Severe plastic deformation of the upper layers of the work-piece is accompanied by an increase of the specific volume of the deformed metal. This causes the development of compressive stresses in the upper layers and the corresponding tensile stresses in the lower layers.

(2) The layers near the surface of the work-piece are plastically elongated in the direction of cutting. This results in compressive stresses in the layers near the surface and tensile ones in the layers further away.

(3) Due to the rise of temperature in the cutting zone, there is a localised heating of the upper layers, leading to plastic deformation in them. This results in residual tensile stresses in the upper layers.

(4) Phase transformations in the surface layers are accompanied by the corresponding changes in the specific volume, resulting in residual stresses of corresponding magnitude and sign in the surface layers.

Matalin[23] was able to explain the experimental results under various cutting conditions by taking a suitable combination of these factors. However, in the absence of quantitative evidence as to the relative effects of the various factors involved, it is not possible to establish the validity of these explanations. Nor will they be of use in successfully predicting the residual stresses to be expected in a given cutting situation.

The need is therefore evident for investigation into the basic cutting process to establish precisely the relative contributions of each of the factors above to the development of residual stresses. In particular, the mechanical effect of the forces in cutting is deemed to be the dominant factor in thick-chip processes.

The following general programme was therefore adopted:-

(1) Construction of an analytical model for determining the residual-stress distributions due to the mechanical effect of the forces in cutting, and

(2) Development of an adequately sensitive experimental technique for the measurement of residual stresses in machining, which involve steep stress gradients confined to narrow layers beneath the surface.

2.2. Existing methods of experimental determination of residual stresses

2.2.1. General

The subject of experimental determination of residual stresses received considerable attention in the past, and a number of qualitative and quantitative methods can be found in the literature. There were contributions to this field in symposia on internal stresses in metals. Books on the subject were produced by Heindlhofer[60], Almen and Black[6], American Society for Metals[61] and National Research Council (U.S.A.)[62]. General reviews were presented from time to time by Barrett[63] (1944), Ford[64] (1948), Martin[65] (1957), and Denton[66] (1966).

The relevant methods of residual-stress determination were examined in the light of recent developments, to enable the choice of a suitable method for the present investigation to be made.

The two main methods of quantitative determination of residual stresses, namely the X-ray method and the mechanical method involving the removal of stressed layers, are discussed in the next two sections. Other methods include qualitative assessments using brittle lacquers[67,68] and strain-etching techniques[69]. Knoop[70] and Hertz's[71,72] hardness tests were employed for quantitative determination of residual stresses. However, in a plastically deformed metal specimen with varying degrees of work-hardening within, the change in hardness

results from the combined effects of work-hardening and the residual stresses and it is difficult to separate their contributions. Stengel and Gaymann[72] pointed out other problems associated with the method and stated the accuracy obtainable to be of the order of ± 10 kp/mm^2 (± 100 MN/m.sq.) on polished steel surfaces.

Hole-drilling methods originally proposed by Mathar[73] were further studied by Lake et al[74]. It appears that these can be employed where a quick assessment of the surface stresses to the accuracy of 20% is adequate.

A number of techniques of ultrasonic stress measurement were recently tried. From Sharpe's[75] review it seems that although the techniques were applied with some success, further development is necessary before they can be employed for precise quantitative determination of residual stresses.

Several methods based on the modifications in the electro-chemical potential[76] and the magnetic properties of ferromagnetic materials[77] were recently explored as possible means of stress detection. Oliver[78] suggested new methods involving electron emission, proton annihilation and nuclear resonance. Again, the value of these methods in the precise determination of residual stresses is yet to be established.

2.2.2. X-ray method

The principles and methods of application of X-ray

stress measurement are treated in detail by several investigators[62,66,79-84]. The method is based on the measurement of lattice strains of specially oriented sets of lattice planes in the region examined. A collimated X-ray beam of a suitable wavelength is used and the high-angle interference lines of the specimen are recorded by means of diffractometers or back-reflection cameras. Lattice strains are determined from these line shifts. Relating the lattice strains to the strain calculated from the theory of elasticity for an isotropic material is the main feature of the X-ray stress analysis.

An assessment of the method in the light of some recent developments[75,80,81,83] brings out the following aspects:

1. Localised stress in a small area limited to a few square millimeters is obtained and again this is determined from the lattice distortion of only a certain group of favourably oriented grains. Hence the values obtained are not representative of the average stress situation, which is often of interest in fatigue and distortion analyses.

2. In polycrystalline metals subjected to plastic deformation, the calculated stress values are due to both macro- and microstresses and these are not easily separable.

3. X-ray elastic constants that must be used to convert lattice strains to stresses are not absolute

constants, but depend on the degree of plastic deformation. In a two-phase alloy these are not only dependent upon the elastic anisotropy of the measured phase, but also upon the interaction effects due to the difference in the elastic properties of the two phases.

4. Only the metals and alloys which give a resolved diffraction ring can be examined. Many high-strength steels, for instance, give very diffuse back-reflection diffraction rings which cannot be measured accurately. Again, if the surface of the specimen is not sufficiently smooth or if the grain size is coarse, diffuse rings will result, making the analysis difficult.

5. The equipment is expensive and the analysis more time-consuming compared with some mechanical methods.

Accuracy of the X-ray stress measurement depends on the accuracy of the diffractometer alignment, diffraction-peak location, specimen preparation and the stress-factor determination. Figures quoted for the accuracy by various investigators are listed in Table 2.1.

In this investigation, X-ray stress measurements were carried out on some specimens to examine the suitability of the method. The accuracy obtained was of the order of ± 2000 psi (± 13.8 MN/m.sq.)

Where depth determinations of stress are required layer removals have to be made with successive exposures of the surface. Thus the method offers no special advantages for the purpose envisaged, and in view of the

limitations cited and the difficulties pointed out the method was not pursued for the present investigation.

2.2.3. Mechanical methods involving layer removal

Essentially, these methods require that a thin layer of stressed metal be removed from the specimen in the region where stress determination is desired, and the resulting strain in the remaining part be measured. The measured strain is then related to the residual stress on certain assumptions*. The distribution of the residual stress from the surface inwards may be obtained by successive layer removals to the required depth.

The various methods that were presented from time to time differed in the geometry of the specimens handled, in the complexity of the stress-state within the specimen and in the resulting expressions employed to relate the strains or deflections with stresses, apart from the details of the experimental technique used for layer removal and strain measurement. Reviews of these methods were made by Barrett[63], Ford[64], Martin[65], Denton[66], and others. A study of these methods indicated that two of them deserved closer consideration for the present investigation. These are the Sachs

---

* e.g. 1. Only elastic re-distributions of stress take place on successive layer removal, and

2. distribution of stress within layers is either uni-form or linearly varying.

boring method, and the bending-deflection method.

Sachs boring method can be applied to determine the axisymmetric stress distribution in solid shafts and tubes. The method involves boring out successive layers of material and measuring the resulting longitudinal and circumferential strains. The strains are then related to the stresses in the original shaft or tube[64].

Although Sachs method can be applied in principle to the measurement of residual stresses due to machining, it is not considered suitable for the purpose for the following reason. In the case of machined surfaces steep gradients confined to narrow region are expected. Hence the layers removed have to be very thin ($\simeq 5\mu$) and the measurement of the resulting small strains in the Sachs method will involve large errors.

The bending-deflection methods have the merit of giving greater deflection for a given thickness of layer removed and hence higher accuracy of stress determination. Moreover, the danger of plastic flow occurring during the redistribution of stress upon layer removal is not there in these methods[66]. The method involves the measurement of changes in the diameter of a slit tube or the curvature of a plate upon the removal of successive layers from the specimen.

The first accurate method of determining the circumferential stresses in thin-walled tubes was given by Davidenkov[86]. The method consisted in slitting the tube along a generator, which resulted in a partial relief

of stresses. The distribution of stresses relieved was calculated from the change in diameter due to slitting. The remaining stresses in the tube were determined from the changes in tube diameter corresponding to successive removal of stressed layers. By superposition, the original stress distribution in the tube could be found. Davidenkov ignored the end effects of the tubular specimen. To justify this assumption the method required the use of a tube of sufficient length ℓ given by[40],

$$\ell \geqslant 12\sqrt{R_m t_o}$$ where R_m = mean radius of the tube
t_o = thickness of the tube

His method for determining the axial stresses in the tube consisted in cutting out a narrow strip parallel to a generator, and measuring the initial change in curvature and the subsequent changes in curvature upon layer removal.

However, Davidenkov as well as Sachs and Espey[85] did not take into account the change ($=\nu\sigma_\theta$) in the longitudinal stresses due to the relief of circumferential stresses σ_θ, upon cutting out the strip. This could result in large errors in the longitudinal stress determined[40,86].

Denton and Alexander[86] considered in detail the earlier methods and pointed out the errors in the treatment of experimental data. They proposed a new method and provided exact expressions for use with the digital computer.

Their [86] method for determining the circumferential and axial stresses requires the measurement of circumferential stresses in two tube specimens one of which is long enough for the end effects to be ignored and the other is short enough for the assumption of complete relief of axial stresses to be valid. If $\sigma_{\theta\ell}$ (y) and $\sigma_{\theta s}$ (y) represent the circumferential stresses at any depth 'y' for long and short tubes respectively, then they may be related as follows:

$$\sigma_{\theta s}\ (y) = \sigma_{\theta \ell}\ (y) - \nu\, \sigma_{z\ell}\ (y) \qquad \text{(4.1)}$$

From this equation $\sigma_{z\ell}$ (y) (the axial stress at depth 'y') can be determined from the known value of ν the Poisson's ratio.

The effect of tube length on anticlastic bending was considered in detail by Pomeroy[87]. On the basis of this work, he concluded that when accurate values of residual stresses were required, the use of a long length of tube to obtain a plane-strain configuration should be avoided.

Pomeroy[88] employed for his experiments the method originally proposed by Birger[40] for thin-walled tubes. This consists in analysing two specimens A and B of narrow width from the same tube, one parallel to the generator and the other perpendicular to it, as shown in Fig.4.1.

It appeared that a bending-deflection method

would be suitable for determining the residual stresses due to machining in a thin-walled tube. Since the 'beam' specimens encountered in Birger's method seemed to offer less difficulties than the long tubes of the method due to Denton and Alexander[86], the former method[88] was used. The details of the method are given in chapter 4.

3. An analytical approach for determining the distribution of residual stresses due to machining

3.1. General

Although there have been several experimental investigations concerned with the problem of determining the residual stresses due to machining, analytical approaches to the problem have been very few. Recent work of Okushima and Kakino[89], and that of Barash and Schoech[90] have only yielded approximate methods for obtaining the depth of the workhardened layer in orthogonal cutting. Valuable contributions have been made by Merwin and Johnson[13,91,92] and by Gurney[12], regarding the analytical determination of residual stresses in rolling and flame heating, respectively. However, no theoretical analysis exists for the determination of residual stresses in machining, doubtless on account of the complexity of the problem.

3.2. Basic approach

To begin with, the case of orthogonal cutting is considered, as this does not involve the needless complications due to the additional parameters arising in practical cutting. Once a solution has been obtained for orthogonal cutting it may be extended for the particular cutting operation by subsequent analysis.

A majority of the metal cutting theories of the past have assumed that the cutting tool is geometrically

sharp[93-98]. Some of these theories concern themselves with the shear zone existing above the cutting edge, as shown in Fig.3.1. (a)-(d), and hence do not account for the plastic deformation and residual stresses in the surface after machining. In certain cases, Fig.3.1. (e)and (f), the shear zone is shown to extend below the cutting edge, but the tool force is considered to be distributed entirely on the rake face. However, the the cutting edge is not geometrically sharp in reality, and experimental results[89,99,100] were found to show better agreement with theory when the effects of the rounded nose of the tool were taken into account.

Fig.3.2. shows the tool with a rounded nose acting on the workpiece through the region ABCD, where AB represents the contact with the rake face, BC with the nose and CD with the clearance face of the tool. The resultant tool force R_f is known to be distributed over the surface ABCD in a complex fashion. The precise distribution particularly around the tool nose and within the contact at the clearance face have not yet been determined, nor the stress and strain fields in the region around the nose and beneath the contact surface.

However, it is evident that the material in the vicinity of the tool edge suffers severe strain, and as the tool advances, a part of the material goes into the chip and the rest into the surface layers of the work-piece. Thus, the material upto a certain depth below the surface would have experienced nonuniform plastic

deformation giving rise to residual stresses beneath the surface.

To arrive at the residual-stress configuration, the stress and strain histories within the work-piece must be considered, as it moves relative to the tool. Thus, the material originally at a point such as 1 (Fig.3.2.) at the section MN which is far ahead of the tool, has negligible stresses to begin with. Stresses rise with the progress of cutting, until a peak value is attained and fall again to low values. However, the material will only have been subjected to elastic strains throughout, if the track 1-1' is sufficiently far below the tool edge, as shown in Fig.3.2. The material at a point such as 2, on the otherhand, is strained plastically, as it passes into the shear zone at E and a stress will remain after exit at F from the plastic shear zone. The magnitude of the residual stress at any point a certain depth below the surface, will depend upon the actual strain history at that depth from the start to the finish of cutting. The material at a point such as 3 is of no interest from the point of view of residual stresses in the work-surface, since it eventually goes into the chip. Thus, from the strain history of the material, the stress history, culminating in residual stresses, may be constructed.

The strain history of the material constituting the surface layers, is governed by the stress and temperature fields prevailing around the tool nose.

These in turn are primarily dependent upon the mechanical, physical and chemical properties of the material of the work and the tool, i.e. cutting conditions (e.g. cutting speed and feed), tool geometry (e.g. rake angle, relief angle and cutting edge radius), tool wear, type and manner of application of the cutting fluid, and the rigidity of the work and the tool set up.

Thus, the problem of predicting the residual stresses, given the properties of the work, tool and the various cutting parameters, may be considered to be two-fold. Firstly, the stress and temperature fields for the given cutting situation are to be determined; secondly, residual stresses are to be deduced from the stress and temperature distributions.

The first part of the problem is a complex one. A solution in the closed form employing elastic-plastic constitutive relations, and equilibrium and compatibility conditions for the machining problem is a far-fetched one, in the present state of the theory. Temperature and strain-rate effects complicate the problem further. Solutions have been obtained in the past, separately for the mechanical and thermal aspects of the problem, employing simplified models[94-98,100-103]. However, these do not yield precise information in the tool-nose region, which is of interest in the present analysis. It is felt that the finite element method applied to an elasto-plastic material[104-106] will prove fruitful in obtaining the required stress, strain and temperature

fields. However, this aspect is considered worthy of a separate investigation.

In the present analysis, a somewhat simplified model has been used for estimating the strain distribution near the tool nose, by considering the mechanical effect of the forces in cutting (sections 3.3. and 3.4.).

Once the strain distribution, and hence the strain history, of the material during cutting has been determined, the second part of the problem requires that the stress history be constructed to arrive at the residual stresses. A step-by-step numerical analysis, employing Hill's[107] total stress-strain relations for a workhardening material, is used in the present investigation. The details are given in section 3.5.

3.3. The model

The work expended by the tool during cutting may be regarded as composed of the work of shear deformation in the chip, and the work of deformation of the material beneath the finished surface. Correspondingly, the resultant cutting force R_f may be considered to be divided into two components P and Q (Fig 3.2.). The component Q along AB on the rake face, is considered responsible for the deformation in the chip, whereas P distributed on the rounded edge BC and the clearance face CD, is taken to be responsible for the deformation in the machined surface.

This concept has been employed by several workers

in the field[89,98-100], and it affords a better explanation of the observed metal-cutting phenomena, than the assumption that the resultant tool force R_f is entirely distributed on the rake face. The component P has been variously termed as 'ploughing force' by Albrecht[99], Boothroyd[100], and Okushima and Kakino[89], 'indentation force' by Masuko, and 'clearance-face force' by Zorev[98]. These investigators have presented various experimental and analytical means of obtaining the component P. In the present analysis, it is assumed that this component P* is responsible for the deformation in the work surface and hence the residual stresses in it.

Thus, the orthogonal-cutting operation is represented, for the purpose of obtaining residual stresses, by the following idealised model:

(1) The system is equivalent to the action of a line load (of constant magnitude and direction) moving on the surface $y = 0$, of a semi-infinite solid $y > 0$ (Fig.3.3.).

(2) The material of the solid is homogeneous and isotropic, and its stress-strain behaviour is of the type $\sigma = k \epsilon^n$

(3) Plane-strain conditions prevail, so that ϵ_z is zero and all other stresses and strains are independent of z.

---

* The term 'ploughing force' will be adopted, since it is the most widly used, to describe the component P.

The outline of the procedure is, first to determine the elastic-plastic strain field under the static concentrated load representing the ploughing force. Then, the distribution of the strain at any particular depth below the surface under the static load is equated to the strain history at any point at that depth, with the load movement along the surface. From the strain history, the elastic-plastic stress history is constructed, to arrive at the residual stresses.

3.4. Strain field within a semi-infinite solid, under a concentrated line load

Considering the equilibrium of a wedge, of a strain-hardening material of the type $\sigma = k \epsilon^n$ in plane-strain, under a concentrated line load, after the analysis given by Sokolovskii[108], the stress and strain components in cylindrical coordinates, at any point (r,θ) (Fig.3.3.), are obtained as (vide Appendix 3.1.) :

$$\sigma_r = 2C \propto P\, g(\theta) / r, \quad \sigma_\theta = \tau_{r\theta} = 0, \quad C = \pm 1 \qquad (3.1)$$

$$\epsilon_r = - \epsilon_\theta = - C \left(\frac{\propto P g(\theta)}{K r} \right)^{1/n}, \quad K = \frac{k}{\sqrt{3}} \left(\frac{2}{\sqrt{3}} \right)^n \qquad (3.2)$$

Here, $g(\theta)$ is a function defined as follows:

$$g(\theta) = \left[\frac{\cos (\ell\theta + \delta)}{\cos \delta} \right]^n \qquad \text{for} \quad n > \frac{1}{2}$$

$$= (1+\delta\theta)^n \qquad \text{for} \quad n = \frac{1}{2}$$

$$= \frac{1}{(1-\delta)^n}\left\{e^{m\theta} - \delta e^{-m\theta}\right\}^n * \qquad \text{for} \quad n < \frac{1}{2} \qquad (3.3)$$

where $\ell^2 = (2n-1)/n^2$

and $m^2 = (1-2n)/n^2$

P = Concentrated edge load per unit length in the z direction.

δ and α are constants determined by applying the conditions of equilibrium, which are:

$$P \sin\beta = -\int_{-\pi/2}^{+\pi/2} \sigma_r \; r \sin\theta \, d\theta$$

$$P \cos\beta = -\int_{-\pi/2}^{+\pi/2} \sigma_r \; r \cos\theta \, d\theta \qquad (3.4)$$

---

* This is a modified and re-derived form of that given by Sokolovskii. The derivation is given in appendix 3.1, and includes the reason why this modification was necessary. Briefly, however, solutions were required for the values of inclination β in the entire range from 0 to $\pi/2$, for which the relationship given by Sokolovskii appeared to require complex variables. The re-derived form used here renders this unnecessary.

To solve equations for α and δ, α is first eliminated by division to yield:

$$\tan\beta = -\frac{\int_{-\pi/2}^{\pi/2} \sigma_r \, r \sin\theta \, d\theta}{\int_{-\pi/2}^{\pi/2} \sigma_r \, r \cos\theta \, d\theta} \qquad (3.5)$$

For a wide range of alloys (e.g. steels, copper and aluminium alloys) $n < \frac{1}{2}$, and the equation (3.5) takes the form

$$\tan\beta = -\frac{\int_{-\pi/2}^{\pi/2} (e^{m\theta} - \delta\, e^{-m\theta})^n \sin\theta \, d\theta}{\int_{-\pi/2}^{\pi/2} (e^{m\theta} - \delta\, e^{-m\theta})^n \cos\theta \, d\theta} \qquad (3.6)$$

For a range of values of δ, the right-hand side of the equation (3.6) was evaluated numerically by Simpson's rule and the corresponding values of β were determined employing the computer programme ALFA (vide appendix 3.2). α was then computed from the relations (3.1) and (3.3) as:

$$\alpha = -\frac{\sin\beta}{\frac{2C}{(1-\delta)^n}\int_{-\pi/2}^{\pi/2} (e^{m\theta} - \delta\, e^{-m\theta})^n \sin\theta \, d\theta} \qquad (3.7)$$

Graphs of $\beta(\alpha)$ and $\beta(\delta)$ are as shown in Fig.3.4. - 3.6. From these, the values of α and δ corresponding to a given value of β can be read off.

The stress and strain distributions under the load could then be computed from equations (3.1) and (3.2). The distributions were obtained, using subroutine STRAIN (vide appendix 3.2), in terms of the Cartesian components. The components of stress and strain at any point (x,y) in the Cartesian system were computed employing the following relations[109]:

$$r^2 = \sqrt{x^2 + y^2}, \quad \tan\theta = x/y$$

$$\sigma_x = \sigma_r \sin^2\theta$$

$$\sigma_y = \sigma_r \cos^2\theta$$

$$\sigma_z = \sigma_r /2$$

$$\tau_{xy} = -\sigma_r \sin\theta \cos\theta$$

$$\epsilon_{xx} = -\epsilon_{yy} = -\epsilon_r \cos 2\theta$$

$$\gamma_{xy} = -2\epsilon_r \sin 2\theta \qquad (3.8)$$

Typical stress and strain distributions at a certain depth are shown in Figs. 3.7 and 3.8.

3.5. Numerical method for the determination of residual-stress distribution within a solid, given its strain history

Merwin and Johnson[13] analysed the plastic deformation in rolling contact and obtained residual stresses. In the present analysis, a similar approach is followed, but a workhardening material is considered, instead of the assumption of rigid-plastic behaviour of Merwin and Johnson. Further, in their analysis, the strain history within the material was obtained considering purely elastic behaviour under static loading, whereas in the present analysis plasticity is taken into account, as given in section 3.4.

In order to obtain the strain history, it is assumed that as the load moved along the surface, the strain field (as under the static load) moved with it through the material. Thus, the strain vs. displacement of load curve is considered to be the same as the strain distribution in the X-direction at that depth, obtained as given in section 3.4.

To begin with, the permissible residual stress and strain distributions in a semi-infinite solid, after the passage of the load are considered[13]. The plane-strain condition implies that the residual stresses $(\tau_{yz})_r$, $(\tau_{zx})_r$, $(\epsilon_z)_r$, $(\gamma_{yz})_r$, $(\gamma_{zx})_r$ * are identically

---

* The suffix 'r' denotes residual stress or strain

zero and the other components are independent of z. Further, under steady and continuous plastic deformation, the solid will retain a plane surface after the passage of load, and hence $(\epsilon_x)_r$ must be zero and the non-zero stress and strain components will also be independent of x. Considering equilibrium, with no load on the surface, it follows that $(\sigma_y)_r$, and $(\tau_{xy})_r$ cannot exist. Therefore, the only possible system of residual stresses reduces to:

$$(\sigma_x)_r = f_1(y) \ , \ (\sigma_z)_r = f_2(y)$$

$$(\sigma_y)_r = (\tau_{xy})_r = (\tau_{yz})_r = 0 \qquad (3.9)$$

Thus, the only non-zero residual stresses are the direct stresses parallel to the surface and these may vary, with depth below the surface. Similarly, the possible residual strains are:

$$(\epsilon_y)_r = f_3(y) \ , \ (\gamma_{xy})_r = f_4(y)$$

$$(\epsilon_x)_r = (\epsilon_z)_r = (\gamma_{yz})_r = (\gamma_{zx})_r = 0 \qquad (3.10)$$

The non-zero residual strains are the direct strain $(\epsilon_y)_r$ which accounts for the compression of the solid normal to its surface and the shear strain $(\gamma_{xy})_r$ which produces a tangential displacement of the surface.

In constructing the stress history, during the

elastic part of the strain cycle, the following elastic stress-strain relationships(Hooke's Law) for plane strain are used:

$$\sigma'_x = 2G\epsilon'_x \quad \text{etc.},$$

$$\tau'_{xy} = G\gamma'_{xy}$$

$$\text{and} \quad \sigma_m = \frac{2(1+\nu)}{(1-2\nu)} G\epsilon_m \qquad (3.11)$$

with $\sigma_m = (\sigma_x + \sigma_y + \sigma_z)/3$ and $\epsilon_m = (\epsilon_x + \epsilon_y + \epsilon_z)/3$

where σ'_x, τ'_{xy} etc. are the deviatoric stresses,

ϵ'_x, γ'_{xy} etc. are the deviatoric strains,

G is the elastic shear modulus, and

ν is the Poissons ratio.

During plastic deformation the complete stress-strain relations of Hill[107], for a work-hardening material, are considered. For plane strain, these may be written, together with von Mises' yield criterion as

$$d\epsilon'_x = \frac{3}{2}\frac{\sigma'_x}{H'}\frac{d\bar{\sigma}}{\bar{\sigma}} + \frac{d\sigma'_x}{2G} \quad \text{etc.},$$

$$\frac{d\gamma_{xy}}{2} = \frac{3}{2}\frac{\tau'_{xy}}{H'}\frac{d\bar{\sigma}}{\bar{\sigma}} + \frac{d\tau_{xy}}{2G},$$

$$d\epsilon_m = \frac{(1-2\nu)}{2(1+\nu)G} d\sigma_m \quad \text{and} \qquad (3.12)$$

$$\bar{\sigma}^2 = \frac{3}{2}(\sigma'^2_x + \sigma'^2_y + \sigma'^2_z + 2\tau'^2_{xy}) \qquad (3.13)$$

In deriving the equations (3.12), it is assumed that $\bar{\sigma}$ can be expressed denoting the plastic strains by the superscript p, as:

$$\bar{\sigma} = H\left(\int \overline{d\epsilon^p}\right)$$

where $\overline{d\epsilon^p}$ is the effective plastic-strain increment given by:

$$\overline{d\epsilon^p} = \sqrt{\frac{2}{3}\left\{(d\epsilon_x^p)^2 + (d\epsilon_y^p)^2 + (d\epsilon_z^p)^2 + (d\gamma_{xy}^p)^2/2\right\}} \qquad (3.14)$$

H' is the slope of the effective stress vs. effective plastic strain curve. For a material whose true stress vs. true strain curve is given by $\bar{\sigma} = k\epsilon^n$, H' may be obtained as follows.

$$\bar{\sigma} = k\left(\epsilon^p + \frac{\bar{\sigma}}{E}\right)^n$$

$$\therefore \quad \frac{1}{H'} = \frac{d\epsilon^p}{d\bar{\sigma}} = \left\{\frac{1}{\sigma n}\left(\frac{\bar{\sigma}}{k}\right)^{\frac{1}{n}} - \frac{1}{E}\right\} \qquad (3.15)$$

Equations (3.12) give strain increments in terms of the stresses and stress increments. However, using the differential form of the yield criterion (3.13)

$$\bar{\sigma}\, d\bar{\sigma} = \frac{3}{2}\left\{(\sigma_x' d\sigma_x' + \sigma_y' d\sigma_y' + \sigma_z' d\sigma_z') + 2\tau_{xy}' d\tau_{xy}'\right\},$$

it is possible to solve for the stress increments explicitly in terms of the strain increments and stresses, as follows.

$$d\sigma_x' = 2G\left\{d\epsilon_x' - \frac{9}{2}\,\frac{\sigma_x' \cdot dW}{\bar{\sigma}^2 (H'/G + 3)}\right\} \quad \text{etc.},$$

$$d\tau_{xy}' = 2G\left\{\frac{d\gamma_{xy}'}{2} - \frac{9}{2}\,\frac{\tau_{xy}' \cdot dW}{\bar{\sigma}^2 (H'/G + 3)}\right\}$$

$$d\sigma_m = \frac{2(1+\nu)\,G}{(1+2\nu)}\, d\epsilon_m \qquad (3.16)$$

where $dW = (d\epsilon'_x\ \sigma'_x + d\epsilon'_y\ \sigma'_y + d\epsilon'_z\ \sigma'_z + d\gamma'_{xy}\ \tau'_{xy})$

$$\text{Also, } \overline{d\epsilon^p} = \frac{3\ dW}{\bar{\sigma}\ (H'/G + 3)} \qquad (3.17)$$

To obtain the residual stress at any point at a given depth y, a step-by-step numerical analysis is performed, starting from a position for the load sufficiently far away so as to cause negligible stresses and strains at the point. The load is then gradually moved towards the point until the stress there is just below the initial yield value. Commencing from this elastic-stress state, the stress increment, corresponding to the strain increment resulting from a small displacement Δx of load, is obtained using the appropriate stress-strain relations, (3.11) or (3.16)*. The process is repeated until the load has moved sufficiently far away from the point so as to cause negligible change in stress upon further movement. The stresses $(\sigma_x)''_r$, $(\sigma_z)''_r$, $(\sigma_y)''_r$, and $(\tau_{xy})''_r$ obtained at the end of such a computation are different from the residual stresses. This is because, the strain history has been assumed

---

* In the event of the strain increment causing partly elastic and partly elastic-plastic modes of stressing, the strain increment is split into the corresponding parts as given in ref. 111.

to be identical to the strain distribution under static load, and the strain is thus allowed to assume zero values at the end of the cycle. As a result, nonzero values $(\sigma_y)''_r$ and $(\tau_{xy})''_r$ might after all be expected. Thus the condition of equilibrium remains to be satisfied (equations (3.9)).

To restore equilibrium, the strains are permitted to relax elastically, until $(\sigma_y)''_r = (\tau_{xy})''_r = 0$. In this relaxation process, conditions of plane strain and symmetry require that $(\epsilon_z)_r = 0$ and $(\epsilon_x)_r = 0$ (equations (3.10)). The residual stresses $(\sigma_x)_r$ and $(\sigma_z)_r$ are thus given by:

$$(\sigma_x)_r = (\sigma_x)''_r - \nu\,(\sigma_y)''_r \;/\; (1-\nu)$$

$$(\sigma_z)_r = (\sigma_z)''_r - \nu\,(\sigma_y)''_r \;/\; (1-\nu) \qquad (3.18)$$

To obtain the distribution of residual stresses with depth below the surface, the process of integration is repeated for different depths below the surface.

3.6. Computer programme

A computer programme (MAIN) was developed for the purpose of computing the residual stress distributions, given the material properties k, n, E and ν and the magnitude of the ploughing force P, and its inclination β, and the associated values of α and δ. Appendix 3.2 contains a flow-chart and listing of the programme, and the main features are described briefly in the following.

Considering the strain distribution such as in Fig. 3.7, it was noted that in general, a strain increment may produce loading or unloading and in the former case, the loading may be purely elastic or elastic-plastic. The programme was therefore written to suit an arbitrary strain history.

The step length Δx was allowed to vary so as to ensure that the strain increment in any component was equal to or less than a chosen value, taken to be 0.001. On account of the finite size of the strain increment, the computed value of plastic-strain increment during loading was sometimes found to be negetive (cf. Yamada et al[111]). Where this was encountered the step size was progressively reduced until the plastic strain increment became positive.

To secure this control of step size while keeping the computation time within reasonable limits, the trapezoidal rule was employed for the numerical integration. Alternative integration schemes (Runge-Kutta, Runge-Kutta-Gill[110]) were tried but abandoned since there was considerable increase in the time of computation which did not appear to warrant the expected minor improvement in results.

The computation was made at intervals of 0.010×10^{-3} m. in depth, starting from $y = 0.025 \times 10^{-3}$ m. The use of the model involving concentrated load was expected to result in excessive values of stress and strain at small depths very near the point of application

of load. Hence the computation for any depth was stopped when a strain gradient larger than a certain value (chosen to be 0.1 for $\Delta x = 0.002 \times 10^{-3}$ m.) was encountered.

Residual-stress distributions were computed for various combinations of the material properties (k and n) and the ploughing force (P and β), to represent a wide range of machining conditions on engineering alloys. Table 3.1. gives the conditions for which computation was performed.

4. Experimental technique and analysis

In this chapter, the general bending-deflectiom method and its analysis is given first (section 4.1). This is followed by a description of the particular experimental technique developed in this investigation (section 4.2).

4.1. The bending-deflection method and analysis

4.1.1. Outline

For the reasons mentioned in section 1, plain turning in a lathe was employed for obtaining the test surfaces. Thus, the specimen used for analysis was a thin-walled tube ($b_o/R_o < 0.1$) with the stressed surface on the outside of the tube.

The review given in section 3.2 indicated that the bending-deflection method originally due to Birger[40] would offer advantages when both the axial and circumferential-stress distributions in the machined tube were to be determined. However, the expressions obtained by Birger for calculating the residual stresses involve the determination of slopes and integrals, and are not in a form convenient for computation.

Hence, equations were developed as given in the following sections, in a form suitable for a digital computer, after the work of Denton and Alexander[86].

The following assumptions have been made,

(1) The material of the tube is isotropic.

(2) The distribution of residual stresses is axially symmetrical.

(3) The tube is circular with concentric inner and outer surfaces.

(4) The tube is thin enough to allow any residual-stress component to be neglected.

(5) The principal stresses are in the circumferential and axial directions.

Essentially, the method consisted in analysing two specimens A and B of narrow width, removed in a stress-free manner from the machined tube, one (B) parallel to a generator and the other (A) perpendicular to it, as shown in Fig. 4.1. After the ring segment A is separated from the tube, the residual circumferential stress f_A (y) in it at a depth 'y' from the surface, may be written as[40],

$$f_A(y) = \sigma_\theta(y) - \nu\sigma_z(y) - R_A(y) \quad \text{or simply}$$

$$f_A \equiv \sigma_\theta - \nu\sigma_z - R_A \qquad (4.1)$$

Where σ_θ and σ_z are the circumferential and axial stresses respectively, in the original tube. R_A is 'reaction stress' due to the distortion of the ring segment upon being removed from the tube and this could be estimated either by mechanical means or by employing resistance strain-gauges (section 4.1.5).

Similarly, for the strip B, the stress existing after separation from the tube is given by,

$$f_B = \sigma_z - \nu \sigma_\theta - R_B \qquad (4.2)$$

Where R_B was determined as indicated before. f_A and f_B were determined (vide sections 4.1.2 - 4.1.5) from successive removal of stressed layers and the measurement of the corresponding changes in the curvature and thickness of layer removed. Equations (4.1) and (4.2) could then be solved to obtain σ_θ and σ_z.

4.1.2. Relationship between the average stress in a layer and the change in curvature

When a layer of small thickness 'a' has been removed from the surface of the 'beam' specimen, the stress σ_u in the layer, just before removal, may be obtained assuming uniform stress distribution accross the layer. Applying Winkler's theory for curved beams, a change in the mean radius of the tube from R to R' is related to a mean stress σ_u in the layer by the equation[86]

$$\sigma_u = \frac{EbR'}{a\left[1 - \frac{1}{\left(1 - \frac{R'}{R}\right)\left(1 - \frac{b'}{b}\right)}\right] \cdot \left[\frac{(a+b)}{2} + R'\left(1 - \frac{b}{b'}\right)\right]} \qquad (4.3)$$

Where b = thickness of tube wall after layer removal

$b' = R' \ln\left(\frac{2R' + b}{2R' - b}\right)$

E = Young's modulus.

4.1.3. Redistribution of stresses due to layer removal

With the removal of each layer, there is a redistribution of stresses, so that the equilibrium of stresses and moments accross the remaining tube wall is maintained. For equilibrium conditions to be satisfied, the direct-force and the bending-moment components borne by the layer before its removal, must be borne by the remaining cross-section, after the layer is removed.

Thus, the increase in stress in the remaining tube wall due to direct-force component in the removed layer with a mean stress of σ_u is given by

$$\sigma_d = \frac{a}{b} \sigma_u \qquad (4.4)$$

The increase in stress due to bending-moment component

$$\sigma_b = - E\left(\frac{b'}{b} - \frac{R'}{h+R'}\right)\left(\frac{1}{\frac{R}{R'-R} - \frac{b'-b}{b}}\right) \qquad (4.5)$$

where h is the distance from the centre of the tube wall to the middle of the layer. The residual stress f' in a layer in the original beam specimen is then obtained:

$$f' = \sigma_u - \Sigma(\sigma_b + \sigma_d) \qquad (4.6)$$

where the term $\Sigma(\sigma_d + \sigma_b)$ is the increase in stress due to the removal of all the previous layers.

4.1.4. Correction for the variation of stress within the layer

The stress within a layer is not uniform, in general, and a better estimate of the stress distribution is obtained by making a correction assuming the stresses to vary linearly accross the layer. If the total variation of the stress within the layer is 2 s, then the component of bending moment per unit length, to be accounted for is $\frac{sa^2}{6}$. Hence the corrected value of stress f is given by

$$f = f' \pm \frac{sa^2}{3a\,(a + b)} \qquad (4.7)$$

The positive sign must be used in equation (4.7) when f' is increasing towards the interior of the wall. Denton and Alexander suggested that s be obtained from the plot of f' vs. y. In the present investigation this was computed directly from the values of f' in the layers.

4.1.5. Determination of reaction stresses

The ring segment A was obtained by first parting off a complete ring from the tube and then making two cuts parallel to the generator. The change in radius of the ring (from R_o to R_1) after the first cut was determined using the technique described in section 4.2. The partial stress-relief on account of slitting is equal to the stress system that would be induced in the

slit ring, if it were forced back to its original radius. Thus, the stresses released may be expressed by Winkler's theory:

$$R_A = E\left(\frac{b_o'}{b_o} - \frac{R_1}{h+R_1}\right)\left[\frac{1}{\frac{R_o}{R_1-R_o} - \frac{b_o'-b_o}{b_o}}\right] \qquad (4.8)$$

where $b_o' = R_1 \ln\left(\frac{2R_1 + b_o}{2R_1 - b_o}\right)$

The reaction stresses for the strip, were obtained by employing two resistance strain gauges attached as shown in Fig. 4.1. The technique is described in section 4.2.4. If the stresses indicated by the outer (B1) and inner (B2) gauges are G1 and G2 respectively, then the reaction stress R_B may be written as

$$R_B = \frac{(G1 - G2)\ h}{b_o} + \frac{(G1 + G2)}{2} \qquad (4.9)$$

4.2. Development of the experimental technique

4.2.1. General requirements:

In developing the experimental technique the following objectives were envisaged:

(1) The technique should yield measurements of stress distribution with adequate resolution over a thickness of the order of 0.05 mm (0.002 in.) to a reasonable degree of accuracy. In the present investigation, an accuracy of $\pm$ 10 MN/m^2 was aimed at.

(2) The complexity and length of time involved in the entire technique should be reduced as far as possible. Residual-stress measurements have normally been both time-consuming and demanding as regards care and skill. In view of the growing need for extensive experimentation in this field, it was felt that an improvement in this respect would in itself be worthwhile.

(3) The method should be applicable to as wide a range of specimen shapes as possible so that it could be used on working components.

The bending-deflection method adopted basically requires a technique for determining the changes in curvature of the specimen for the progressive removal of known thicknesses of stressed metal.

4.2.2. Considerations leading to the technique involving continuous removal of stressed layers

Most investigators in the past (e.g. ref. 20, 30, 66) have employed layer removal in discrete steps, the corresponding deflection and thickness of layer removed being measured at each step. Denton[14] described one such technique for the determination of residual stresses in sunk tubes. In the early part of the present investigation, the technique due to Denton was modified and improved to make it suitable for the determination of stresses due to machining. These modifications consisted in developing:

(1) a method for uniform and stress-free removal of layers by electropolishing, and

(2) an interferometric method, using a combination of monochromatic and white light sources, for the measurement of deflection. This enabled direct measurement of deflection in terms of wavelengths of light to be made.

A detailed account of the technique and an analysis of the accuracy of stress determination by this method have been given elsewhere[112]. Although this technique gave stress distributions to a reasonable degree of accuracy, ($\pm$ 9.0 MN/m^2 ($\pm$ 1300 psi.) in a layer of thickness 0.00625 mm (0.00025 in.)), it required a considerable amount of time and labour. At this stage, stress determination by X-ray method was

carried out to investigate its suitability for the present purpose. It was found that the accuracy obtained was less ($\simeq \pm$ 2000 psi.) and that the time consumed was greater than the mechanical method. Hence the X-ray method was not pursued.

A technique involving continuous removal of layers and continuous monitoring of deflection was subsequently developed. A comparison of the X-ray technique, the 'discrete step' mechanical method, and the continuous layer removal technique, is given in Table 4.1. This clearly indicates the merits of the continuous-layer removal technique. An account of its development follows.

4.2.3. Development of the technique involving continuous layer removal

Principally, the technique required that the following aspects should be both continuous, and automatically recorded:

(1) layer removal in the stressed region and the assessment of the thickness of metal removed with elapsed time, and

(2) monitoring of specimen deflection.

To begin with, the following basic set up was considered. The narrow 'beam' specimen from the work-piece was held vertically in a suitable holder, so that it became, in effect, a cantilever beam built in at the lower end. Stressed metal was then removed over a

certain area from the specimen and the deflection of the free end of the specimen was recorded.

4.2.3.1. Method of material removal

In earlier investigations, stressed layers have been removed by acid etching, grinding, mechanical polishing and spark erosion. The unsuitability of such methods has been discussed previously[112]. Electropolishing provides continuous material removal in a uniform and stress-free manner, and therefore was employed. Also it has been increasingly used in other recent investigations[49,88,113].

Various electrolytes have been suggested for different materials and the details of these can be found in references 114 and 115. Of the two different electrolytes tried, the composition of the one found more suitable is given in table 4.2.

To select suitable values for voltage and current during electropolishing, the process was studied over a range of values of the applied voltage. Fig. 4.2. shows that upto a voltage of V_1, the relationship between current density and voltage is almost linear. A 'matt' surface was obtained on the specimen. A slight increase of voltage from V_1 to V_2 resulted in a decrease in current density. Beyond this point the current strength remained substantially constant with increase in voltage, upto V_3. Further increase in voltage produced a rapid rise in the current density. When the

voltage was held within the portion CD of the characteristic, a steady current condition and a bright polished surface were obtained. These observations agree with the earlier work reported in this field[114]. Thus, a voltage V = 10 volts and the corresponding current density I_d = 0.65 amperes per square inch (900 amp/sq.m) were employed.

Fig. 4.3 shows the experimental arrangement with the specimen (1) held in a glass holder (2) and then positioned in a tank (3) containing the electrolyte. The cathode was a suitably shaped stainless-steel strip (4) fixed to the glass holder, with a uniform gap of about 1" between the electrodes. The specimen surface was marked outside the layer-removal area with a non-conducting paint. Vertical positioning of the specimen aided the dispersion of gas bubbles formed during polishing, ensuring that non-uniform metal removal did not result from the accumulation of the bubbles.

4.2.3.2. Assessment of the thickness of layer removed

With the "discontinuous" technique the amount of material removed at each stage can be assessed by direct measurements of the average thickness of the specimen. In the continuous method this must be done either by some means of monitoring the average thickness of the specimen while it is being electropolished and without interfering with the measurement of deflection, or by predicting the thickness removed from the

conditions of polishing. The latter method was used in this investigation.

The volume of metal removed (U) is related, by Faraday's law , to the current (I) and the time (t) for which it is passed:

$$U = K_f \int I.\, dt = K_f.\, q$$

where K_f is a constant involving the equivalent weight of the metal. Hence the average thickness (a) of metal removed

$$a = K_f.\, q/A$$

where A is the area of the anode. However, K_f cannot be evaluated analytically due to the uncertain valency of the Fe-ions during the actual process, there being either divalent or trivalent Fe-ions during the different phases of the electolysis[114]. Further, there is also evolution of some oxygen, with the expenditure of energy which cannot be easily account for. Direct calibration was therefore employed.

Results obtained (Fig. 4.4) show that the volume of metal removed may be regarded as varying linearly with the quantity of charge (q). This is also borne out by the experiments of Fedotev et al[114], Pomeroy[88], and Doi[116].

Thus the thickness of layer removed at any instant during electropolishing was obtained by calculating the average metal removal rate from the

measured initial and final thicknesses of the specimen and the magnitude of the charge passed. The magnitude of the charge was determined by obtaining a continuous record of current with time and by integrating the I-t curve, using a digital computer (vide computer programme, appendix 4.1).

4.2.3.3. Measurement of deflection

As the stressed metal was continuously removed by electropolishing, the deflection was continuously monitored by a sensitive capacitive transducer* (12), and a U.V. recorder (13), as indicated in Fig. 4.3.

The changes in the curvature of the specimen could be related to the recorded displacements by calculation from the measured geometry of the specimen-extension arm combination. However, a more direct method was employed, which incidentally afforded a check on the linearity of the transducer readings. The method involved calibrating the deflection readings with the slope changes of the free end of the specimen.

---

* This was a Distance Meter (DM 100B) by Wayne Kerr, and with the probe employed (MB1) it was nominally capable of 2% accurcy in distance measurement over the range of 125 μm, with a discrimination better than 0.5% of the range.

Calibration of the displacement readings

To obtain the slope changes, a sensitive photo-microptic autocollimator (15) (Hilger and Watts) was positioned at the level of the metal plate (10) behind which a front-silvered mirror (9) was fixed (Fig. 4.3.). The accuracy of measurement by the autocollimator was $\pm$ 0.2 seconds of arc (see appendix 4.2). From the autocollimator readings, taken simultaneously with the U.V. recording of the deflection, calibration curves were obtained; a typical example is shown in Fig. 4.5. A linear relationship exists; thus a distance of 1 mm on the U.V. trace corresponds to approximately 1.5 sec. at the autocollimator. The accuracy of reading from either was of the same order. In addition to the advantage of continuous recording, the distance meter enabled a data logger to be used, so that the results could be directly processed by a digital computer. Nevertheless, in this work, the autocollimator readings have been employed for the majority of the specimens.

Readings by the autocollimator were related to the changes in curvature, as in appendix 4.3.

Assessment of deflection due to stress relief

The deflection measured was found to be influenced by the following:

(1) the bending-deflection due to stress-relief upon layer removal

(2) changes in curvature due to thermal gradients across the specimen

(3) any spurious effects due to improper clamping, 'settling' at the supporting feet of the specimen-holder or tank, and the deformation of the mounting of the measuring unit.

Factor (3) was made negligible only after a considerable period of development. This led to the use of glass for the material of the holder. The holder, tank and tray (5) (Fig. 4.3.) were each mounted on three glass 'feet'. A robust support was employed for the transducer probe. The complete apparatus was mounted on a surface table with antivibration mountings, and situated in a metrology laboratory with temperature control to within $\pm$ 1.0 ^{o}c. (see Fig. 4.6). Further improvements in the techique were effected until the deflection due to sources (3) was negligible. The autocollimator was used here to check the drift of a specimen mounted as for an actual test, but without electropolishing.

During electropolishing, the deflections observed were due to the combined thermal effects and stress-relief. It was therefore necessary either to account for the thermally-induced bending, or to make it negligibly small.

Attempts were made to avoid the thermal effects by 'intermittent' layer removal, allowing a uniform temperature to be reached in between, at which readings

were taken. Although the method avoided resetting operations, the overall time required was practically the same. In addition, the deflections measured included spurious effects associated with switching on and off.

Further attention was therefore paid to the continuous technique. It was observed that upon switching on, both the current and the voltage quickly reached their maximum values (Fig.4.7). It was expected that this would cause a quick release of heat at the 'exposed' surface of the specimen. The resulting temperature gradient within it would initially produce a deflection of the specimen soon after switch on, as observed. However due to rapid heat conduction through the specimen, the temperature differential should fall, reducing the thermal deflection after a short period of time, and the deflection observed thereafter should be substantially due to stress-relief.

A number of tests under various voltages and current densities were performed on annealed specimens, to study the thermal deflection alone. A typical record of the current, voltage and the specimen deflection is shown in Fig. 4.7. These indicated an initial deflection cycle, thence attaining a stable condition within a relatively short time (less than 2 minutes under the range of polishing conditions employed). The temperature of the electrolyte increased slowly during polishing, but without affecting the deflection of the annealed specimen. The average temperature was

therefore unimportant, for the reasons already given. Thus the deflection due to stress-relief alone could be obtained, commencing about two minutes after switch-on. To obtain stress-measurements as near as possible to the original surface, a low current-density was employed to minimise the material removed during the initial 'settling' period.

4.2.4. Experimental details

4.2.4.1. Specimen preparation

Specimens for analysis were prepared from a hot-rolled bar of OECD - XC45 steel. The composition (percent by weight) and properties of the material were as follows:

C	Mn	Si	P	S
0.47	0.80	0.50	0.01	0.01

Physical properties :-

Vicker's Hardness	1890 MN/m^2
Elastic limit	400 MN/m^2
Ultimate tensile strength	690 MN/m^2

The specimens were turned on a VDF high-speed lathe. The bar was turned down to the outside diameter of 2.30 in. (58.5 mm), followed by drilling and boring, by using a similar procedure, to a nominal bore size of 2 in. ($\simeq$51 mm). A close-fitting clearance plug was glued to the open end using Araldite so that this end

could be supported in the tail-stock centre.

The surfaces for investigation were then produced using STORA P20 N2 triangular carbide bits held in clamped tool holders. Details of the cutting conditions for the specimens are given in Table 4.3. After the required length of surface was turned, the tube was parted off using a low cutting speed (<40 sfpm, 12.2 m/min.) and low feed. The specimens for circumferential stresses were obtained in the form of rings of 3/8 in. ($\simeq 9.5$ mm) width, by parting off in the same manner.

4.2.4.2. Measurement of reaction stresses

Circumferential specimen

The change in radius upon slitting the ring was determined. Two fine parallel lines spaced about 0.14 in. (3.6 mm) apart were scribed, using the Measuring Machine (MU214B). The initial spacing (g_1) between the lines was measured and the ring was slit open by a cut along a generator, between the scribed lines. Spark erosion, was employed since it enabled the specimens to be clamped lightly, without the risk of imposing further stresses. After slitting, the spacing (g_2) between the lines was measured again. The change in radius was then calculated from the following relationship (derived in appendix 4.4).

$$2\pi(R_1 - R_o) = R_1\left\{2\sin^{-1}\left(\frac{g_2}{2R_1}\right)\right\} - R_o\left\{2\sin^{-1}\left(\frac{g_1}{2R_o}\right)\right\}$$

The reaction stresses R_A could then be obtained from equation (4.8).

Axial specimen

Two bonded wire strain gauges were employed, one at the outer and the other at the inner surfaces, along the length of the tube (Fig. 4.1). The gauges were of Type PS - 20 (Tokyo Sokki Kenkyujo), active dimensions 20 mm X 3 mm, resistance 120 $\pm$ 0.3 Ω and gauge factor 2.10. The gauges were fixed with a recommended polyester adhesive. For strain measurement, Carrier Amplifier and Demodulator, Type SE 423/1E of SE laboratories, was used in conjunction with a U.V. recorder (Type SE2005). After initially balancing the gauge circuits, the specimen strip carrying the strain gauges was cut out by spark erosion. The strains indicated by the inner and outer gauges were determined, and the corresponding stresses G1 and G2 were calculated. The reaction stresses R_B could then be determined from equation (4.9).

4.2.4.3. Analysis by layer removal

The initial thickness of the specimen was measured on a Matrix Diameter Measuring Machine (1) (Fig.4.8), of N.P.L. design, fitted with a fiducial pressure indicator (2). The machine had a least count

of 0.00001 in. (0.25 μm) and repeatability was better than this. The specimen (3) was mounted during the measurement on a perspex bench (4). Two brass sleeves (5) carrying 1 mm dia. steel balls each, were mounted on the anvils to minimise errors of misalignment. The measurement was obtained on the micrometer drum (6) after orientating the specimen to give the minimum reading with the aid of the fiducial indicator.

It was shown earlier that the measurement of thickness was quite critical for the precise determination of stress. Hence, thickness was assessed as the mean of 28 readings taken at different positions along the width and length of the specimen. Accuracy attained thereby in the measurement of thickness was of the order of $\pm$ 16 $\times$ 10^{-5} in. (see appendix 4.2).

The D.C. supply was arranged by using a Majoreg rectifier unit to provide a constant voltage of 10 volts at a setting limiting the current to 1.0 amp. (max.). After the specimen was set up, sufficient time was allowed for drift to settle down; this was checked with the help of the sensitive null indicator of the photo-microptic autocollimator. Electropolishing was then performed, usually for a period of about 40 minutes to obtain a depth of removal of 0.002 in. (0.05 mm).

From the current and deflection traces and the other measurements data were prepared for the computer programme which was developed for computing the residual- stress distributions and for plotting these

by Calcomp (graph plotter). A flow chart, listing and other details of the programme are given in appendix 4.1. Appendix 4.2 includes an analysis of the accuracy attained in stress determination.

5. Results and discussion

5.1. Analytical results

Figs. 5.1 - 5.8 show the residual-stress distributions computed on the basis of the analytical model for the conditions listed in Table 3.1. A dimensional analysis, given in appendix 5.1, indicated that it would be advantageous to represent the distributions in terms of non-dimensional stress (σ/K) and non-dimensional depth below the surface ($\frac{y}{P/K}$). This would facilitate comparisons of stress distributions in different materials, since the stress is given in relation to the strength coefficient K. Further, with this representation identical distributions were obtained, as expected, for different magnitudes of the ploughing force P (other conditions being unchanged). Thus the parameters for investigation were reduced to

(a) the angle of inclination β of the ploughing force with the normal to the surface,

(b) the strength coefficient K and

(c) the strain-hardening index n (from the assumed stress-strain behaviour of the type $S_s = KE_s^n$)

Effects of K and n

For a typical value of $\beta = -30^\circ$, Figs. 5.1 - 5.4 show that over the range of computation, n has a dominant effect upon the general shape of the stress distribution in the direction of cutting. Thus, as n is

reduced from 0.4 to 0.1 the stress gradient increases, the depth of distribution of tensile stresses decreases and the compressive region of the distribution becomes more pronounced. The effect of K is seen to be relatively minor.

Effect of β

Figs. 5.5 - 5.8 reveal the effect of β for a typical value K = 0.6 X 10^3 MN/m^2. Fig. 5.5 shows that for n = 0.4 there is a marked change in the shape of the distribution between the cases $\beta = -35^\circ$ and -40°. As n increases the value of β where this transition occurs increases until below n = 0.2 no such transition is seen for values of β upto -60°. This behaviour is associated with the changes in the stress and strain fields, brought about by a change in β. When the load is normal to the surface ($\beta = 0$) the stress and strain fields (at a certain depth below surface) are as shown in Fig. 3.7. As $|\beta|$ increases, the tangential force component increases introducing assymetry into the distributions, as shown in Fig. 3.8. Beyond a certain value of β, the influence of the tangential force will be sufficient to cause a change in the shape of the residual-stress distribution, the value of β for this transition obviously depending upon the value of n.

Prediction of the residual-stress distributions from the cutting conditions

On the basis of the foregoing analytical results, the influence of the cutting conditions on the residual-stress distributions in orthogonal cutting is now considered. It is necessary to know therefore the manner in which the values of P, K, n and β vary with the cutting conditions. No independent tests have been undertaken in this investigation; the pertinent information is available in the literature[89,97-99,117]. Table 5.1 lists the values of K and n for various materials. From this, the effects of cold work and alloying can be inferred. Stress-strain curves of the form $\sigma = K\epsilon^n$ are shown in Fig. 5.9 for various values of K and n to facilitate visualisation of the effects of these parameters, on the shape of the curve.

Cutting speed

With an increase in cutting speed, the strain rate increases. The work of Oxley and Fenton[118] on low-carbon steel indicates that an increase in strain rate results in a decrease in the value of n, and a comparatively small increase in K. Results of Okushima and Kakino[89] indicate that there is no significant change in the magnitude of P, with increase in speed. Thus the effect of increasing the cutting speed is felt largely through a decrease in n.

From Figs. 5.1 - 5.4, the effect of this can be seen to be an increase in the stress gradient and a reduction in the depth of distribution of stresses. The results of the present investigation given later on, show overall agreement with this. However, increase in the cutting speed is usually accompanied by changes in the mode of chip formation and the flow around the cutting edge, in addition to changes in the temperature in the zone of cutting. Consideration of the effect of cutting speed should therefore take account of these factors.

In the machining of two-phase alloys an important influence is exerted by the built-up edge, whose size and shape is determined by the composition of the material and the cutting conditions[120]. This is discussed in section 5.2, with reference to the experimental results obtained in the present investigation.

In a material which does not undergo structural transformations, the increase in temperature in the cutting zone is expected to cause an increase in the tensile stresses in the layers near the surface. If structural changes occur, however, the accompanying volume changes have to be taken into account in inferring the changes in the stress distribution. In steels that are sensitive to hardening, a martensitic transformation would result in an increase in the specific volume leading to a reduction in the tensile stresses near the surface. This picture is consistent with Matalin's[23]

results showing that the stresses beneath the surface change from tensile to compressive with an increase in cutting speed.

Rake angle

Results[99] on 81B45 steel show that with a decrease in the rake angle from + 30° to - 15°, β changes from - 34° to - 15°, while P decreases by a factor of about 2. Assuming that n remains sensibly constant, it can be inferred from Figs. 5.5 - 5.8 that smaller tensile stresses are to be expected for less positive rake angles. Results of Kravchenko[53] (Fig. 2.5) show this trend.

Matalin[23] reported in some cases compressive stresses near the surface at large negetive rake angles and high speeds (Fig. 2.4). The explanation given was the occurrence of martensitic transformation. The model, however shows (e.g. Fig. 5.5) that such distritutions can possibly arise due to purely mechanical effects, provided $|\beta|$ is sufficiently large. The appearance of large compressive stresses near the surface in grinding and milling of low-carbon steels and materials which are not susceptible to phase changes, can be explained on this basis.

Depth of cut

Okushima's[89] results indicate that the ploughing force remains unaffected by changes in depth of cut

above a certain minimum value (< 0.2 mm in Okushima's tests). Thus no change is expected in the residual-stress distribution with depth of cut other than at low values of the latter. This is supported by Okushima's measurements of the depth of deformed layer at various depths of cut, showing no significant change. At depths of cut smaller than this minimum, the ploughing force increases with depth of cut, and stresses increase correspondingly. Henriksen's results (Fig. 2.2) at low depths of cut show this effect.

Cutting-edge radius

Ploughing force has been found to increase linearly with the cutting-edge radius[89]. Thus, considerable influence is seen to be exerted by the latter, an increase in the radius bringing about a proportionate increase in the depth of distribution of the stresses (see Figs. 5.1 - 5.8). Results obtained by Okushima[89] bear this out.

Tool wear

Extensive results reported by Zorev[98] show that the clearance face force increases with the flank-wear land approximately linearly. Thus, with tool wear an increase in P and a decrease in $|\beta|$ may be expected. For this change, the model predicts an increase in the tensile stresses and the depth of their distribution (see e.g. Figs. 5.5 - 5.8). This condition is of course

detrimental to the surface integrity. However, increased heat generation at the clearance face will affect the distribution favourably in the case of hardenable steels, if the temperatures are high enough for the martensitic transformation to occur.

Material of the work-piece

From Table 5.1 it can be seen that, in general, increasing alloying in steel causes an increase in K and a decrease in n. Further, an increase in cold work appears to decrease n.

The model shows that these changes result in steeper stress distributions confined to shallower depths, considering that under similar conditions of cut, (P/K) has been shown[98] to remain approximately constant. Conversely, a decrease in carbon content in plain-carbon steels causes a deeper penetration of the stress distribution and it is apparent that this accounts for the increase in the 'resultant stress' (see Fig. 2.3) found by Henriksen[30].

Copper alloys are expected to give rise to distributions with tensile stresses extending over comparatively large depths with low stress gradients.

Hardness distributions

The flow stress at any given depth below surface corresponding to the effective plastic strain has been taken to be an index of hardness achieved as a result

of deformation. The distributions of 'hardness' thus obtained are shown in terms of the nondimensional hardness index ($\bar{\sigma}/K$) and the nondimensional depth ($\frac{y}{P/K}$) in Figs. 5.10 - 5.15.

Figs. 5.10 - 5.11 show that the hardness near the surface is little affected by K. The effect of β can be seen to be small (Figs. 5.12 - 5.15). Large values of β ($= -60^{\circ}$) produce a lower degree of hardening throughout the range investigated. The value of n is seen to exert a dominant effect on the degree and depth of hardening, these increasing with increase in n.

Thus while the residual-stress distributions show significant changes with both β and n, the corresponding changes in the nature of the hardness distributions are comparatively small. It is noteworthy that no indication as to the sign of the stresses beneath the surface can be estimated from the hardness distributions. The value of the latter in determining the surface integrity of the component is therefore limited.

The depth of hardening should decrease with an increase in cutting speed and carbon content. This is supported by Russian investigations[24], but not by results obtained by Camatini[119]. A decrease in rake angle should increase the depth of hardening, as also found by Camatini. The large increase in the depth of hardening reported by Herbert[31], and Digges[32] with the increased wear and bluntness of the tool can be explained

by considering that P increases proportionately with the wear land[98] and the cutting-edge radius[99].

5.2. Experimental results

Test conditions used in the experimental work have been given in Table 4.3.

Repeatability

An analysis of the accuracy of stress determined by the continuous process (see appendix 4.2) gives the zone of uncertainty to be $\pm$ 4.2 MN/m^2 in a layer of 5 μm thick, as compared with $\pm$ 13.1 MN/m^2 for the discrete-layer-removal technique, and $\pm$ 13.8 MN/m^2 for the X-ray technique.

Fig. 5.16 shows the superimposition of three distributions obtained on three segments taken from the same specimen. The close agreement between the distributions demonstrates the repeatability of the experimental technique.

In Fig. 5.17 are superimposed the distributions in two segments from a single specimen, determined by employing different values of current (average values 0.196 and 0.146 amperes). Good agreement is evident, showing that reduced current can be successfully employed for obtaining stress measurements nearer to the surface.

Circumferential stress in the machined tube

Fig. 5.18 shows circumferential and axial residual-stress distributions in the turned tube, derived from the distributions for the ring and strip specimens taken from the tube. It can be seen that the circumferential stress distribution in the tube is nearly the same as that in the ring specimen in the region where tensile stresses exist (depth = 0.02 mm). Below this depth, the stresses in the ring have lower compressive values than in the original tube. The axial stresses in the tube are limited to low compressive values ($\simeq$150 MN/m^2). Thus, the stresses of importance are the tensile circumferential stresses, these being given to a fair degree of accuracy by the circumferential stresses in a ring specimen. This lends support to the view taken by most investigators in the past that the stresses of significance are those in the direction of cut.

Comparison between the experimental and predicted stress distributions

Fig. 5.19 shows a typical stress distribution obtained experimentally, together with the pridicted distribution for the corresponding condition. The values of n and K taken for the material (XC-45 steel) were 0.26 and 0.368 X 10^9 N/m^2 (see Table 5.1). The values of P and β yielding a fair comparison were found to be respectively 0.156 X 10^5 N/m and - 30°.

Comparison of the analytical curve for these conditions and the experimental results shows reasonbly good agreement.

General features of the residual-stress distributions

The distributions in Figs. 5.16, 5.17, 5.20 - 5.35 exibit high tensile stresses beneath the surface falling sharply to low compressive values within a small depth (0.01 - 0.04 mm). The magnitude of the tensile stress can reach values up to 600 MN/m^2 (1.5 times the initial yield strength) near the surface (at a depth of $\simeq$ 0.005 mm). Stresses of this nature are known to be deleterious to the fatigue strength and corrosion resistance of the component. Thus it can be seen that the residual stresses in turning are of considerable practical importance.

Results obtained by Kravchenko (Fig. 2.5), and Matalin[23] during turning of steel 45 (R), (of a composition similar to that of the present work) also show these essential features. The typical distribution given in ref. 24 for plain turning of 0.4% carbon steel (Fig. 2.6) also follows similar features except that it exhibits in a layer of 1 - 2 μm from the surface, high compressive stresses which abruptly change to large tensile values. In view of the fact that the primary finish of a turned surface is usually worse than about 2 μm, it is considered that measurement of the stress distributions within the 1 - 2 μm range is not realistic.

In the present investigation, careful studies of the nature of the specimen deflection at low currents have not revealed any evidence of the existence of this first compressive layer.

Influence of the cutting speed

The following characteristics of the distributions have been considered for comparison over the speed range 15 - 478 m/min.*

(1) Peak tensile stress

(2) Stress at 0.005 mm below surface

(3) Depth of the tensile region

(4) Average slope of the tensile portion of the distribution

From the curve A - A of the Fig. 5.36 it can be seen that stress at a depth 0.005 mm below the surface has low values (50 MN/m^2) at cutting speeds up to 40 m/min. With an increase in speed above 40 m/min, the stress rapidly rises reaching a peak value at 53 m/min. and then falls with a further increase in speed. Studies of the mode of chip formation, and an examination of the finished surface and the underside of the chip, suggested that this could be attributed to the changes in the size and shape of the built-up edge. Thus, the incidence of a negative-wedge type of built-up edge revealed in the

---

* For the range 15 - 75 m/min, results from an earlier investigation[112] by the author have been used.

investigations of Heginbotham and Gogia[121], is considered responsible for the large increase in the level of stress with the increase in speed from 41 to 53 m/min[98]. Further increase in speed causes the built-up edge to diminish, the disappearance occuring for XC-45 steel at about 80 m/min[120]. Correspondingly, the stress is found to decrease with increase in speed up to 70 m/min. Russian investigations in turning of steel 45 (R) have revealed similar behaviour in this speed range (Fig. 5.37) and it was attributed to the built-up edge.

Beyond this point the stress shows a gradual increase with increase in speed up to about 160 m/min. A significant fall then occurs between 160 - 200 m/min. The reason for this may be found from the recent work of Betz[122] on XC45N steel (a material of composition similar to the one employed in this investigation) showing a marked change in the conditions around the tool point at a cutting speed of about 200 m/min. Photographs obtained by using an electron scanning microscope showed the existence of a stagnant ('dead') zone of metal in front of the cutting edge over a wide range of speeds. At 200 m/min., the 'dead zone' was found to move clear of that part of the tool-edge giving rise to the cut surface, whence the tool edge produced a 'burnished' effect on the cut surface. The onset of this burnishing may be expected to result in a decrease in the magnitude of the ploughing force P, leading to a decrease in the residual stresses.

Increase in speed beyond 200 m/min. causes a gradual increase in the stress. The rise of temperature in the cutting zone with speed is considered to have a dual effect. It superimposes thermal residual stresses, tensile in nature, near the surface. Also it has a stress-relieving effect, tending to reduce the magnitude of stresses near the surface. The net increase in the tensile stresses with cutting speed that has been observed suggests that the stress-relieving effect has a secondary role. Towards the higher range, the stresses increase less rapidly indicating that this effect gains in importance as speed is increased.

Depth of tensile stresses

The general decrease in depth with cutting speed shown in Fig. 5.36, is as predicted by the model. This may also be explained considering the established[97,98] changes in the shape of the shear zone. An increase in speed reduces the extent of the shear zone below the cut surface. Correspondingly, the total depth of spread of the stresses and that of the tensile region decrease. However, in the range of speeds over which built-up edge exists, the changes in depth of distribution are associated with the changes in the built-up edge configuration. The average slope of the tensile region shows a gradual increase with increase in speed (Fig. 5.38), in accordance with the prediction.

Effect of depth of cut

Fig. 5.20 shows that when the depth of cut was increased from 1.19 mm to 2.4 mm, the depth of distribution has decreased slightly without a significant change in the average slope of the tensile region. It might appear that this is not in accord with the prediction. However, in turning an increase in depth of cut alters the direction of chip flow and the resultant force, giving rise to the observed effect.

Effect of rake angle

Fig. 5.33 reveals that there was no significant change in the stress distributions with a change of rake angle from + 6^{o} to - 6^{o}. Albrecht's[99] results indicate that a large change in rake angle would be necessary to affect a significant change in β. Hence, the change in rake angle in this work is evidently too small to result in any discernible change in the stress distribution.

Effect of tool-wear

Fig. 5.34 shows that a wear land of 0.15 mm produced no significant change in the residual-stress pattern, compared with a 'sharp' tool. However the wear land, produced by simulated cutting, was on the side-cutting edge and hence for small values this might not have much effect on the ploughing force responsible for

the residual stresses in turning. Significant wear in the nose-radius region however, might be expected to result in increased depth of the distribution of stresses.

Effect of approach angle

The change of the cutting-edge angle from 90° to 45° resulted in a marked rise of the stresses, as well as the depth below the surface of the significant stresses (Fig. 5.35). It would seem that it is beneficial, from stand point of residual stresses, to use as large a cutting-edge angle as possible.

6. Conclusions and suggestions for further work

6.1. Conclusions

(1) The predictions of the analytical model show good agreement with experiment. The model can be employed to predict the nature of residual-stress distributions due to the mechanical effect of forces in cutting.

(2) The bending-deflection techinique developed gives reproducible results with an accuracy of stress determination of $\pm$ 4.6 MN/m^2 in a layer 5 μm thick, and is to be preferred to the mechanical method of 'discrete' layer removal, or the X-ray method.

(3) High tensile stresses, of the order of 1.5 times the initial yield strength of the material, can be induced beneath the surface due to turning. Since such stresses are detrimental to fatigue life, they constitute an aspect of considerable practical importance.

(4) In the turning of 0.47% carbon steel (XC-45), cutting speed has a pronounced effect upon the nature of the residual-stress distribution.

At low cutting speeds (< 40 m/min.) comparatively low tensile stresses ($\simeq 100$ MN/m^2) extending to depths upto 0.1 mm beneath the surface are found under the conditions employed.

In the range (40 - 80 m/min.), changes in the peak stress values occur with changes in the built-up edge, the maximum value in speed range being at about 50 m/min.

A marked fall in the stress occurs between 160 - 170 m/min., which appears to correspond to the reported changes taking place in the flow round the cutting edge, influenced by the dead-metal zone. At these conditions the tool edge is in effective cutting contact with the surface, which becomes burnished, and of good finish. Beyond 260 m/min. the stresses show a further increase.

Thus, under the conditions employed, the desirable cutting speed is between 200 - 250 m/min., to give relatively low residual stresses together with a good surface finish.

The subcutaneous stresses are tensile in nature over a wide range of speeds (15 - 480 m/min.) and generally the depth of distribution of the stress is reduced, and the stress gradient increased, with increase in speed.

(5) The present analysis confirms experimental work reported in the literature, indicating that large negative rake angles, radiussed cutting edges and flank-worn tools produce large tensile stresses distributed over comparatively large depths, in steels which do not undergo phase transformations during cutting.

(6) Results of the analytical model show that an increase in strain rate, alloying or degree of cold-work tends to reduce the depth of the distributions of stress and increase the stress gradient. Also copper alloys give rise to residual stresses extending to

deeper layers and with lower stress gradients than plain-carbon or alloy steels.

(7) The depth of the work-hardened layer and the degree of hardening are primarily dependent on the strain-hardening index n of the material (in the stress-strain behaviour of the type $\sigma = k\epsilon^n$). Thus the depth of hardening is greater for copper alloys than for plain-carbon and alloy steels.

Increase in the cutting-edge radius causes a proportionate increase in the depth of the work-hardened layer. Rake angle has a negligible effect.

(8) Although residual stresses are usually accompanied by changes in hardness in the surface layers, the latter do not indicate the magnitude and the nature of stresses. The hardness distribution therefore has no other specially relevant or unique value as an indicator of the important effects of the machining process upon the surfaces it produces.

6.2. Suggestions for further work

(1) A detailed study of the conditions of flow around the cutting edge to reveal the precise manner in which P and β change with cutting conditions. Thus a more accurate quantitative prediction may be possible, which takes into account the situation actually existing at the cutting edge.

(2) The use of the finite element method would enable a more realistic strain distribution within the

work-piece to be obtained and residual stresses to be evaluated at the surface as well as within the material. It may be possible to incorporate the effects of strain rate and temperature using this approach, thus yielding a better estimate of the stress distribution in cutting.

Table 2.1

Accuracy of stress determination by X-ray technique in steel, quoted by various investigators.

Investigators	Accuracy ($\pm$ MN/m^2)
Sharpe[75]	20.7
Grimaldi et al.[84]	15.0
Taira and Yoshioka[83]	10.0
Norton and Rosanthal[14]	10.3

Table 3.1

Conditions for which residual-stress distributions based on the analytical model, were computed

Figure No.*	K (X 10^3 MN/m^2)	n	(degrees)
5.1	0.2,0.4,0.6,0.8	0.4	-30
5.2	"	0.3	"
5.3	"	0.2	"
5.4	"	0.1	"
5.5	0.6	0.4	0,-15,-30,-45,-60
5.6	"	0.3	"
5.7	"	0.2	"
5.8	"	0.1	"

For all the cases,

$E = 0.2067 \times 10^{12}\ N/m^2$

$\nu = 0.3$

* Figures show stress distributions in the direction of cutting.

	X-ray method	Mechanical method with layer removal in discrete steps	Mechanical method involving continuous layer removal
Special equipment and facilities necessary	X-ray unit, back-reflection camera, facilities for developing the film, photodensitometer.	Universal Measuring Machine, Twymann-Green interferometer, monochromatic and white light sources, Angle-dekkor.	Displacement transducer, and either a U.V. recorder or an autocollimator.
Time for experiment	Two exposures (minimum) taking 2 hours each, 15 minutes for developing and analysis.	½ hour (minimum) per layer, including 10 minutes for setting up per layer.	15 minutes of set-up time and 45 minutes of actual layer removal, per specimen.
Costs	Cost of equipment, film and developing.	Cost of equipment.	Cost of equipment, U.V. recorder paper.
Accuracy obtained	$\pm$ 13.8 MN/m^2	$\pm$ 13.1 MN/m^2 in a layer 5μm thick.	4.2 MN/m^2 in a layer 5μm thick.
Special features	Expensive equipment.	High demands on care and skill.	Suitable for data-logging and on-line computation.

Table 4.1

Table 4.2

Conditions employed for electropolishing the specimens.

Constituent	% Composition by volume
Perchloric acid (60%)	20
Glycerol	10
Alcohol	70

Voltage = 10 Volts D.C.

Current density = 900 Amperes/m^2

Spacing between the electrodes = 25 mm.

Table 4.3

Summary of conditions employed for turning the test surfaces.

A feed of 0.24 mm/rev. was employed for all specimens.

Specimen No.	Cutting speed m/min.	Depth of cut (mm)	Tool geometry* ($\gamma - \alpha - \lambda - \kappa - \varepsilon - r_\varepsilon$)
1	15	1.19	(6 5 0 90 60 0.76)
2	26	"	"
3	41	"	"
4	54	"	"
5	67	"	"
6	75	"	"
7	96	"	"
8	112	"	"
9A	187	"	"
10A	264	"	"
11A,11B,11C	155	"	"
12A,12B	319	"	"
13A	472	"	"
14A	159	"	"
15A	319	"	"
16A,17A	240	2.40	"
18A	238	1.19	(6 5 0 45 60 0.76)
19A	238	"	(-6 5 0 90 60 0.76)
21A	241	"	(6 5 0 90 60 0.76)
22A	112	"	"

* The tool geometry is shown in Fig 4.9.

Table 5.1

Typical values for K and n at low-strain rates and room temperature (from Kalpakjian[117])

No.	Material	K (10^9 N/m^2)	n
1	Low C-steel, ann.	0.318	0.26
2*	XC-45 steel, HR.	0.368	0.26
3	1112 steel, ann.	0.449	0.19
4	1112 steel, CR.	0.444	0.08
5	4135 steel, ann.	0.600	0.17
6	4135 steel, CR.	0.650	0.14
7	4340 steel, ann.	0.378	0.15
8	1100-0 Aℓ.	0.106	0.20
9	2024-T4 Aℓ.	0.407	0.16
10	6061-T6 Aℓ.	0.240	0.05
11	Copper, ann.	0.198	0.54
12	70-30 Brass ann.	0.555	0.49
13	85-15 Brass CR.	0.351	0.34
14	304 stainless, ann.	0.785	0.45

* From tensile tests performed in the present investigation.

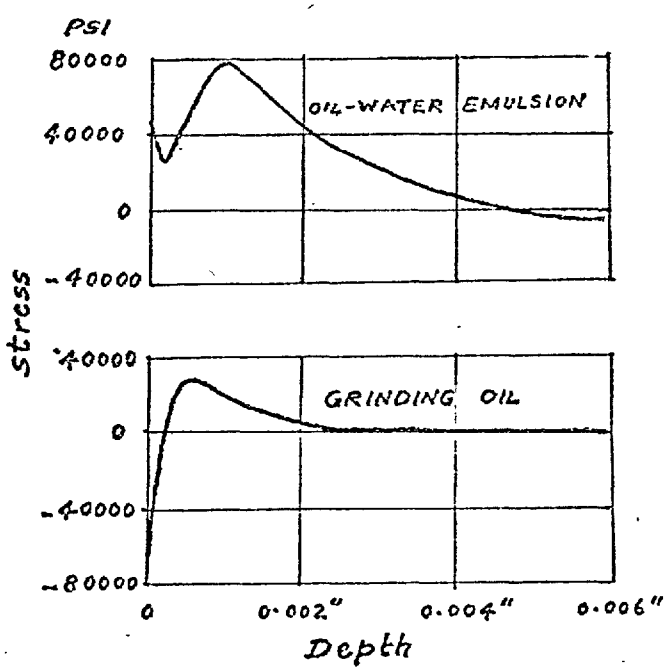

Fig.2.1. Grinding stresses in hardened steel. (After Letner.[19])

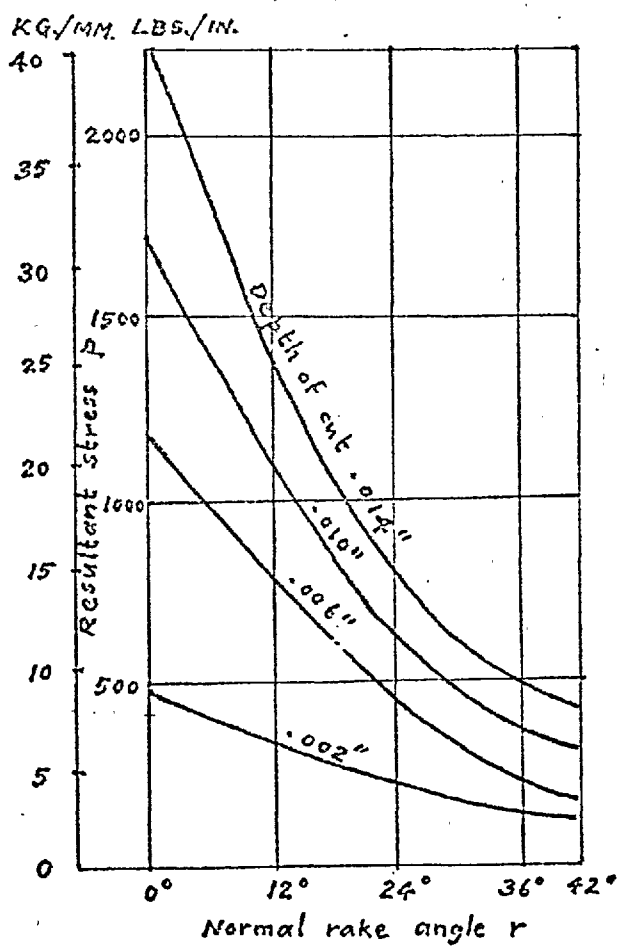

Fig. 2.2. Variation of resultant machining stress p in relation to normal rake angle r of tool and depth of cut. (Orthogonal cutting, 0.1% carbon steel, cutting speed 15.7 sfpm.)
(After Henriksen[30])

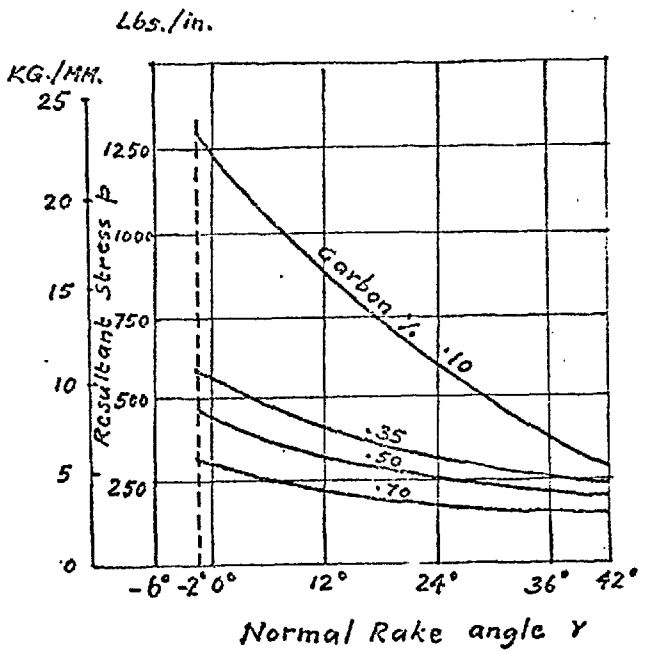

Fig.2.3. Variation of resultant maching stress p in relation to normal rake angle r of tool and carbon content of material. (Orthogonal cutting , 0.008 in. depth of cut , cutting sp. 15.7 sfpm). (After Henriksen[30])

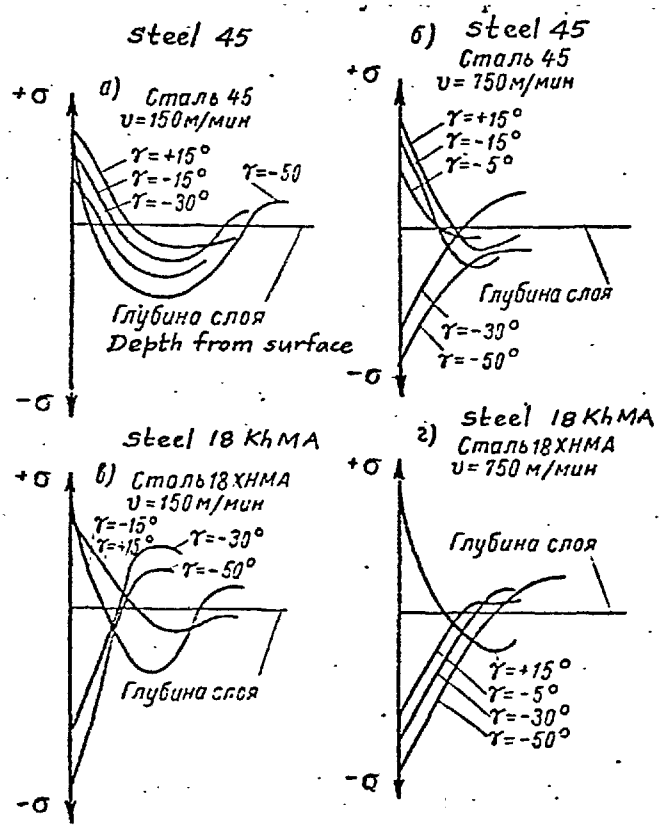

Фиг. 146. Влияние переднего угла на характер распределения остаточных напряжений при точении (П. Е. Дьяченко и А. П. Добычина).

Fig. 2.4. Influence of rake angle on residual-stress distributions (by experiment) in turning, shown schematically.

σ – Residual stress.
γ – Rake angle
v – cutting speed.

(after Matalin[23])

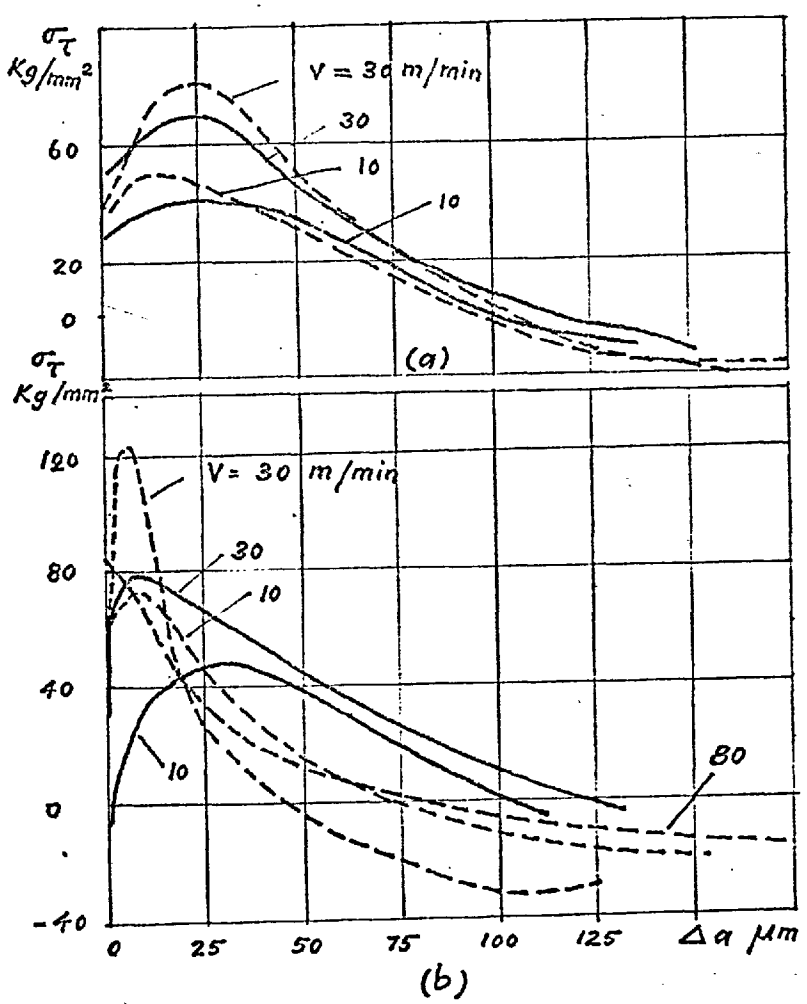

Fig. 2.5. Relationship between the residual tangential stresses σ_τ and the depth of the layer Δa in the machining of KHN77TYUR alloy steel at various speeds (a) rake angle = +7° (b) rake angle −10°. (After Kravchenko)[53]

—— without coolant
--- with coolant

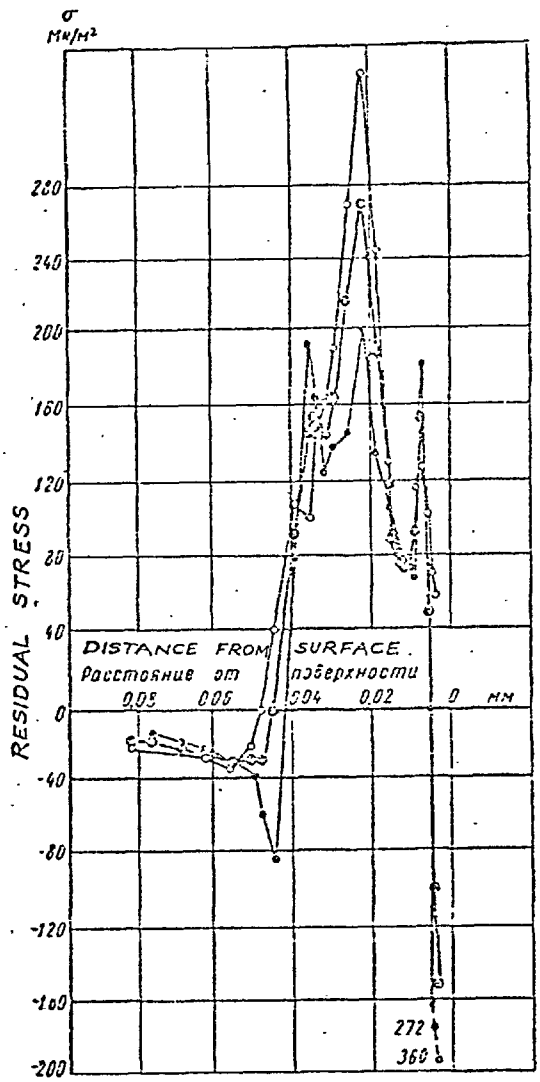

Fig. 2.6. A typical residual-stress distribution in steel 45 (R) due to finish turning. (From ref. 24)

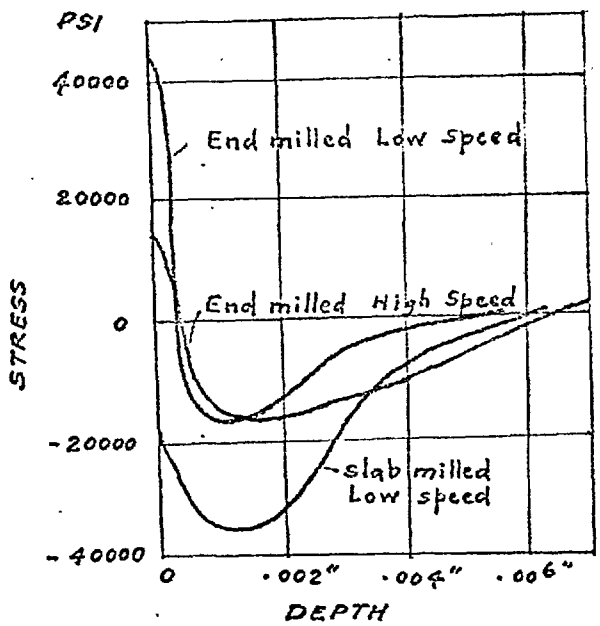

Fig.2.7. Machining stresses from milling.

End milled, Low sp. — Ordinary end milling.
End milled, High Sp. — Face milling.
Slab milled, Low Sp. — Side milling.

(After Field and Zlatin[34])

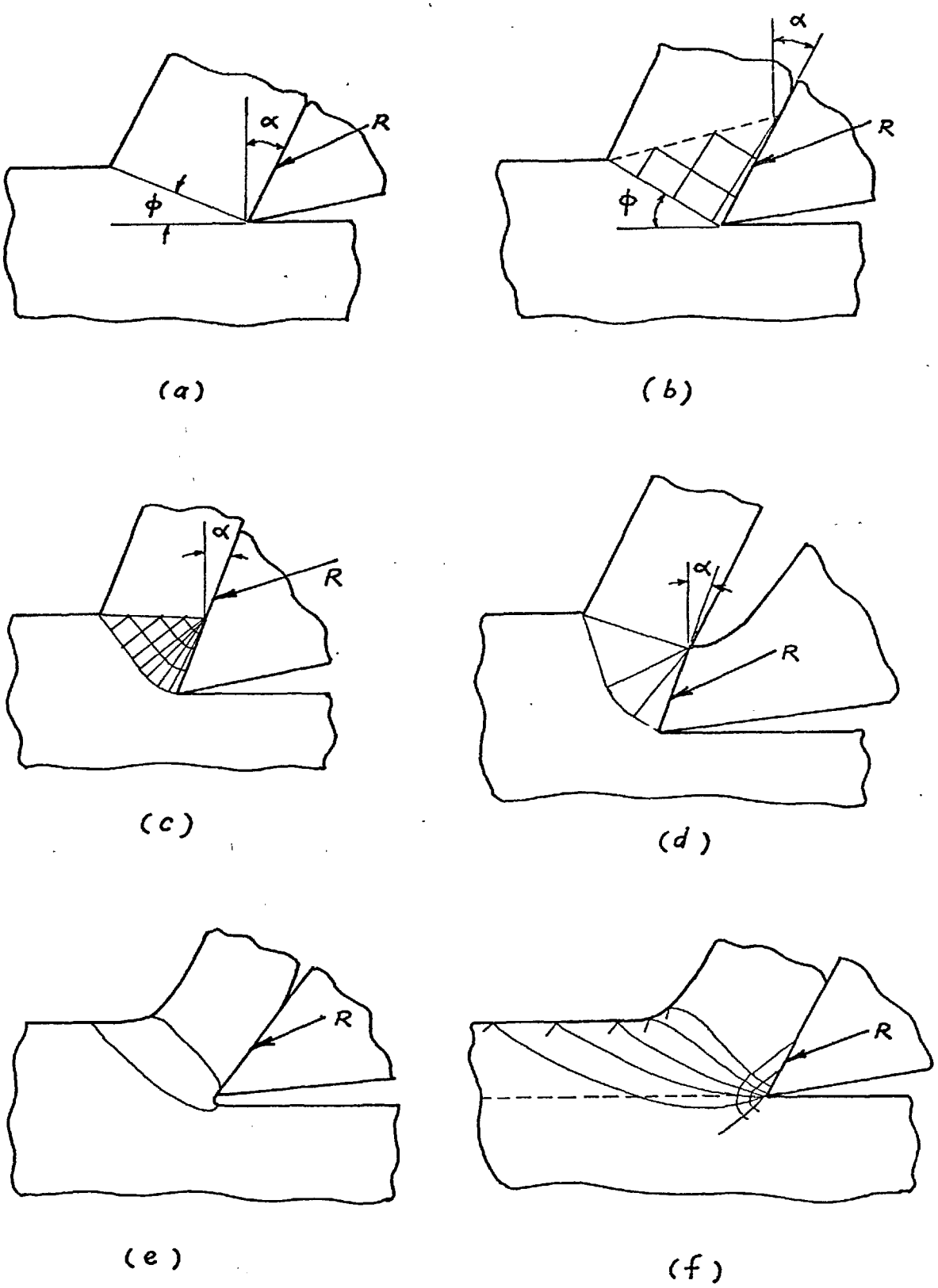

Fig. 3.1. Orthogonal cutting models due to

(a) Merchant.[93] (b) Lee and Shaffer.[94]

(c) Usui and Hoshi.[95] (d) Johnson.[96]

(e) Oxley.[97] (f) Zorev.[98]

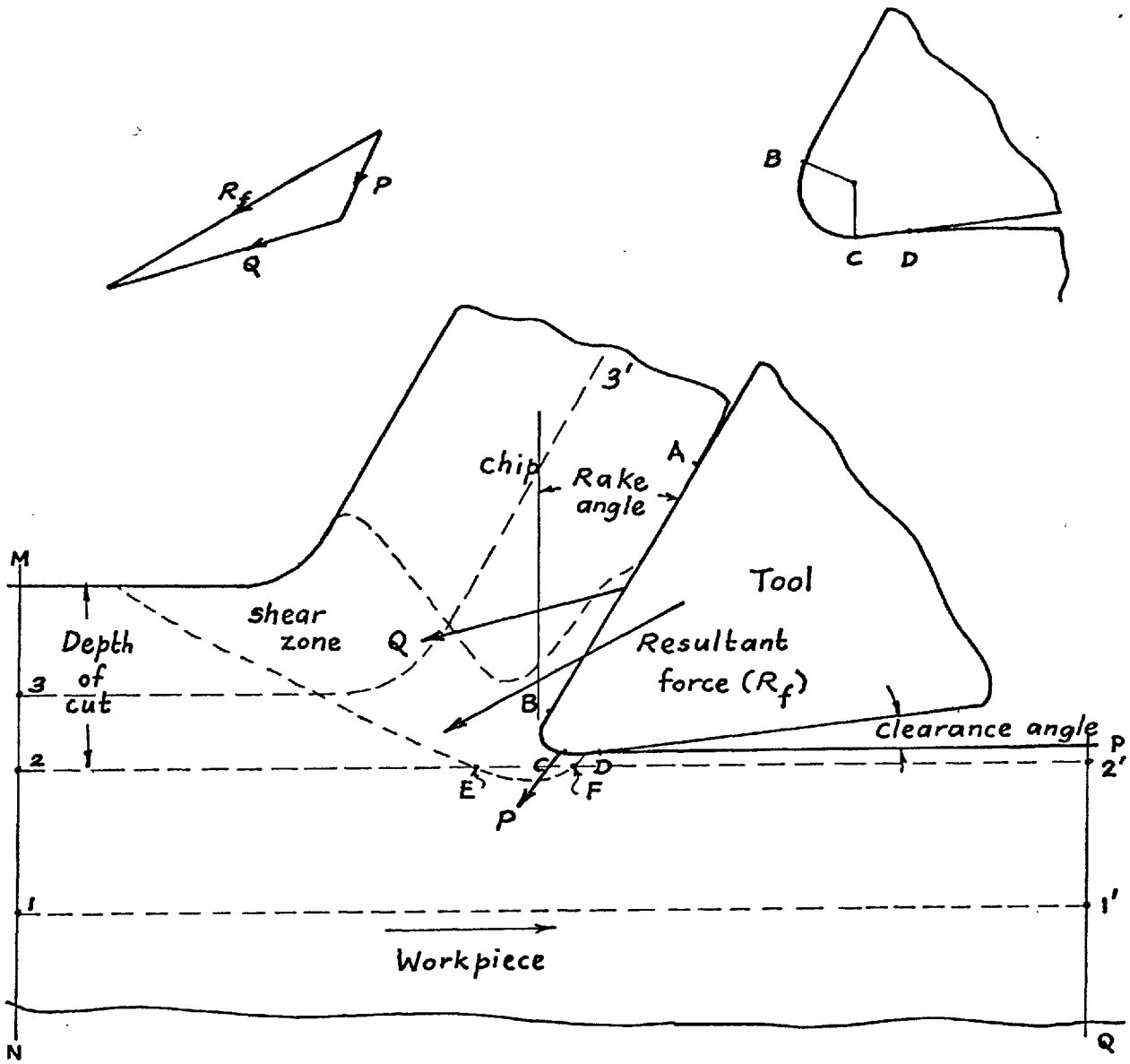

Fig. 3.2. Contact regions and forces on a tool in orthogonal cutting.

AB — Rake-face contact region
BC — Nose contact region
CD — clearance face contact region

P — Ploughing force
Q — Rake-face force
R_f — Resultant force

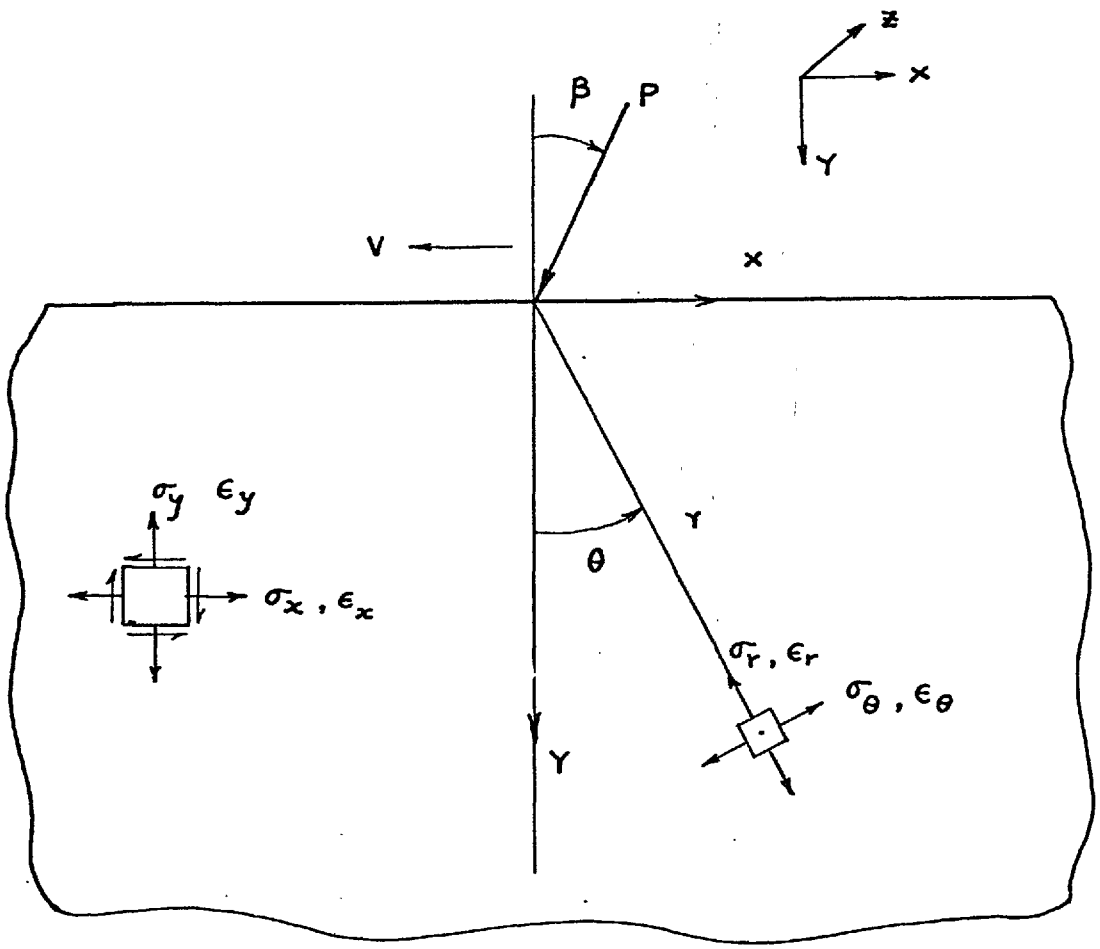

Fig. 3.3. Coordinate systems and notation for stresses.

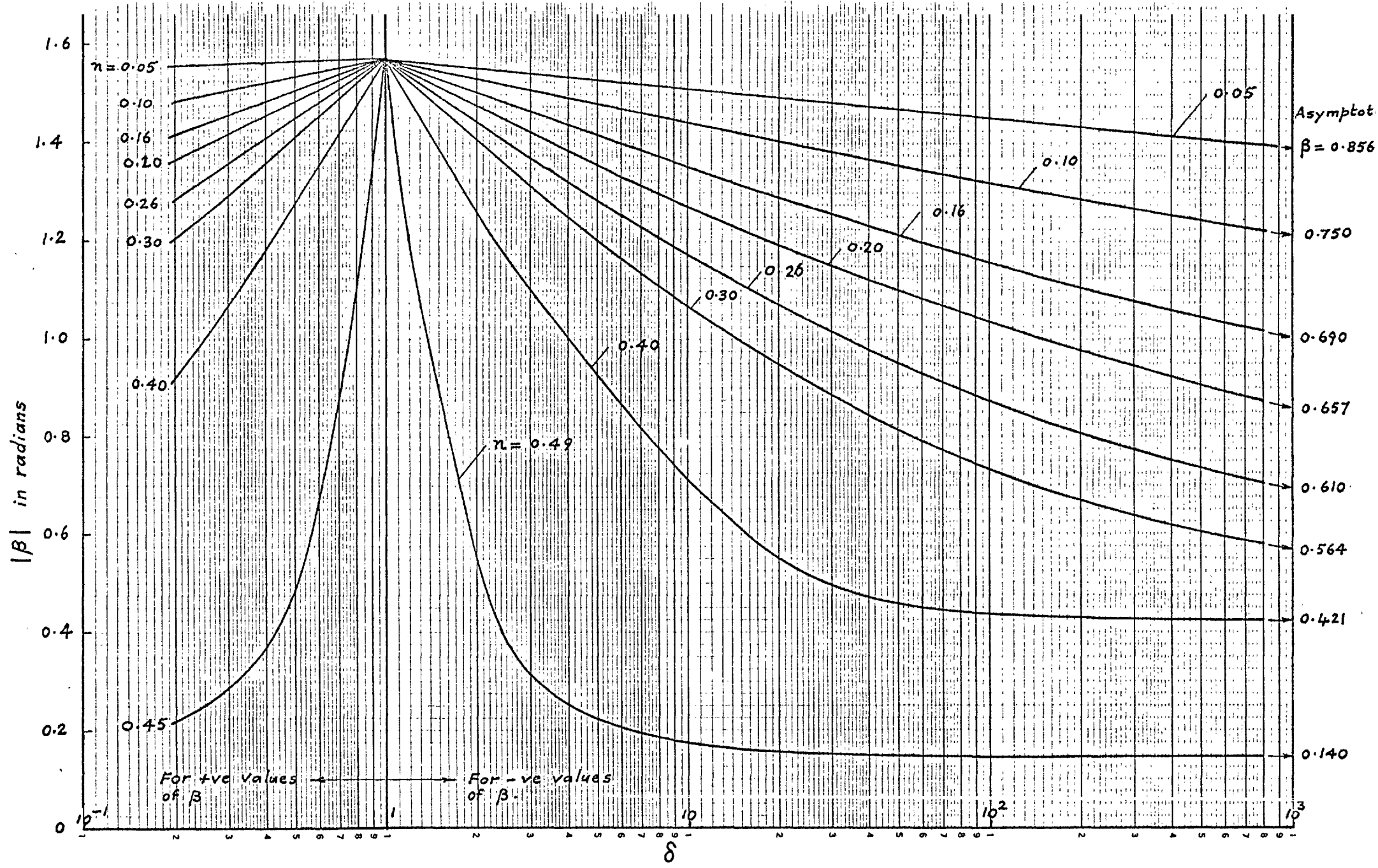

Fig. 3.4. Relationship between β and δ for various values of n. (See also Fig. 3.5)

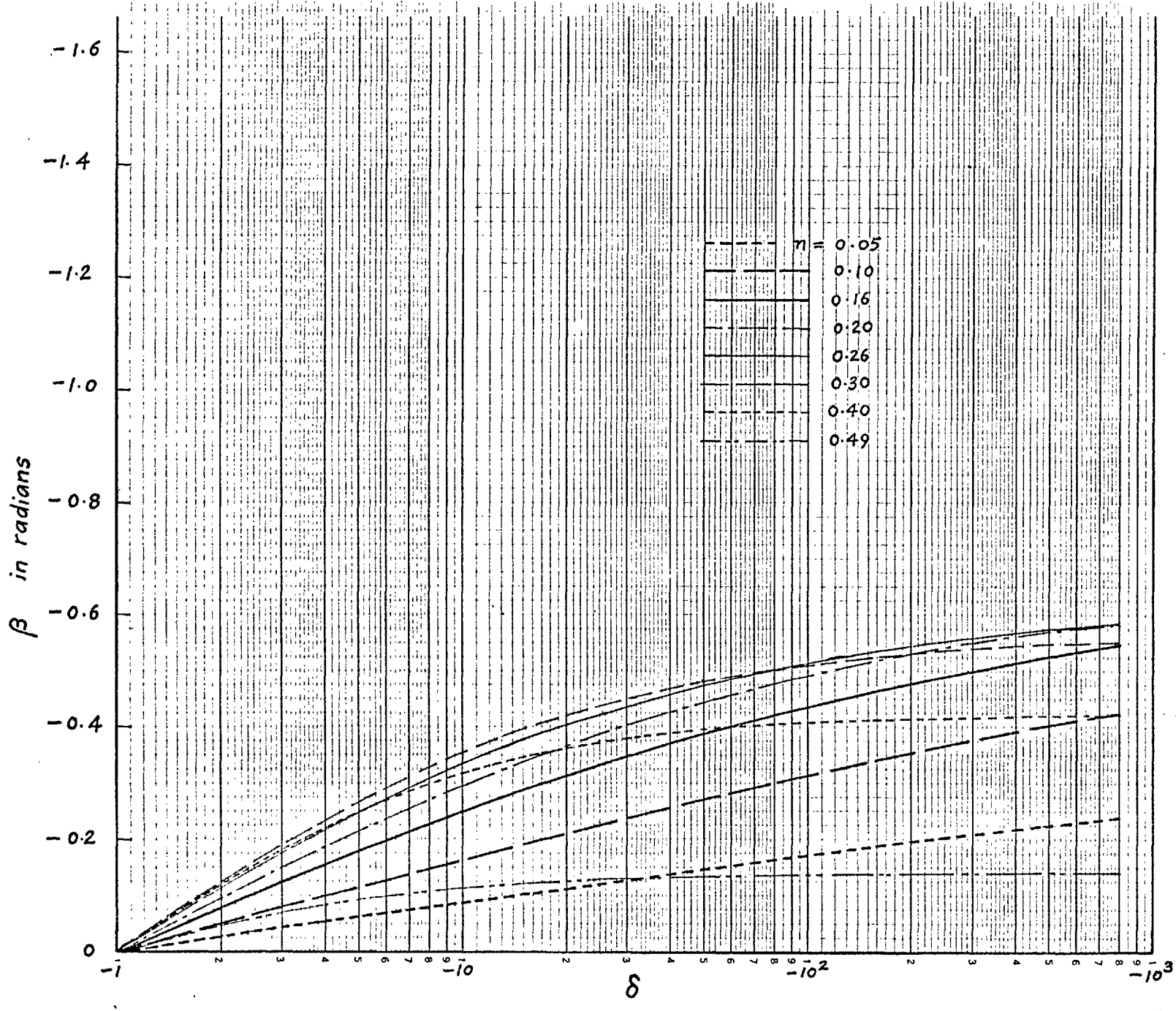

Fig. 3.5. Relationship between β and δ for various values of n. (See also Fig. 3.4)

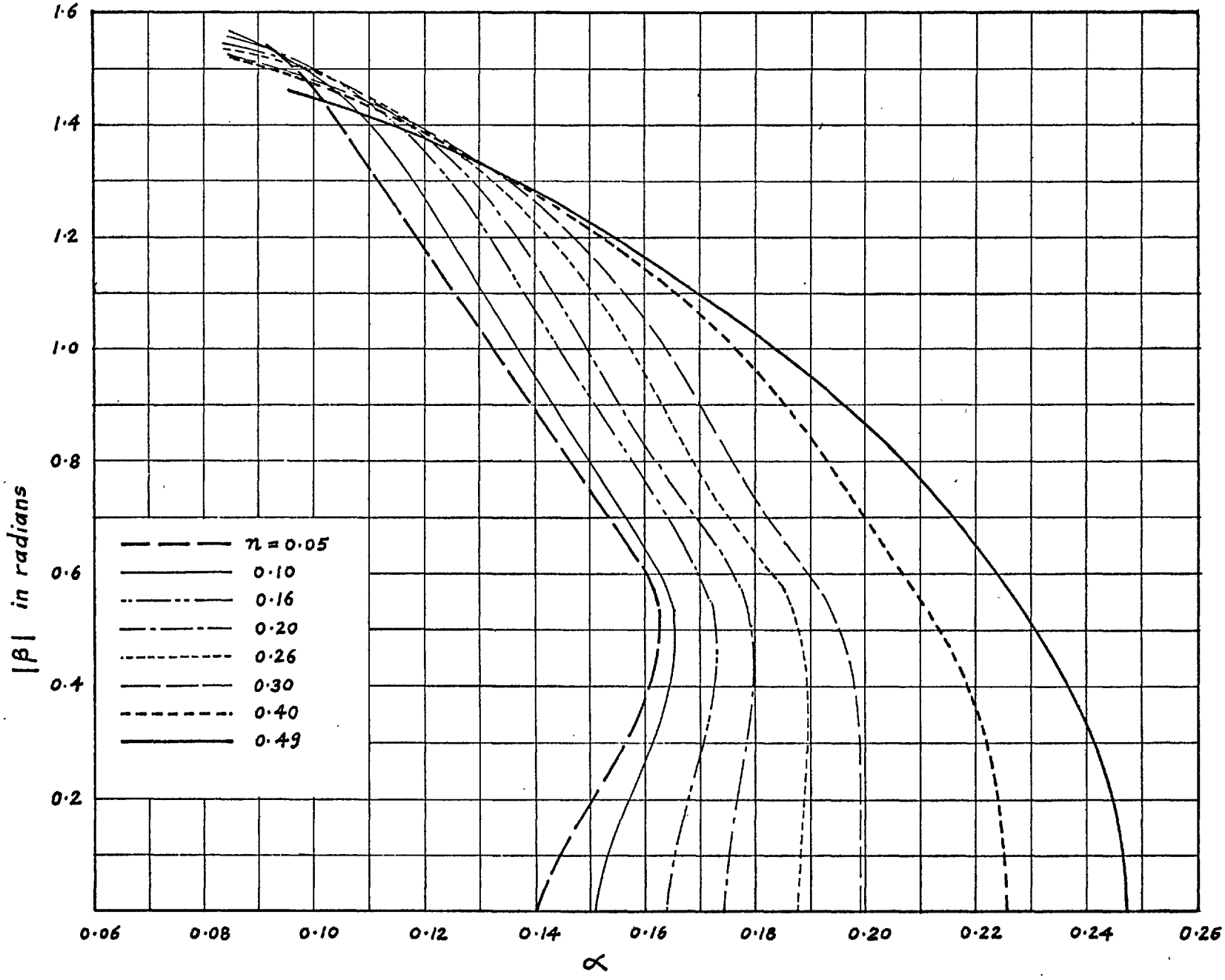

Fig. 3.6. Relationship between β and α for various values of n less than 0·5.

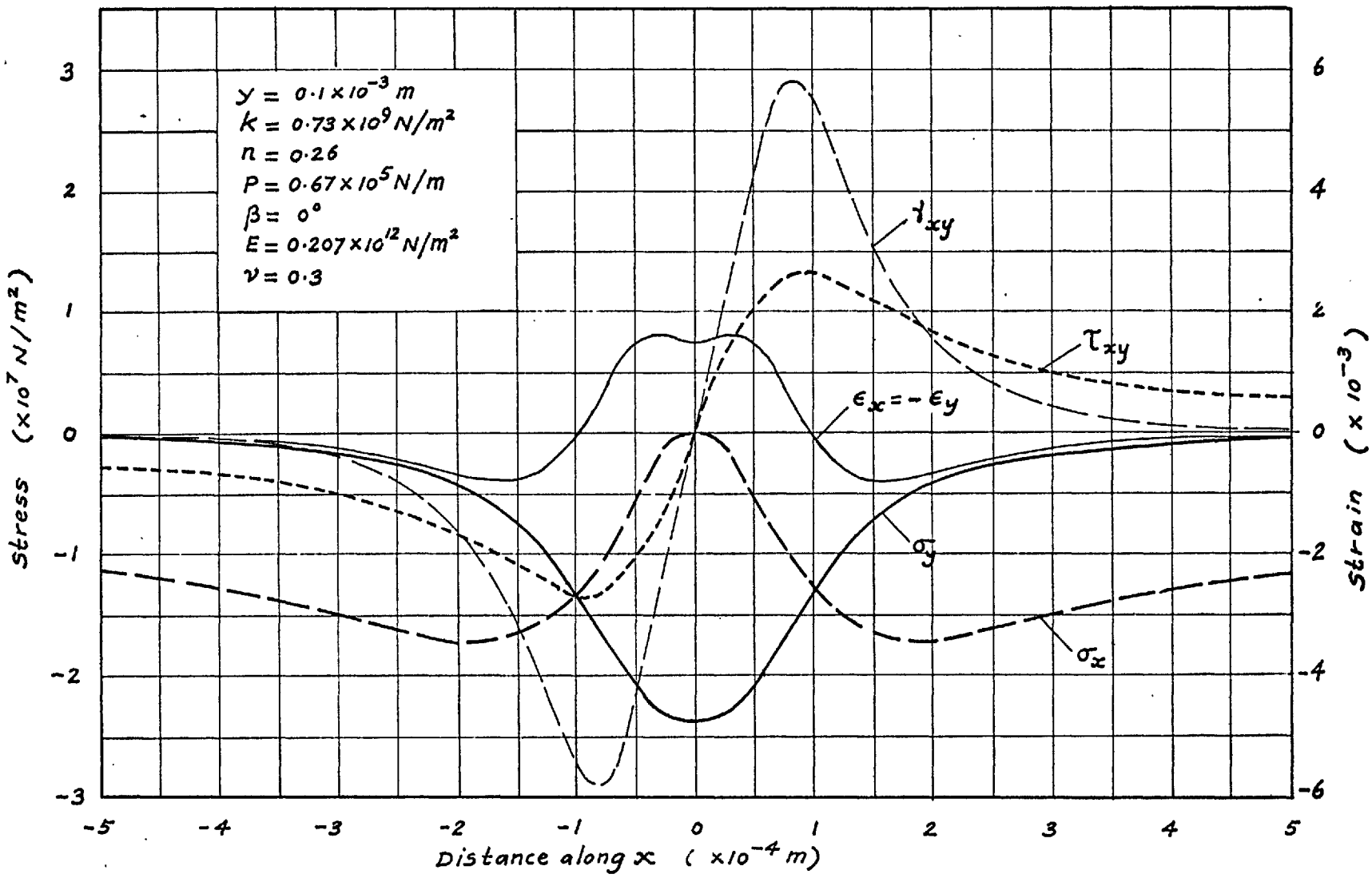

Fig. 3.7. Stress and strain distributions at a constant depth y below surface of a semi-infinite solid under a static line load P, assuming the stress-strain behaviour to be of the type $\sigma = k\epsilon^n$. Load acts normal to the surface.

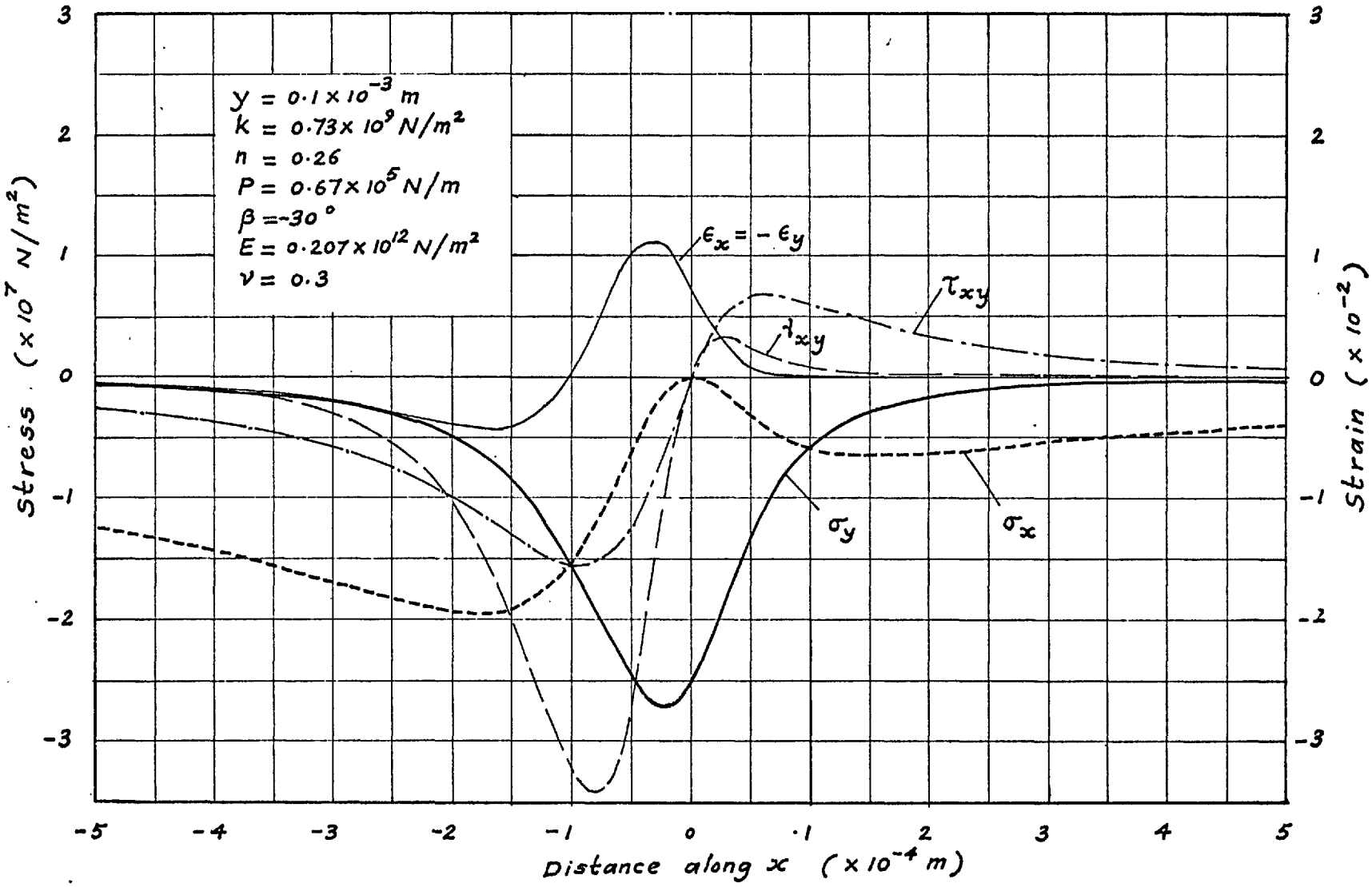

Fig. 3.8. Stress and strain distributions at a constant depth below surface of a semi-infinite solid under a static line load P, assuming the stress - strain behaviour to be of the type $\sigma = k\epsilon^n$. Load acts at 30° to the normal.

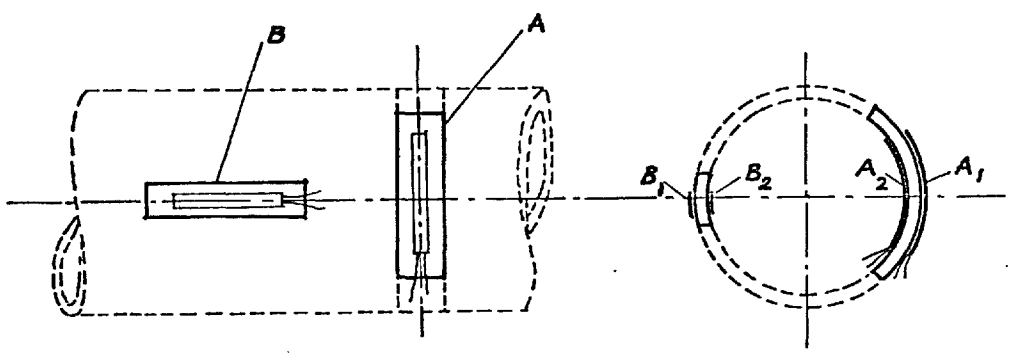

Fig. 4.1. Orientation of specimens A and B, and location of strain gauges A_1, A_2, B_1 and B_2

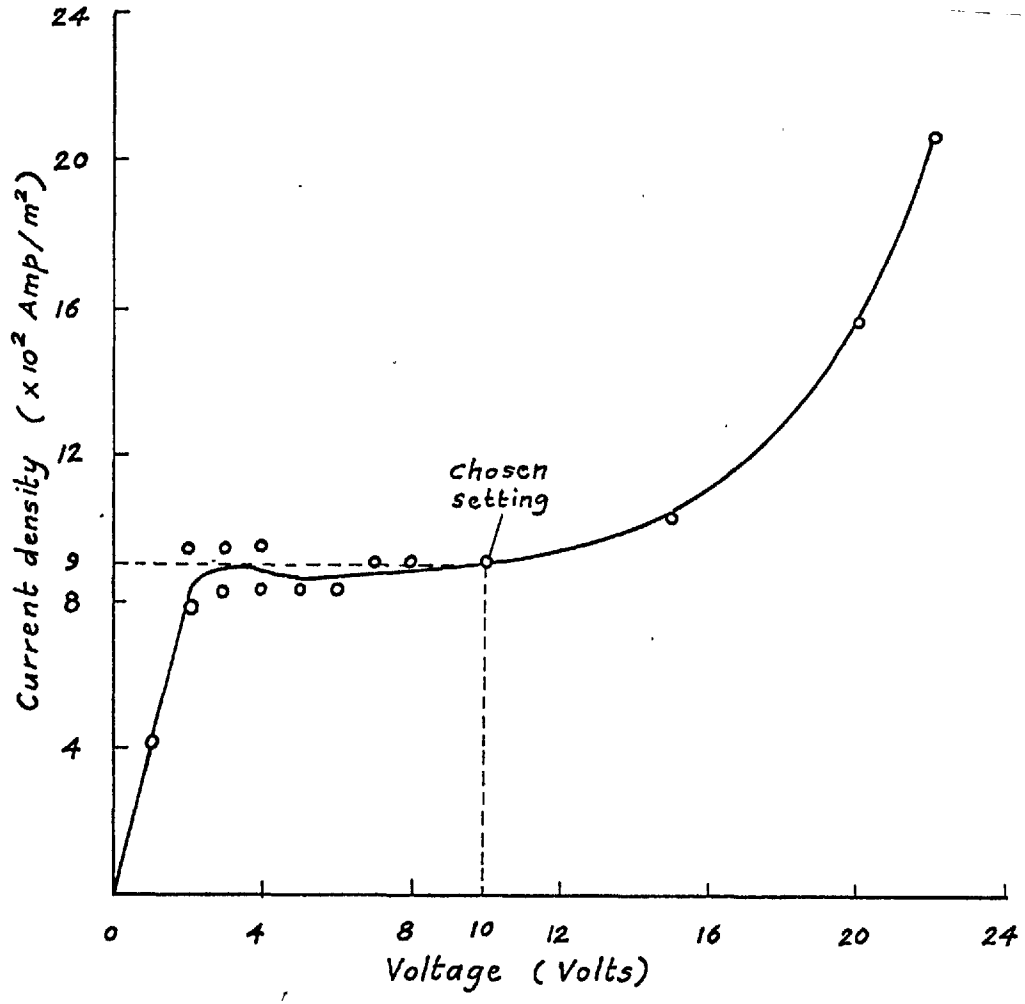

Fig. 4.2. Relationship between anodic current density and voltage in electropolishing steel, using perchloric-acid based electrolyte.

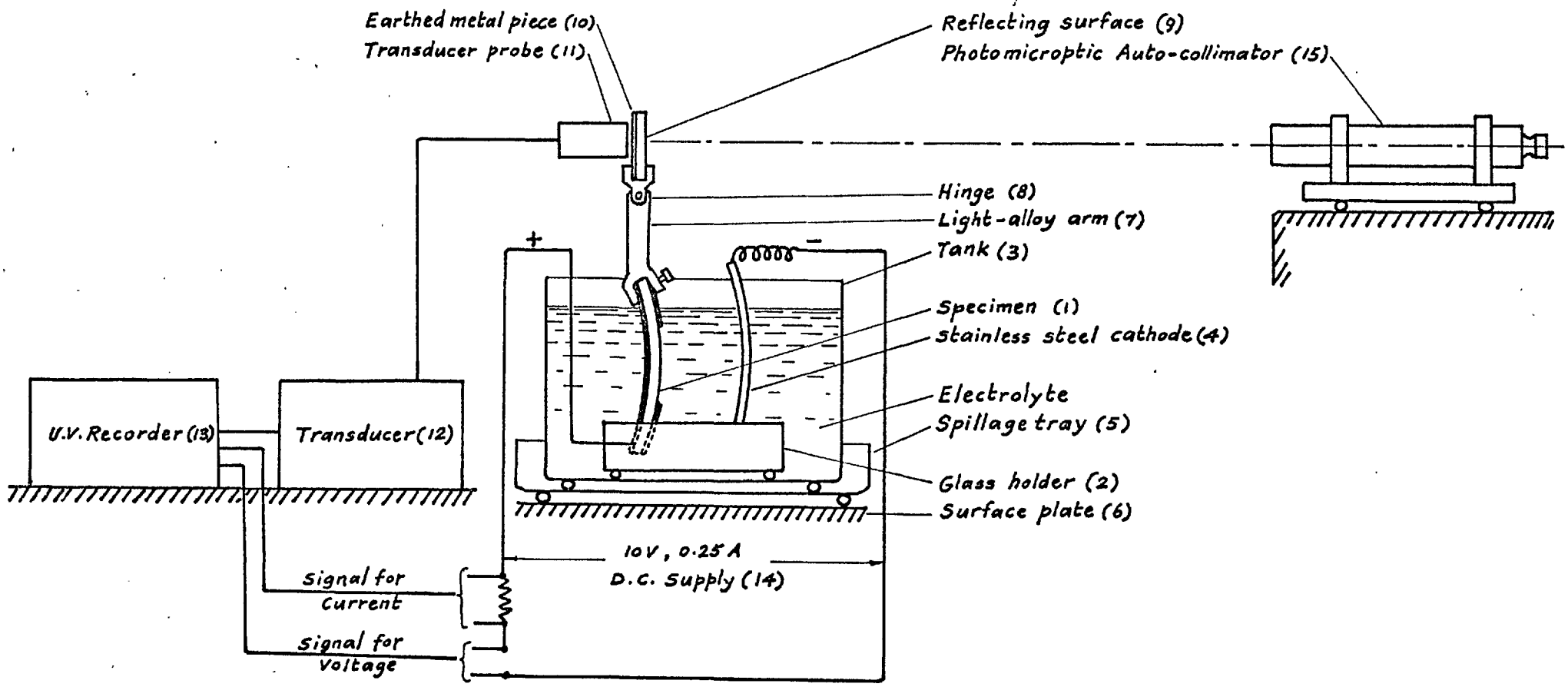

Fig. 4.3 Schematic diagram of the general arrangement for the measurement of residual stresses.

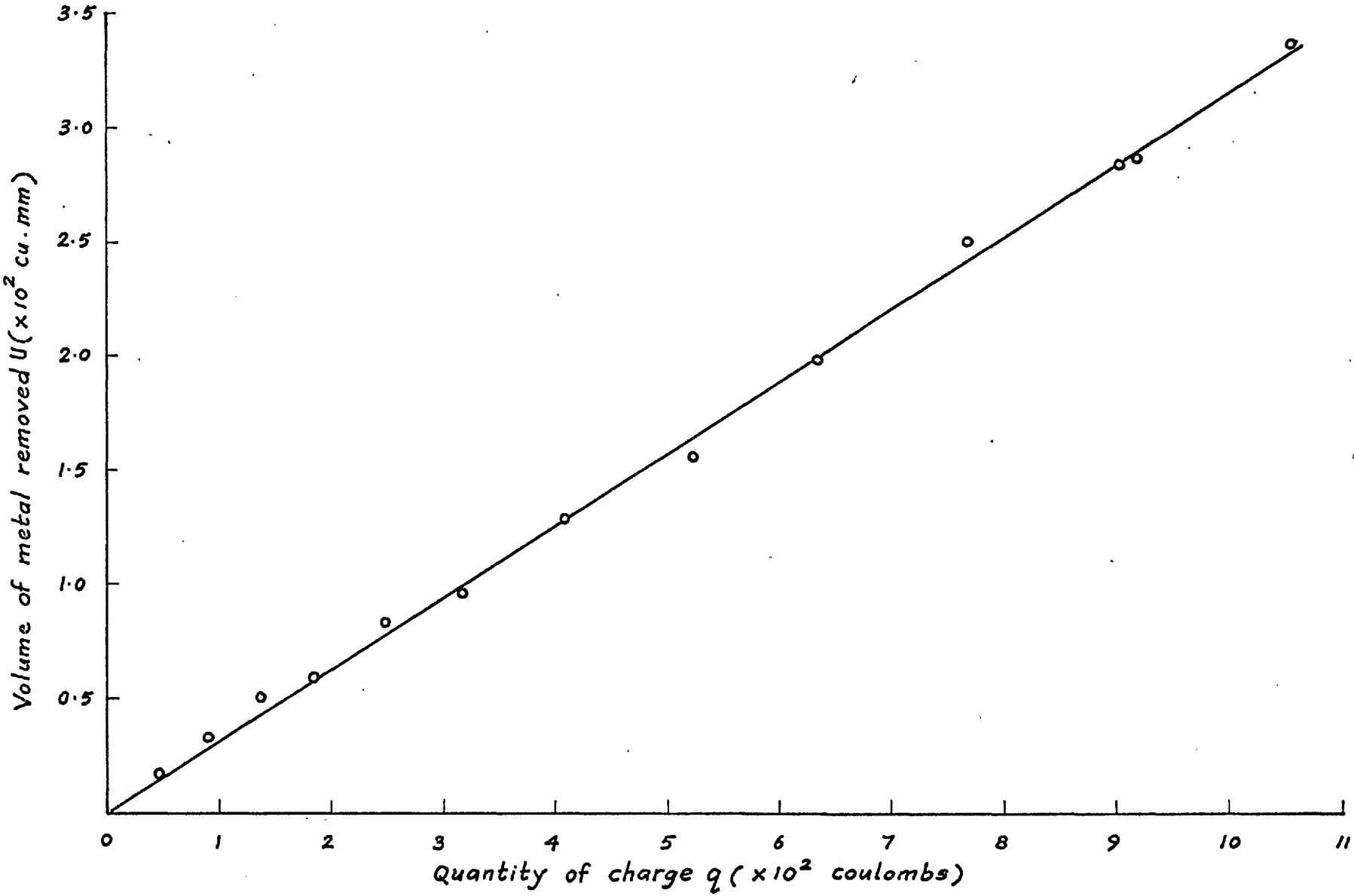

Fig. 4.4. Relationship between the quantity of charge passed and the amount of metal removed by electropolishing.

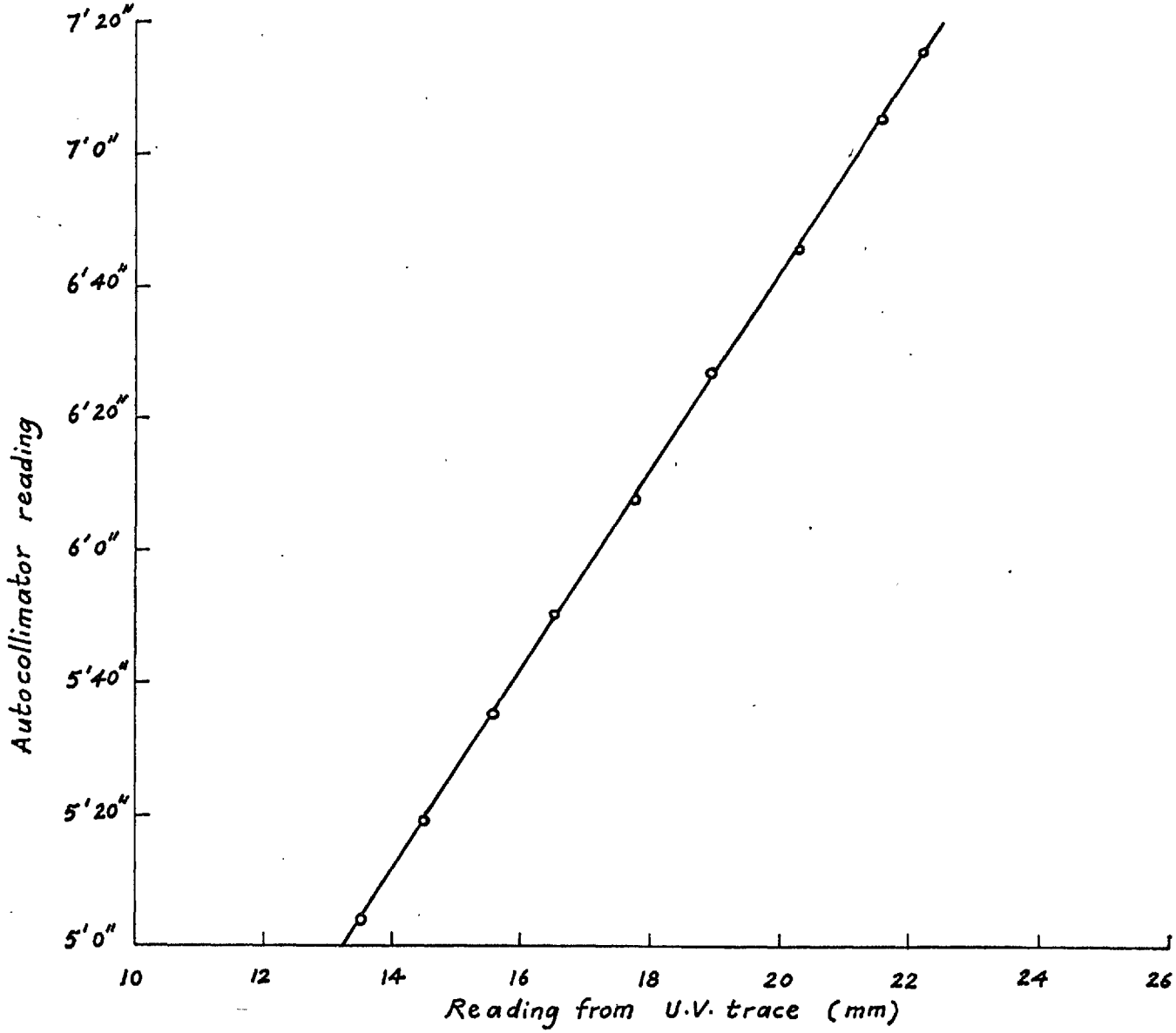

Fig. 4.5 Calibration of deflection readings from the U.V. Chart using photo-microptic autocollimator.

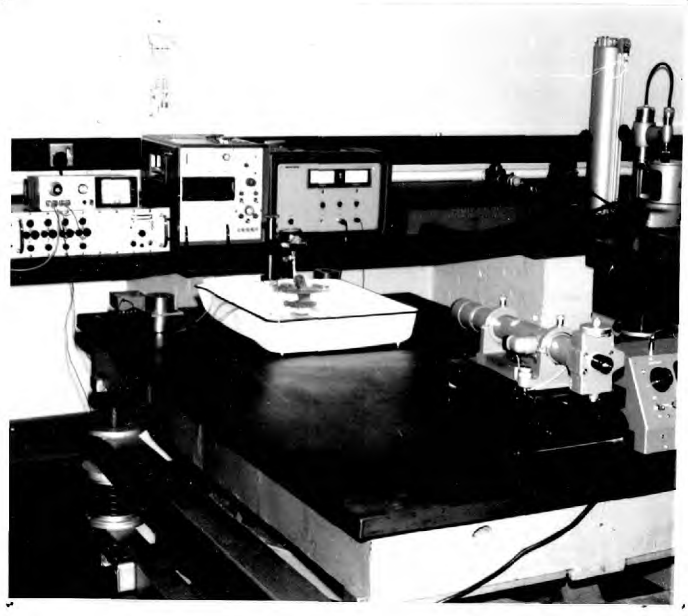

Fig. 4.6 (a) General arrangement.

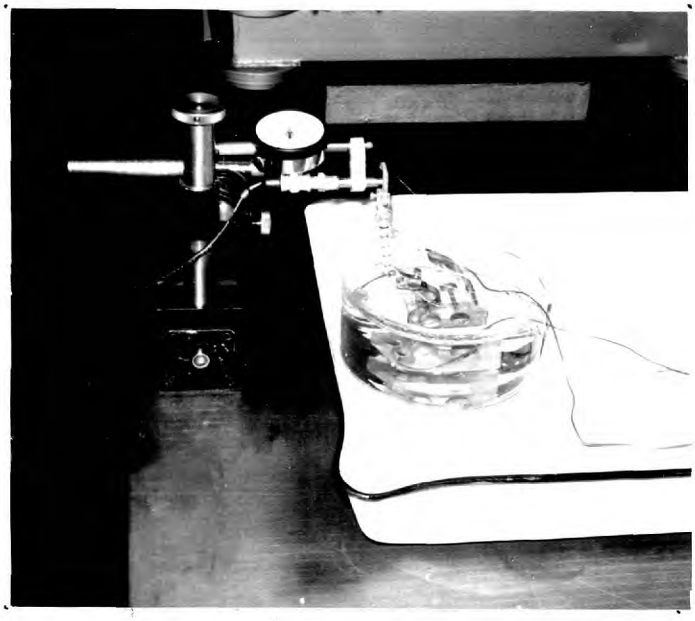

Fig. 4.6 (b) Transducer-probe mounting and the electropolishing unit.

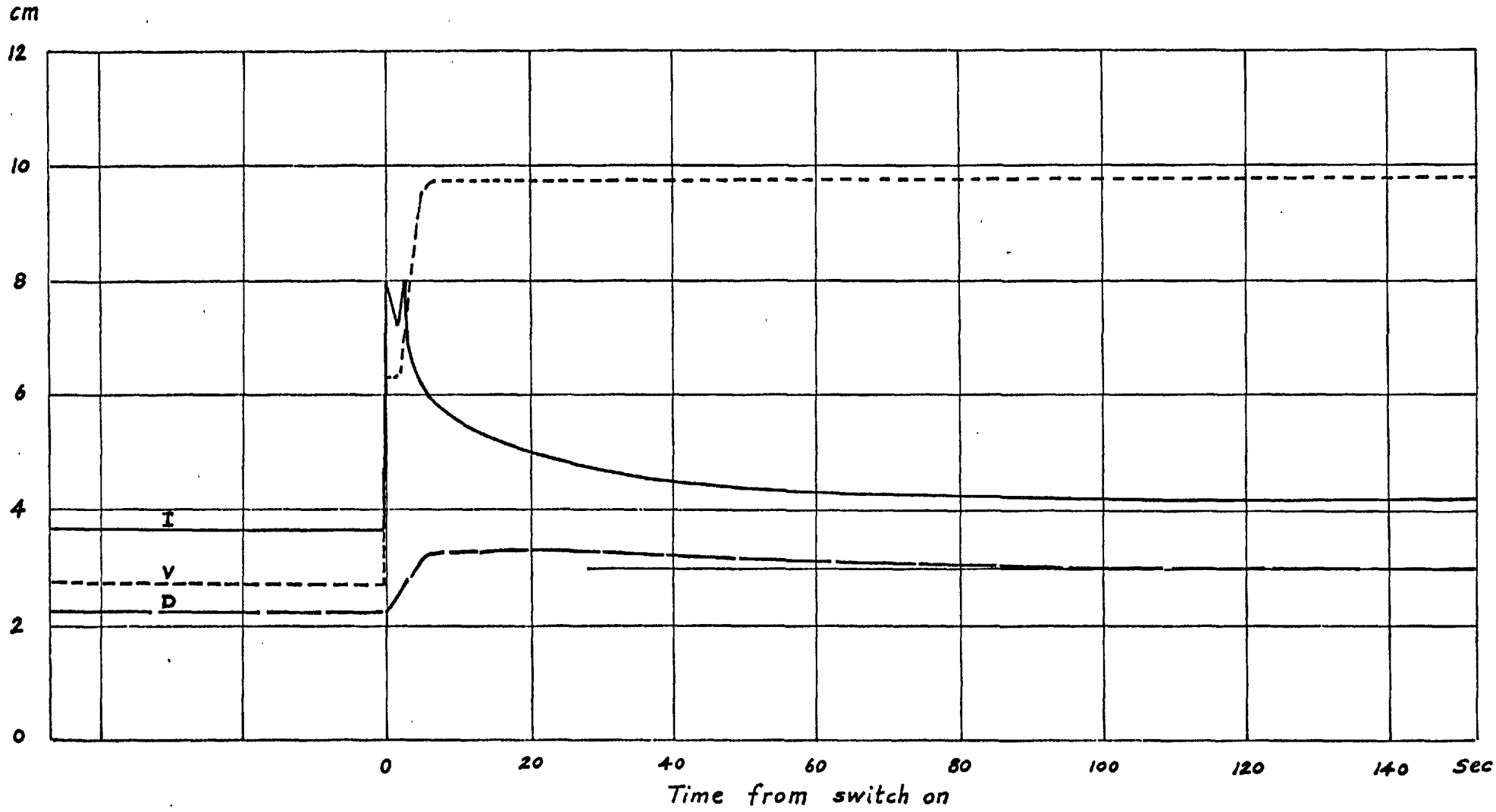

Fig. 4.7. A typical trace of current I, voltage V and deflection D from a U.V. Recorder, at the commencement of electropolishing, for an annealed specimen.

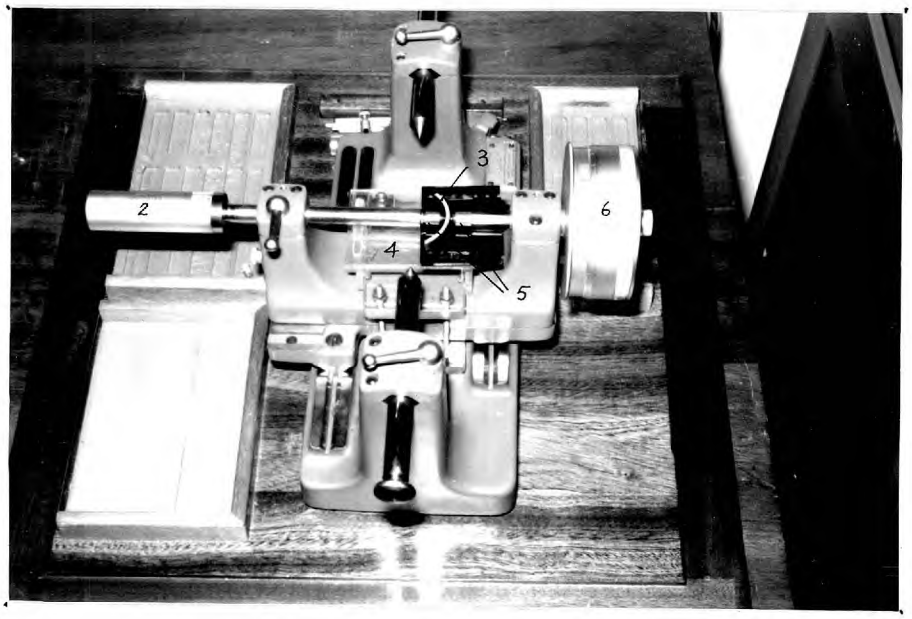

Fig. 4.8. Arrangement for the measurement of thickness.

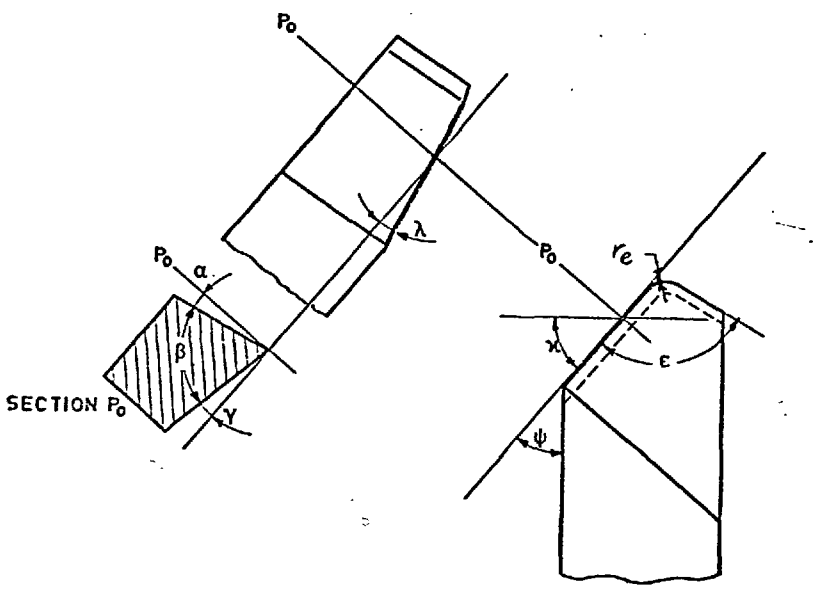

ALL ANGLES ARE POSITIVE IN THIS DRAWING, EXEPT λ WHICH IS NEGATIVE.

Fig. 4.9. Tool geometry.

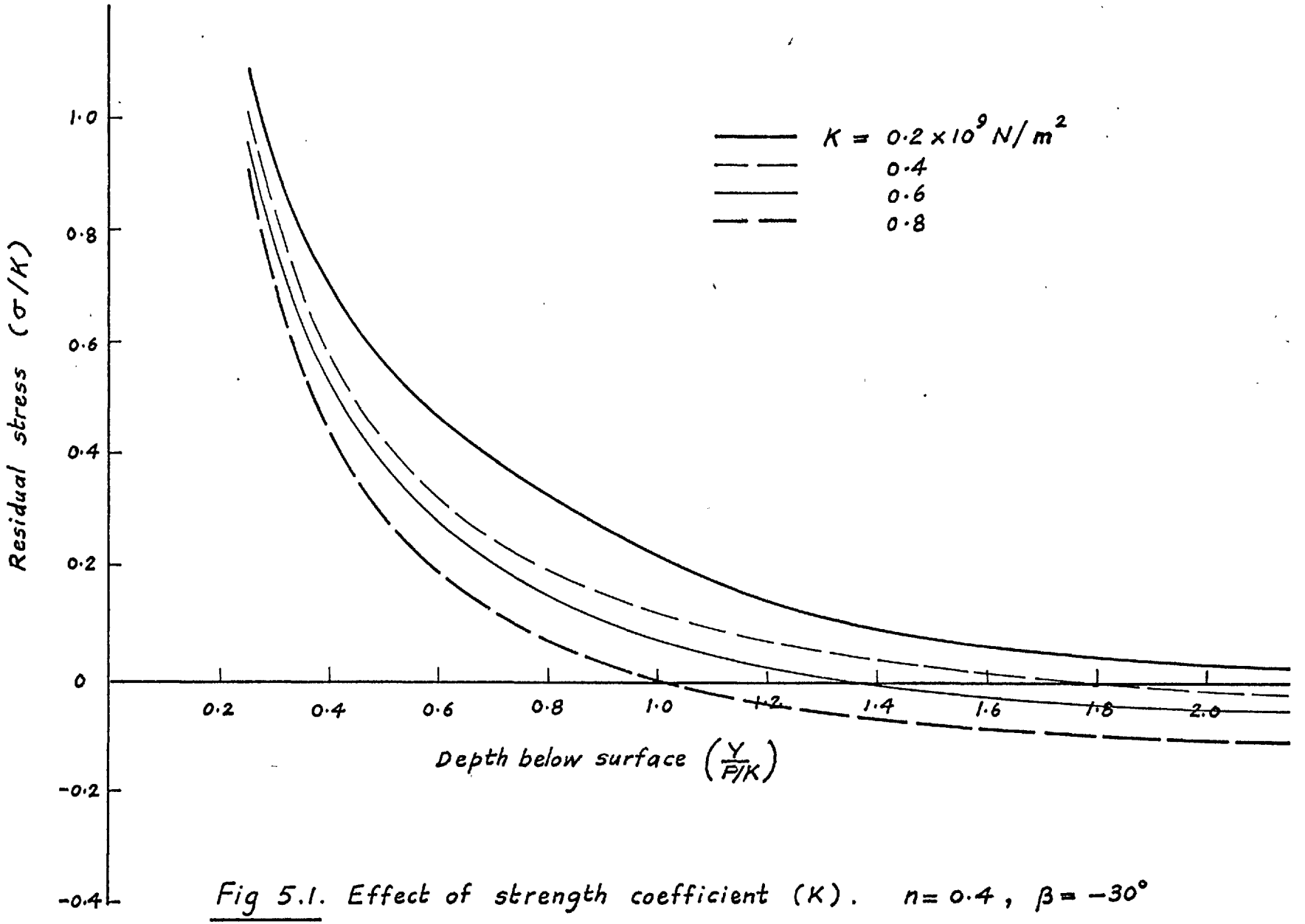

Fig 5.1. Effect of strength coefficient (K). $n = 0.4$, $\beta = -30°$

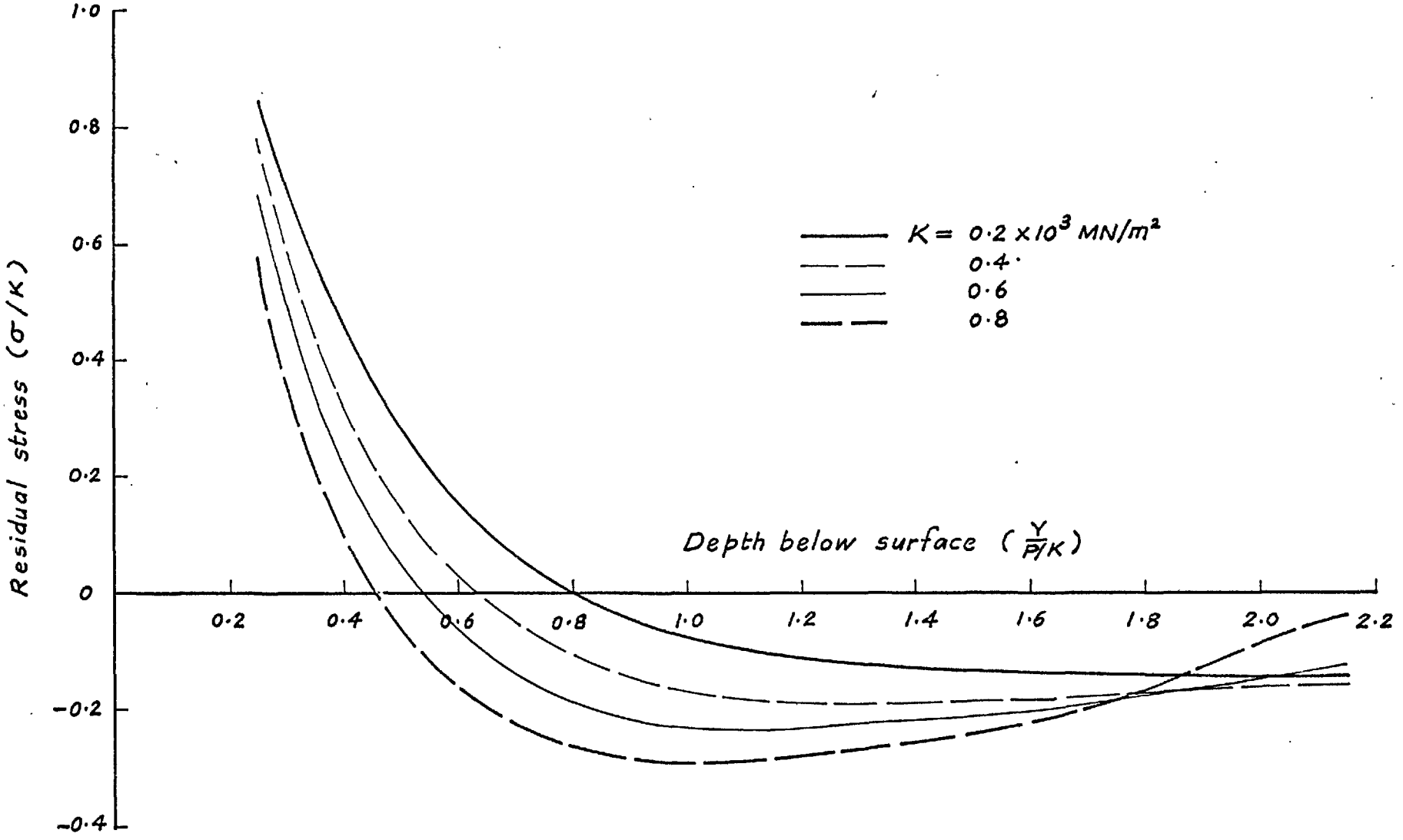

Fig. 5.2. Effect of strength coefficient (K). $n = 0.3$, $\beta = -30°$

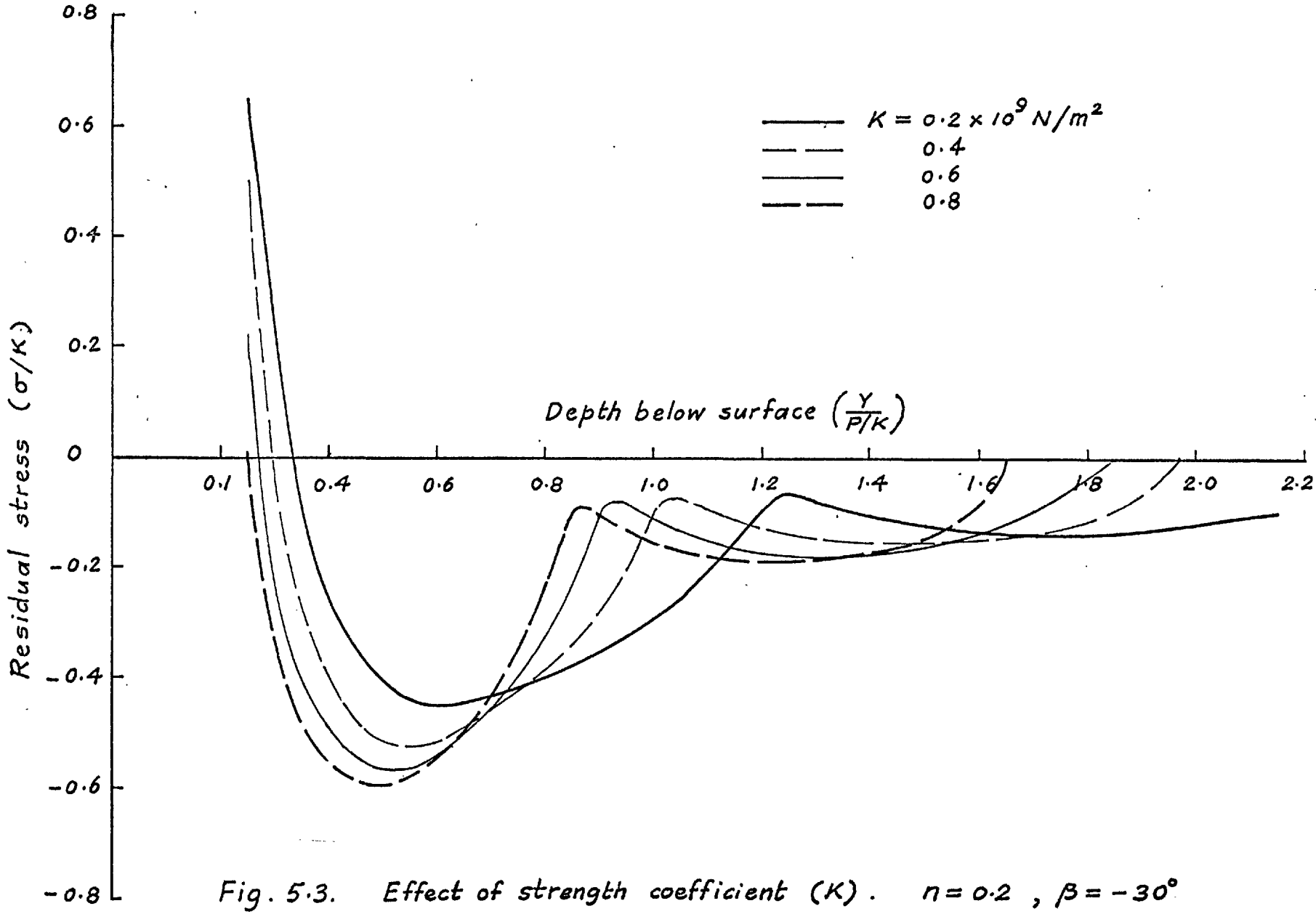

Fig. 5.3. Effect of strength coefficient (K). $n = 0.2$, $\beta = -30°$

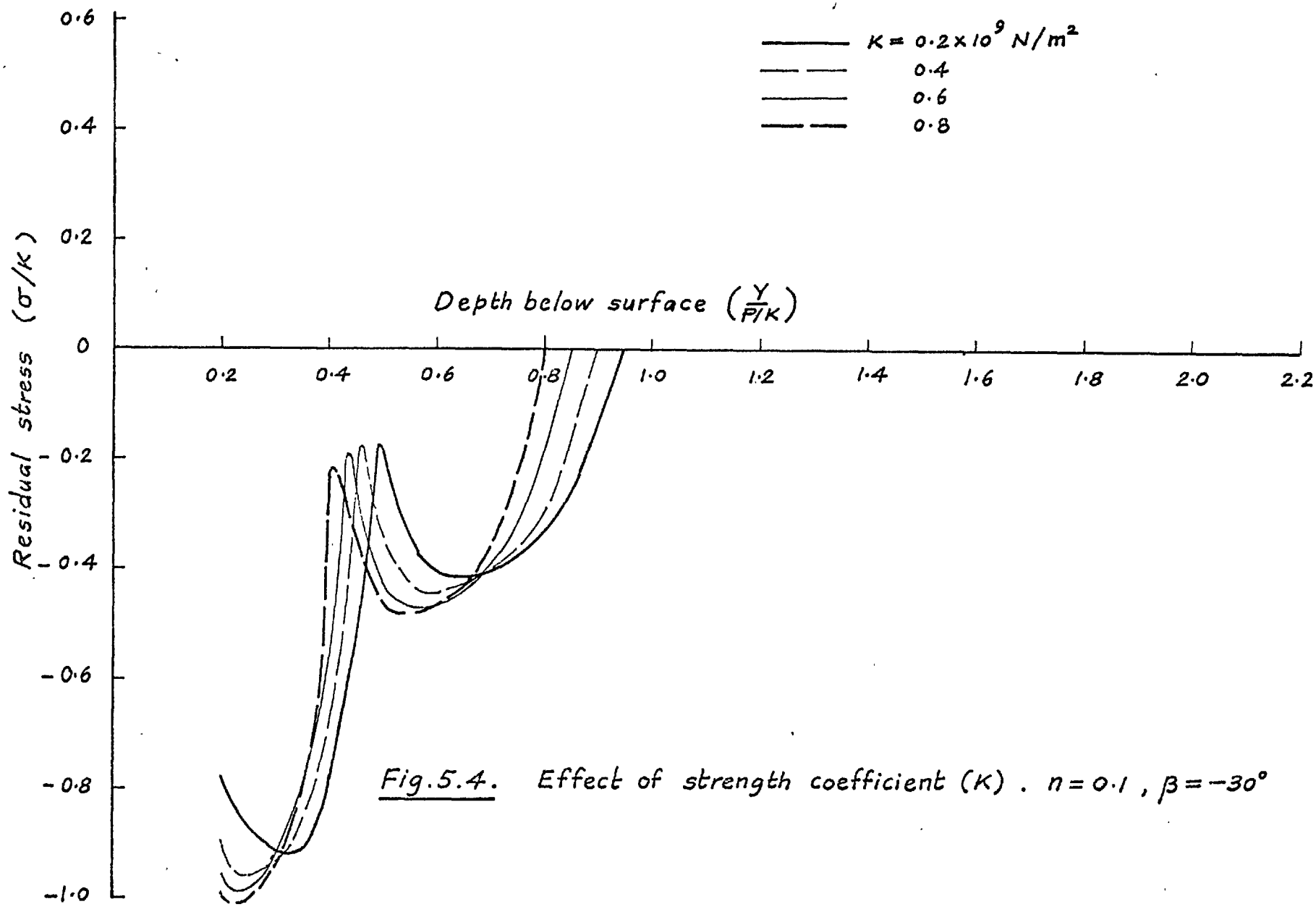

Fig.5.4. Effect of strength coefficient (K) . $n = 0.1$, $\beta = -30°$

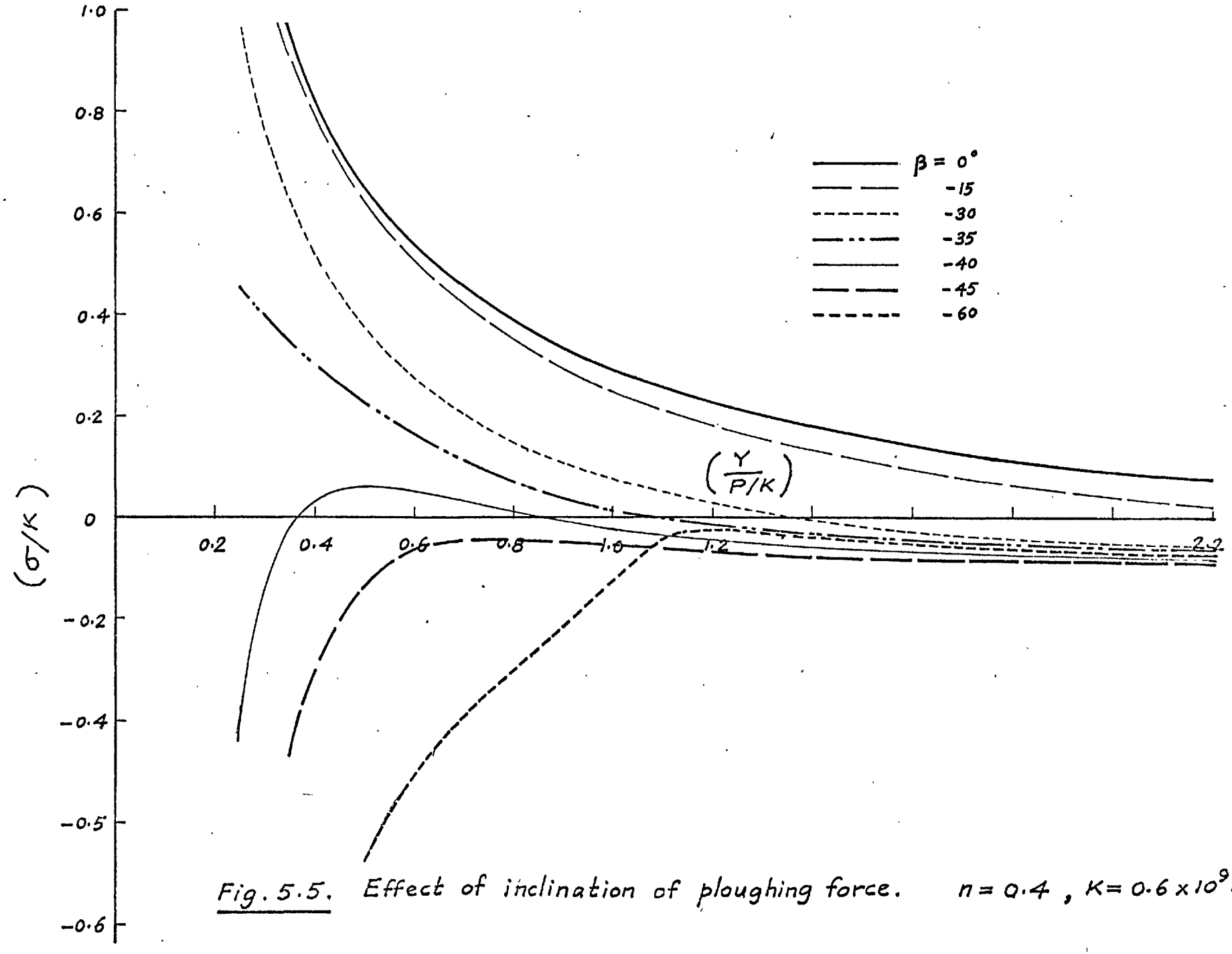

Fig. 5.5. Effect of inclination of ploughing force. $n = 0.4$, $K = 0.6 \times 10^9 N/m^2$

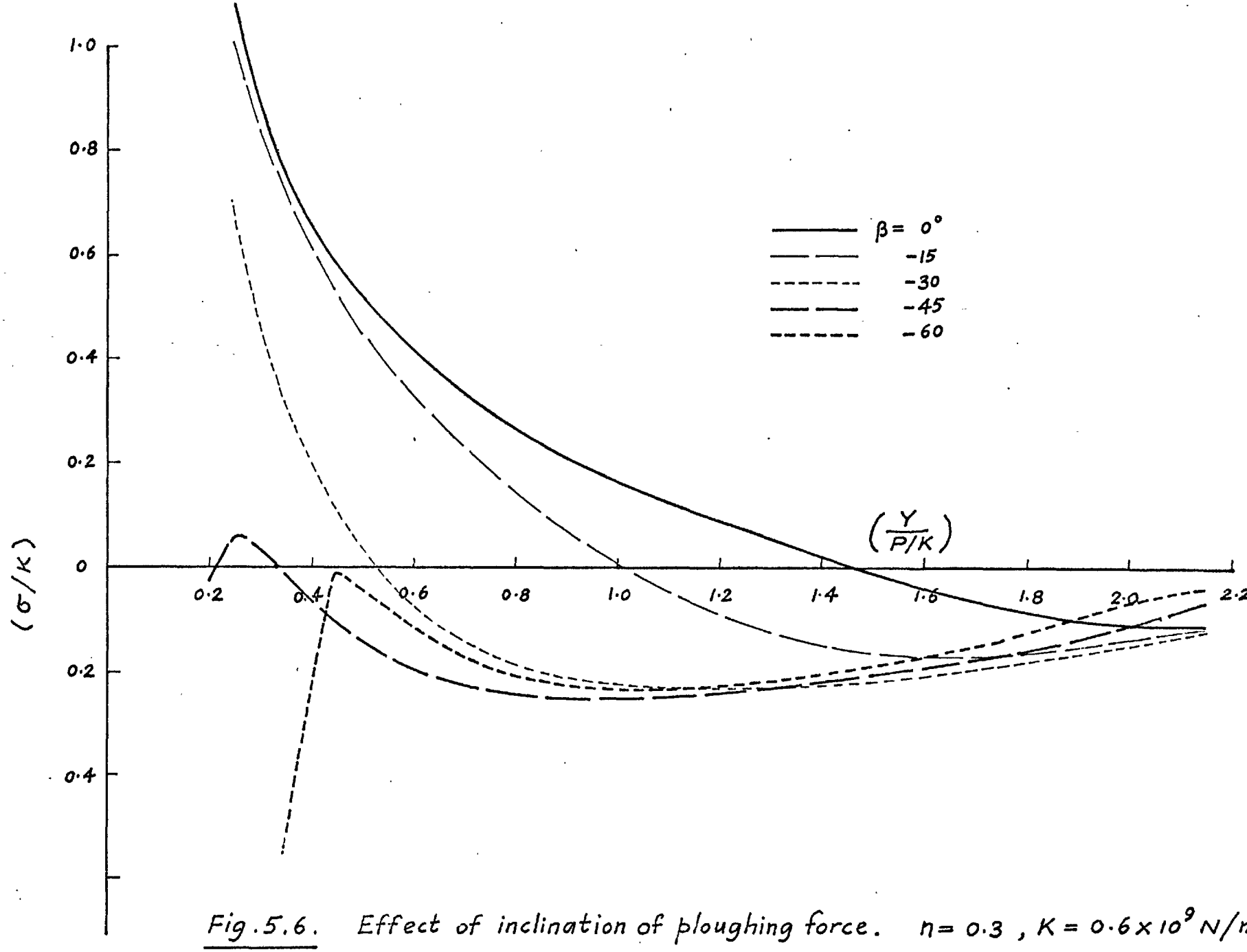

Fig. 5.6. Effect of inclination of ploughing force. $n = 0.3$, $K = 0.6 \times 10^9 N/m^2$

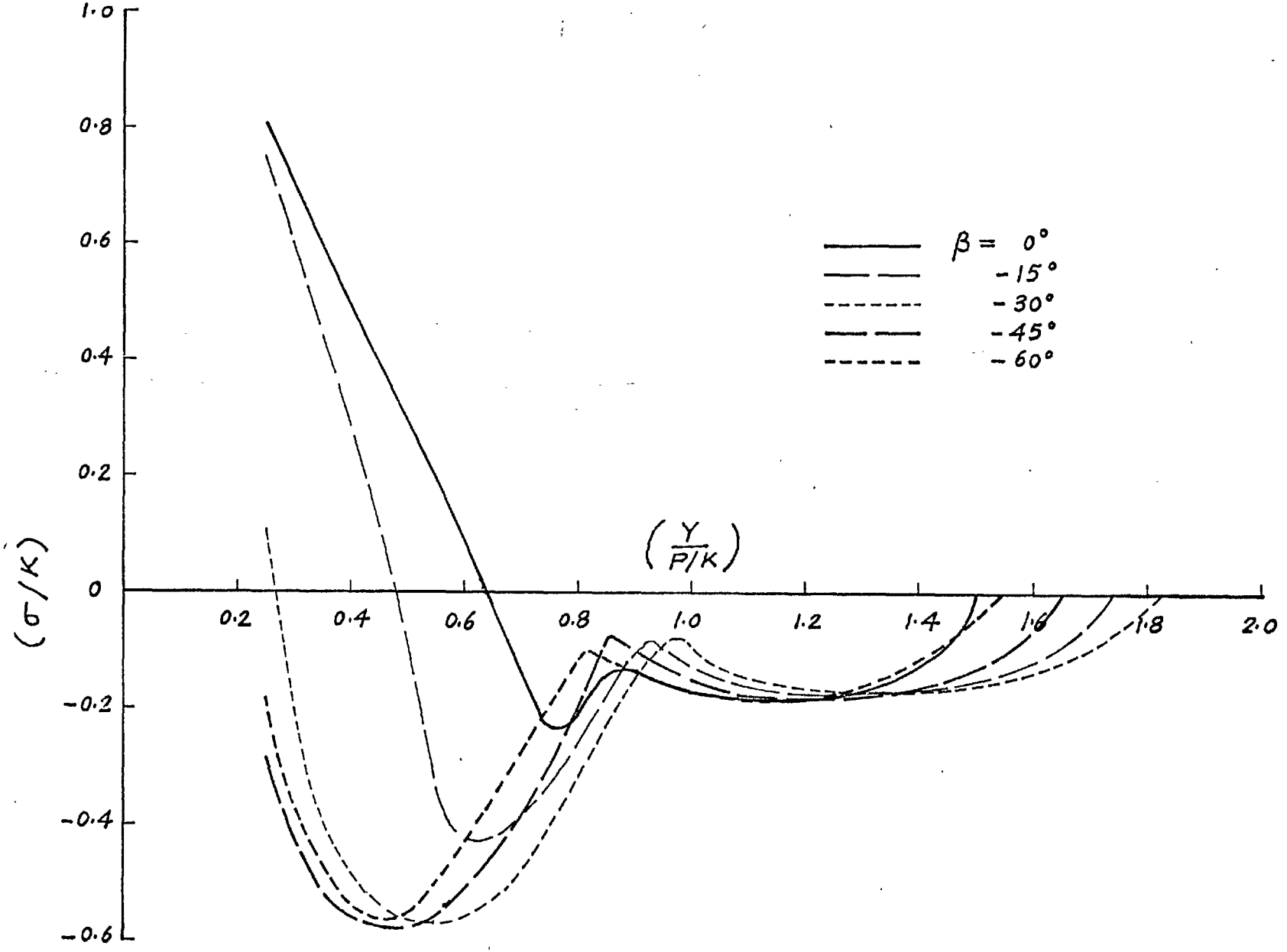

Fig. 5.7 Effect of inclination of ploughing force. $n = 0.2$, $K = 0.6 \times 10^9 N/m^2$

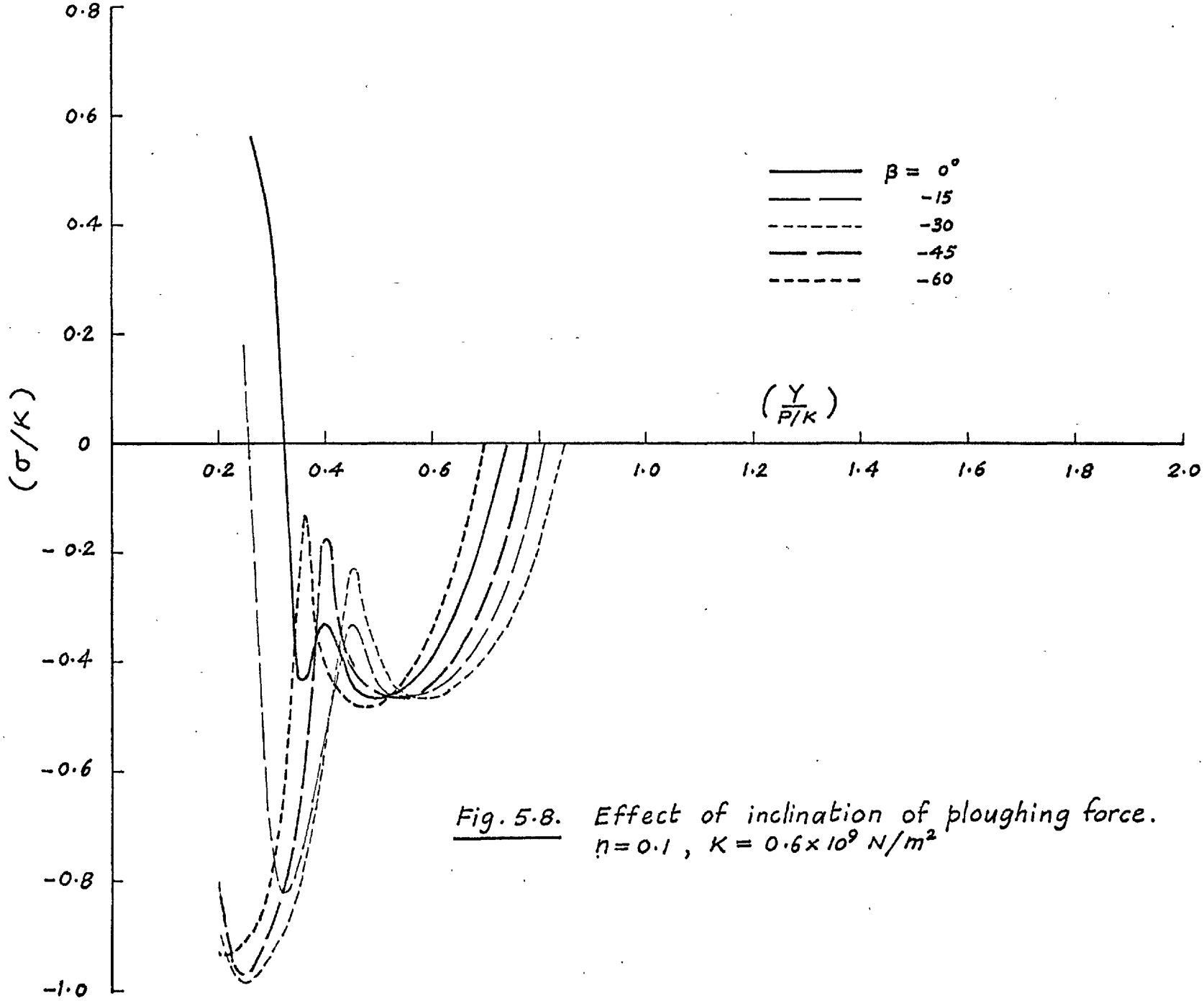

Fig. 5·8. Effect of inclination of ploughing force.
$n = 0.1$, $K = 0.6 \times 10^9\ N/m^2$

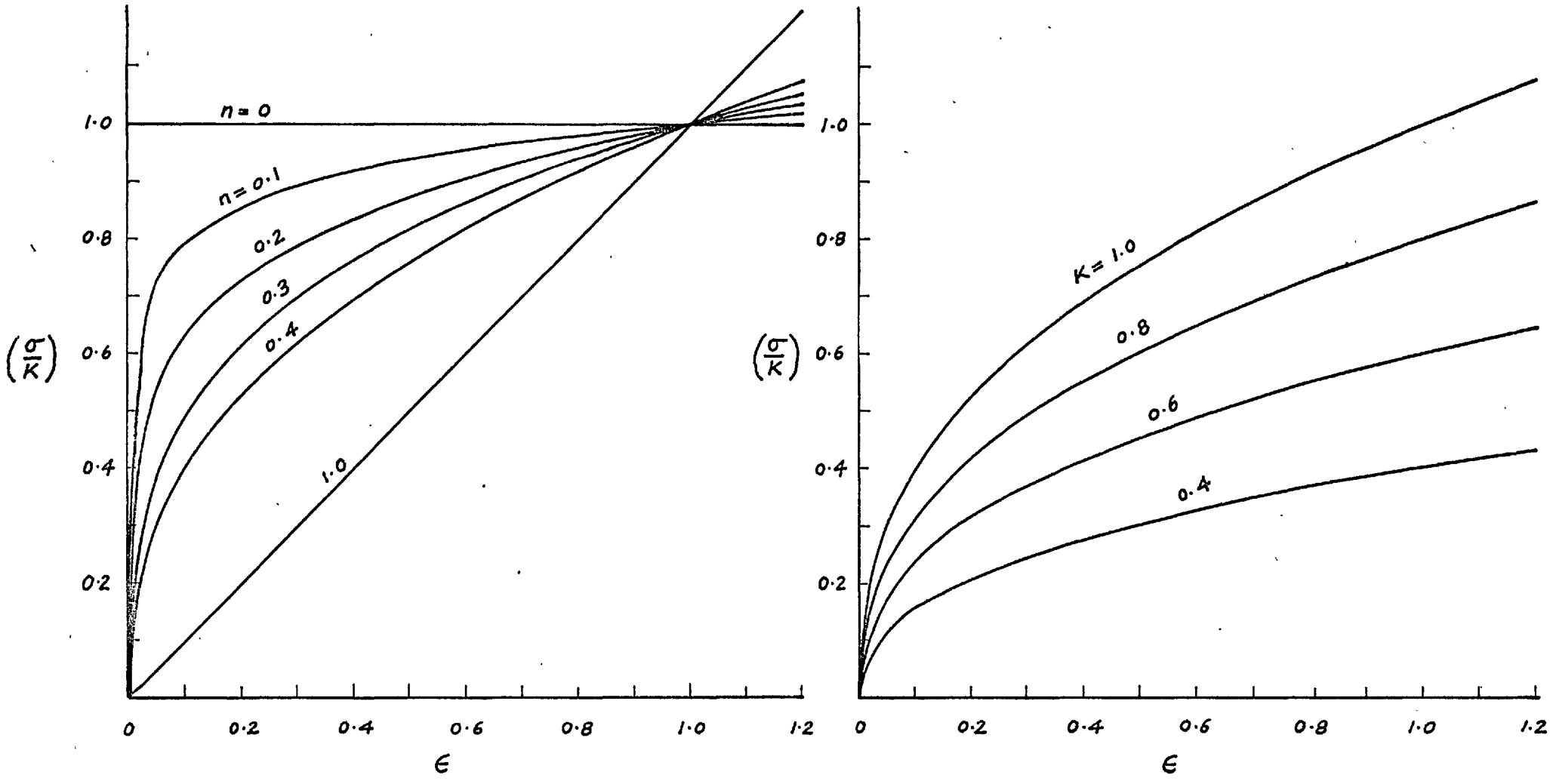

Fig. 5.9. Influence of K and n on the shape of the stress - strain curves of the form $\sigma = K\epsilon^n$.

(a) $K = 1$, $n = 0.1, 0.2, 0.3, 0.4$
(b) $K = 1, 0.8, 0.6, 0.4$, $n = 0.4$

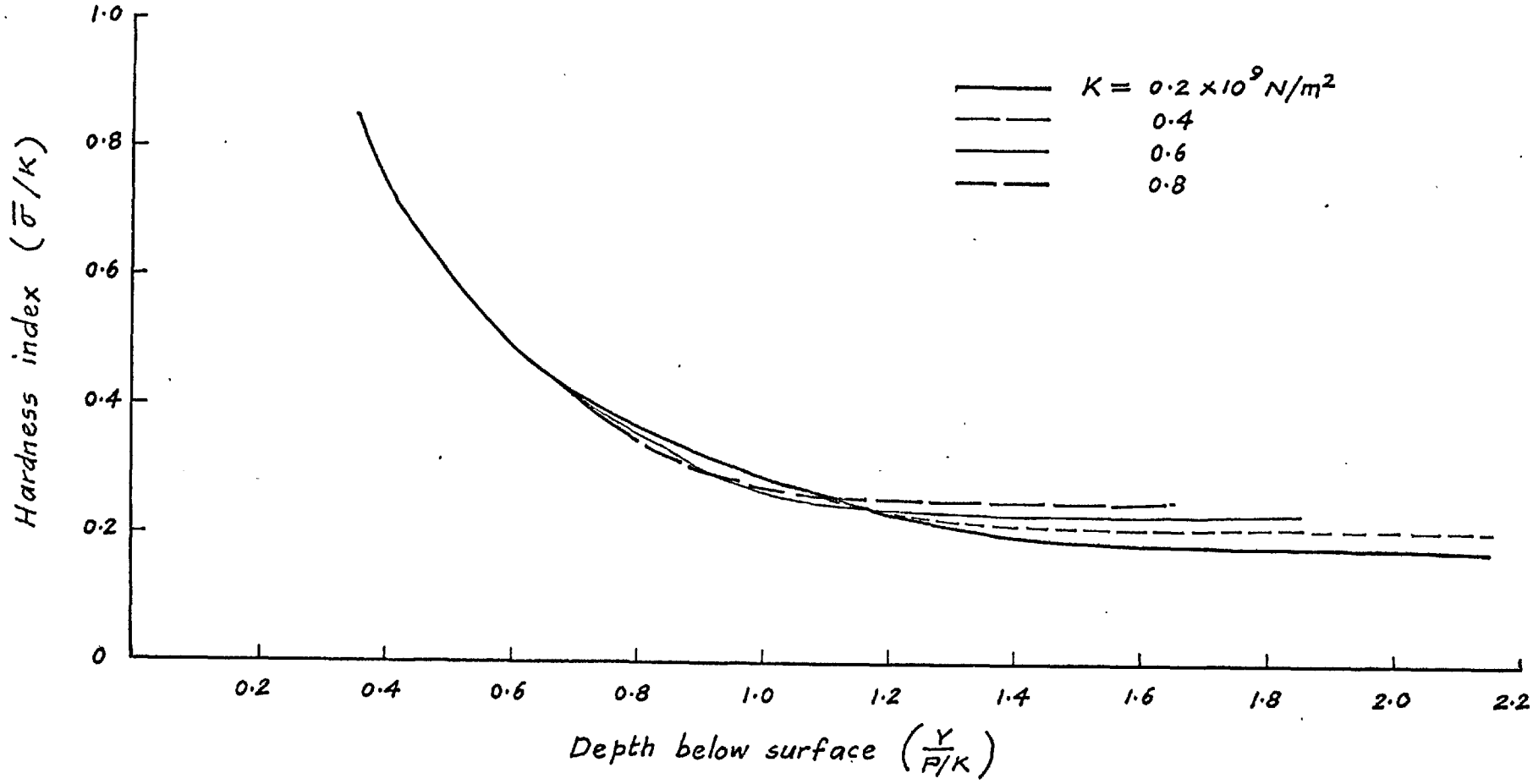

Fig. 5.10. Effect of strength coefficient. $n = 0{\cdot}2$, $\beta = -30°$

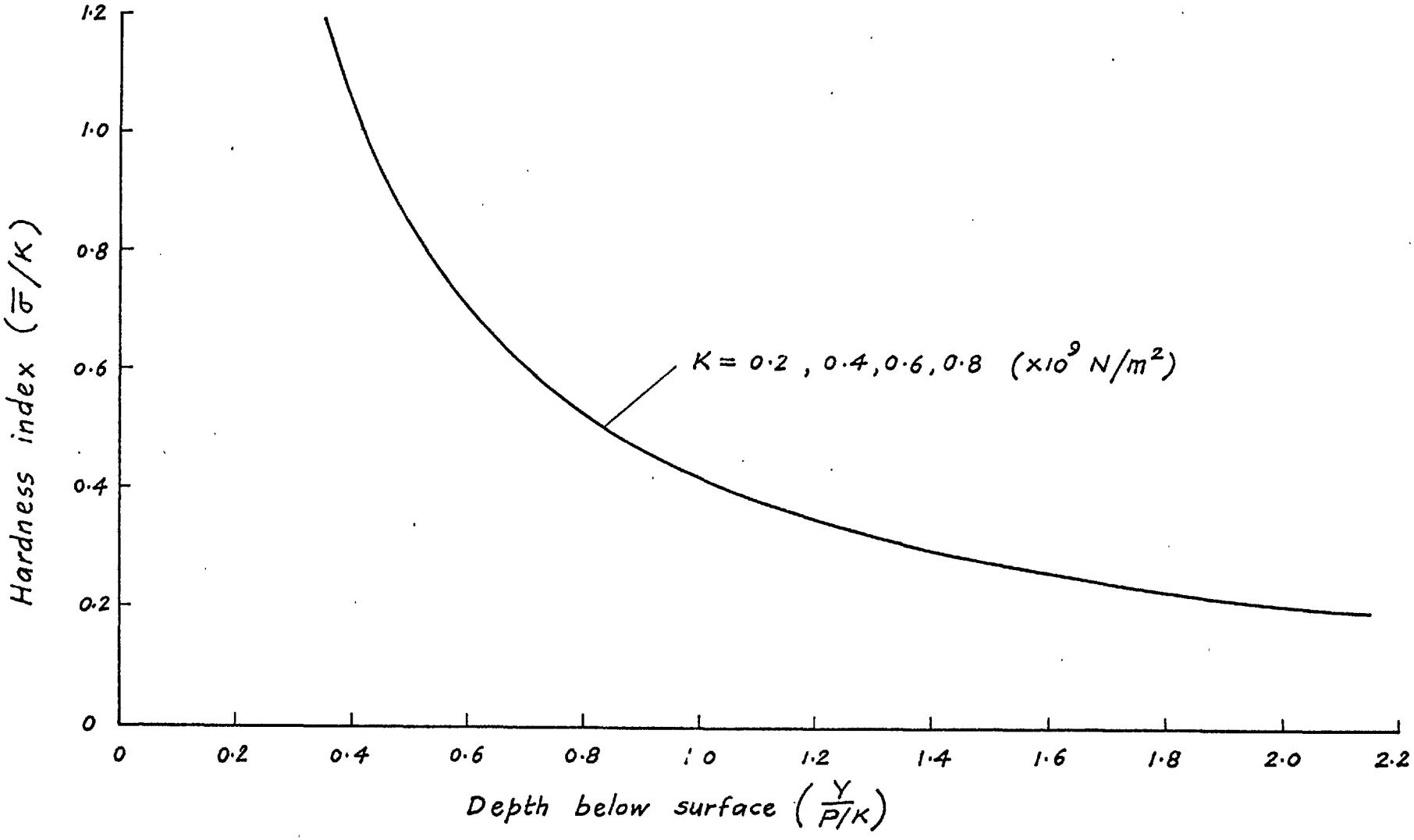

Fig. 5.11. Effect of strength coefficient. $n = 0.4$, $\beta = -30°$

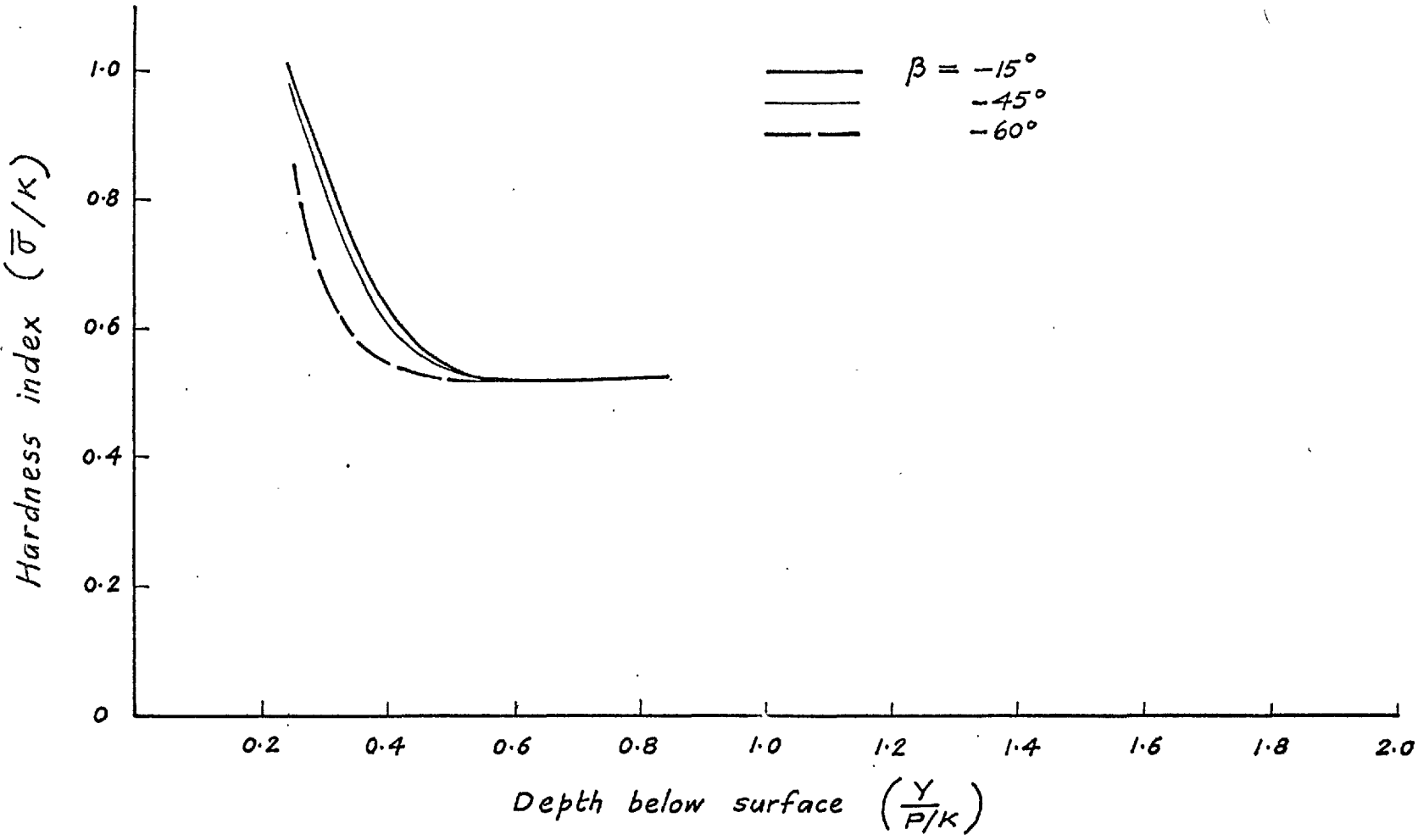

Fig. 5.12. Effect of the inclination of the ploughing force.
$n = 0.1$, $K = 0.6 \times 10^3$ MN/m^2

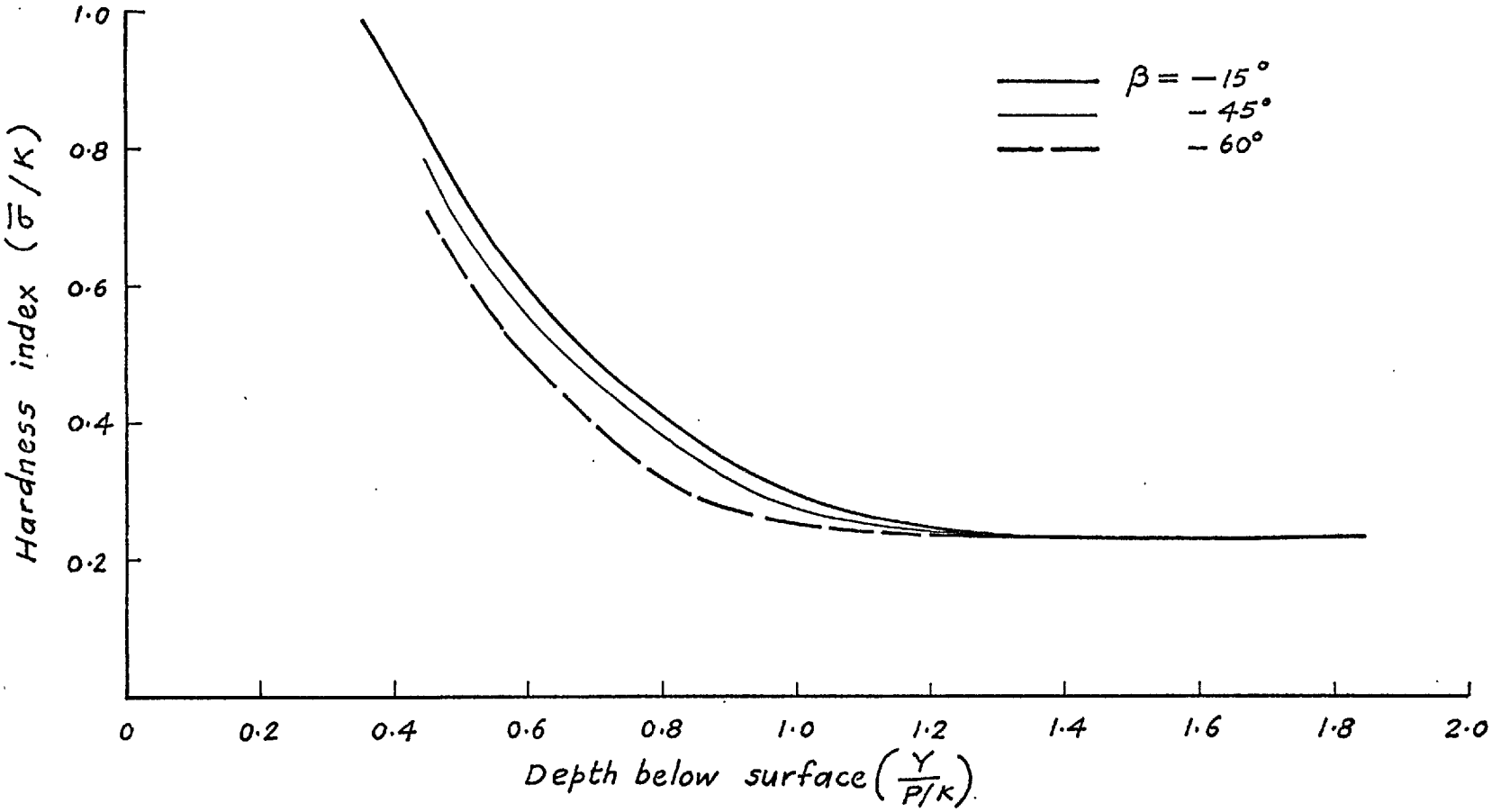

Fig. 5.13. Effect of the inclination of ploughing force.
$n = 0.2$, $K = 0.6 \times 10^9 N/m^2$

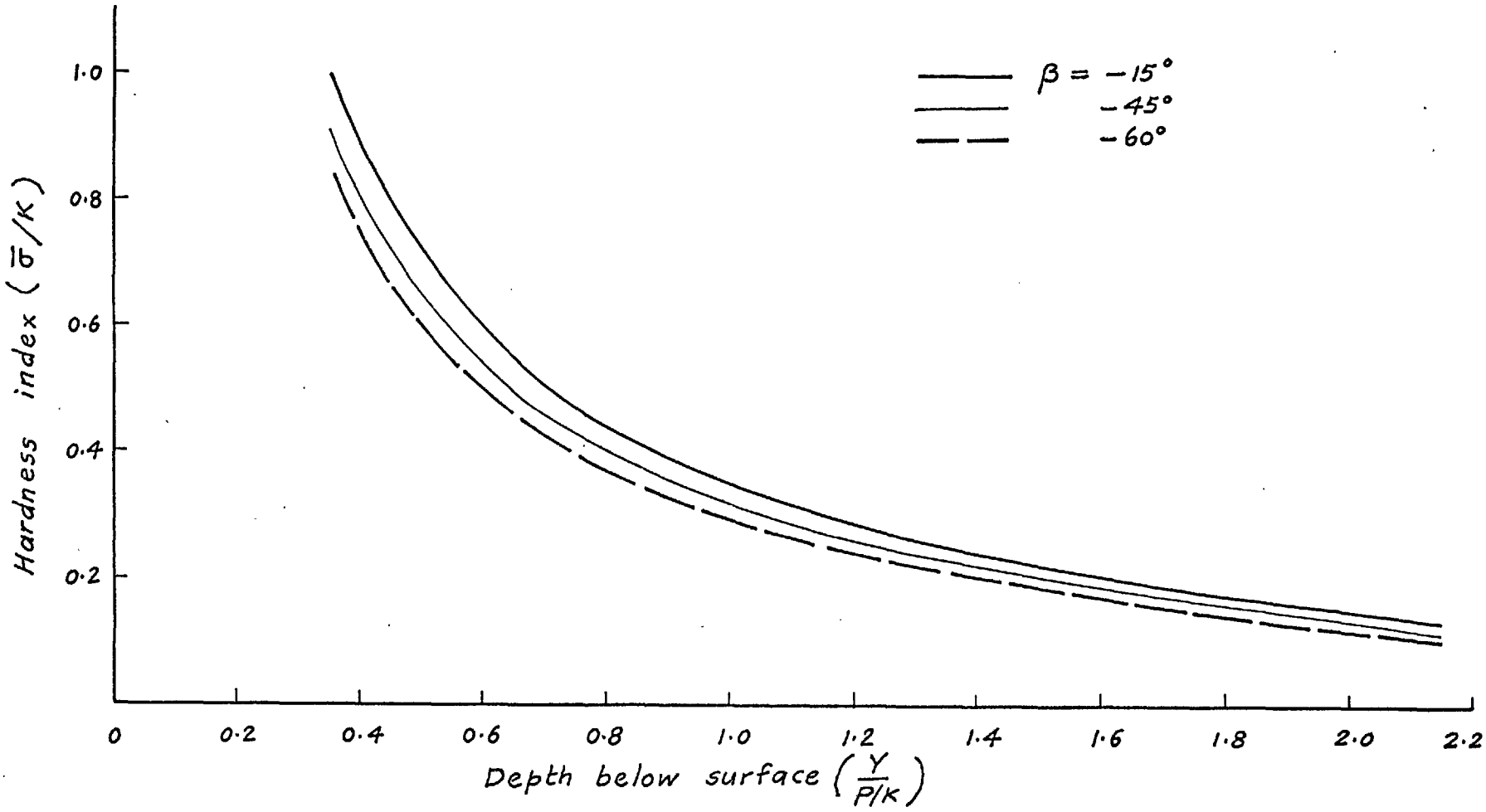

Fig. 5.14. Effect of the inclination of ploughing force.
$\eta = 0.3$, $K = 0.6 \times 10^9\ N/m^2$.

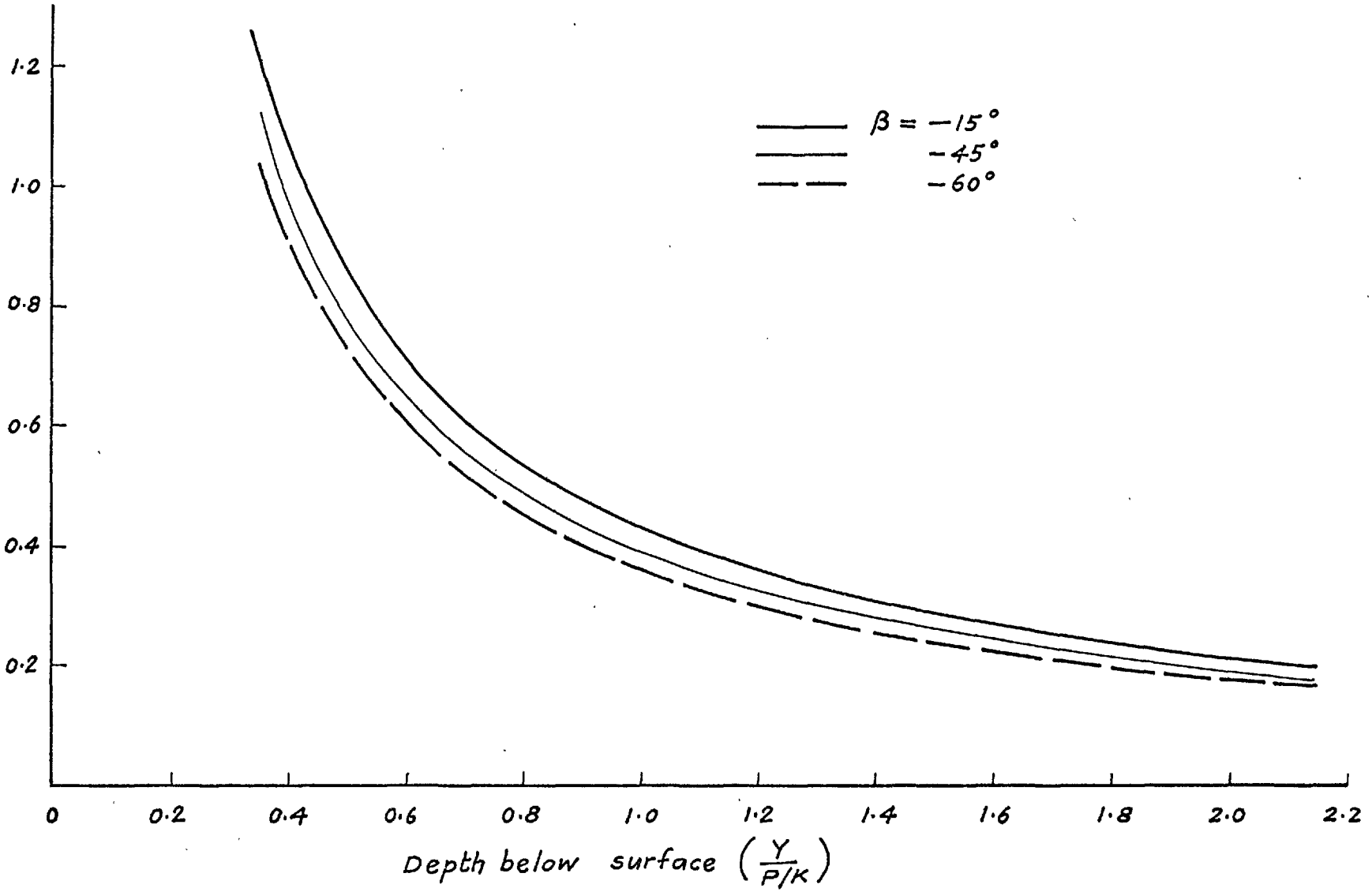

Fig. 5.15. Effect of the inclination of the ploughing force.
$n = 0.4$, $K = 0.6 \times 10^9\ N/m^2$

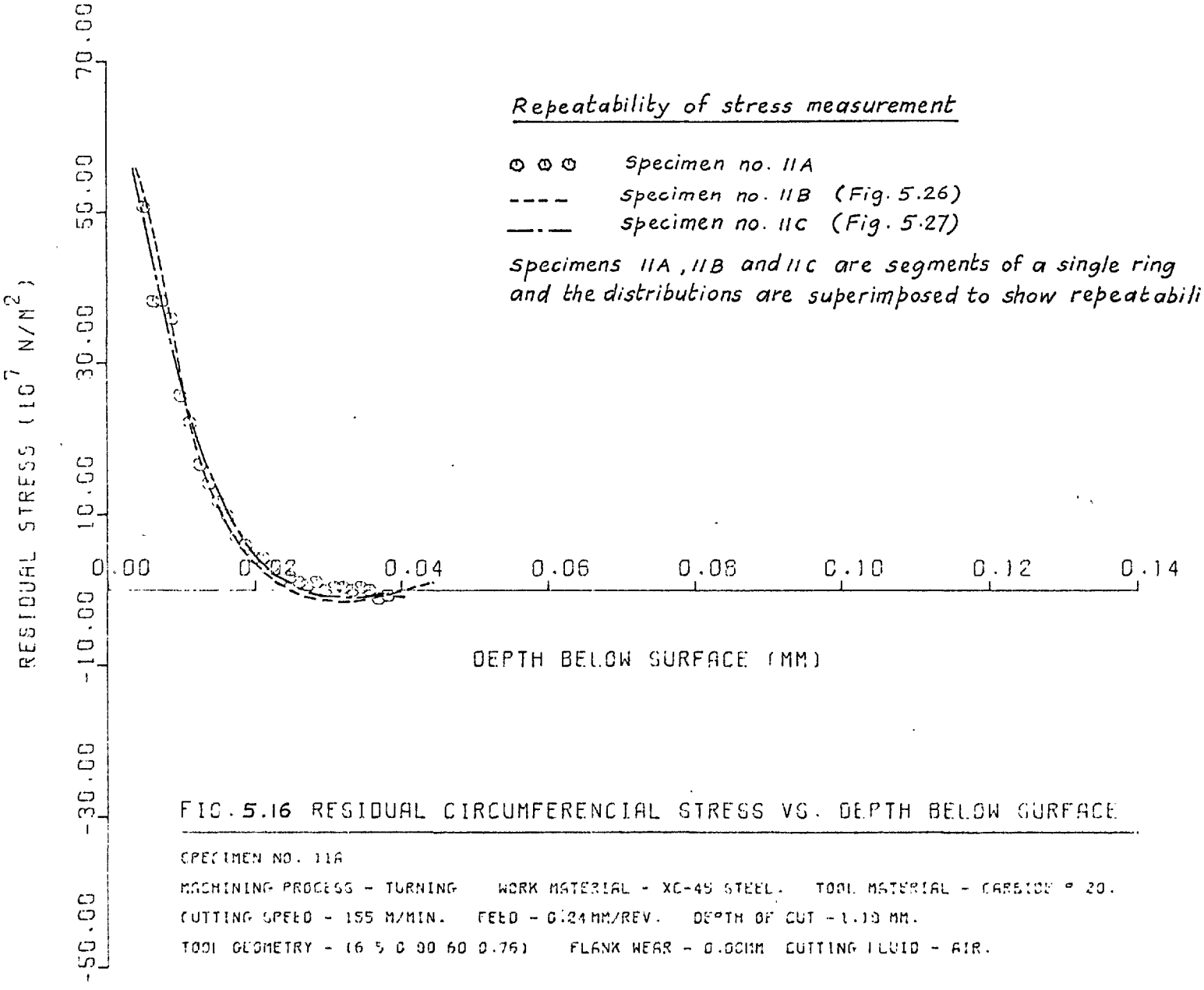

FIG. 5.16 RESIDUAL CIRCUMFERENCIAL STRESS VS. DEPTH BELOW SURFACE

SPECIMEN NO. 11A

MACHINING PROCESS - TURNING WORK MATERIAL - XC-45 STEEL. TOOL MATERIAL - CARBIDE P 20.

CUTTING SPEED - 155 M/MIN. FEED - 0.24 MM/REV. DEPTH OF CUT - 1.19 MM.

TOOL GEOMETRY - (6 5 0 90 60 0.76) FLANK WEAR - 0.00MM CUTTING FLUID - AIR.

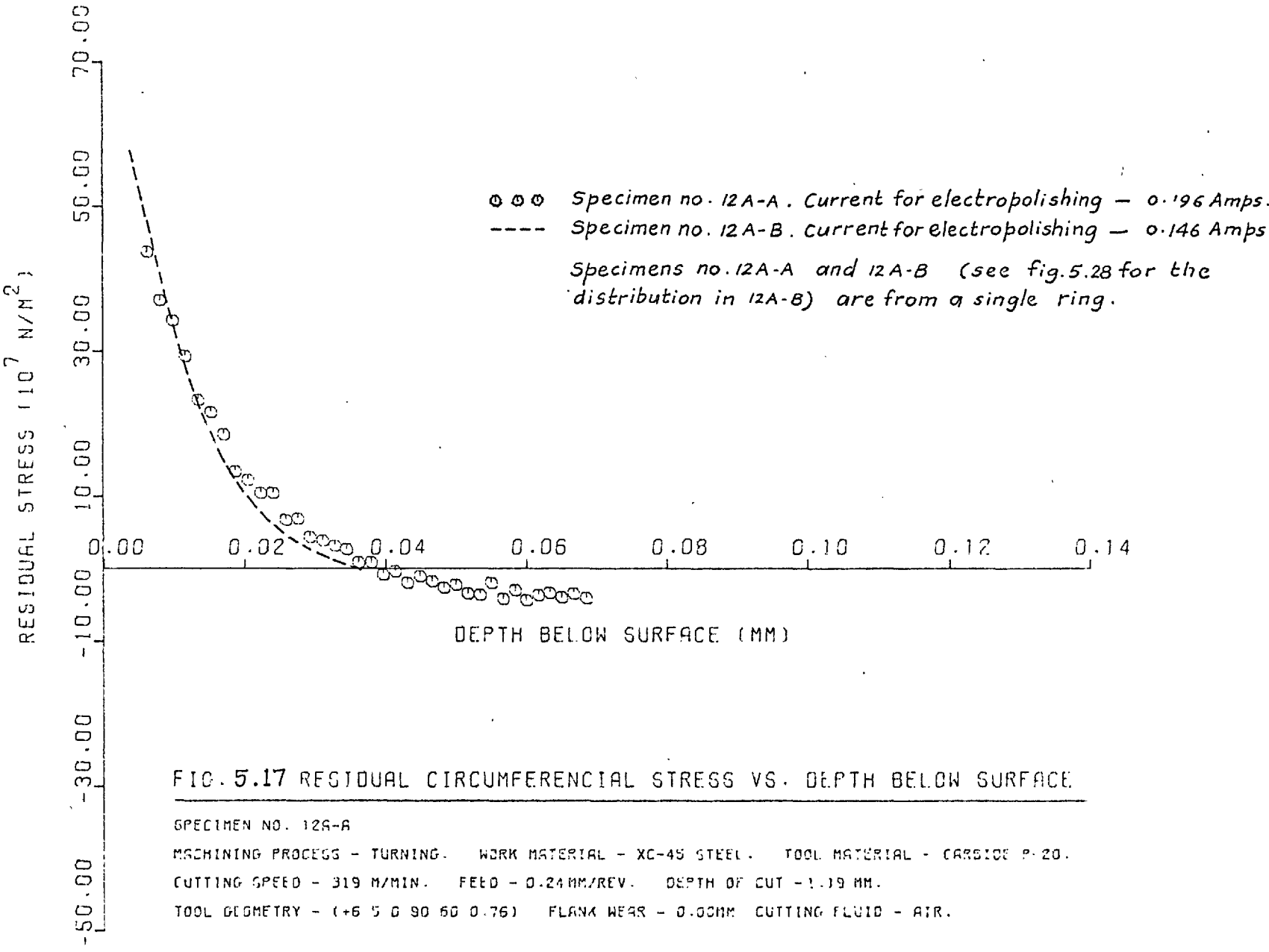

FIG. 5.17 RESIDUAL CIRCUMFERENCIAL STRESS VS. DEPTH BELOW SURFACE

SPECIMEN NO. 12A-A

MACHINING PROCESS - TURNING. WORK MATERIAL - XC-45 STEEL. TOOL MATERIAL - CARBIDE P-20.

CUTTING SPEED - 319 M/MIN. FEED - 0.24 MM/REV. DEPTH OF CUT - 1.19 MM.

TOOL GEOMETRY - (+6 5 6 90 60 0.76) FLANK WEAR - 0.00MM CUTTING FLUID - AIR.

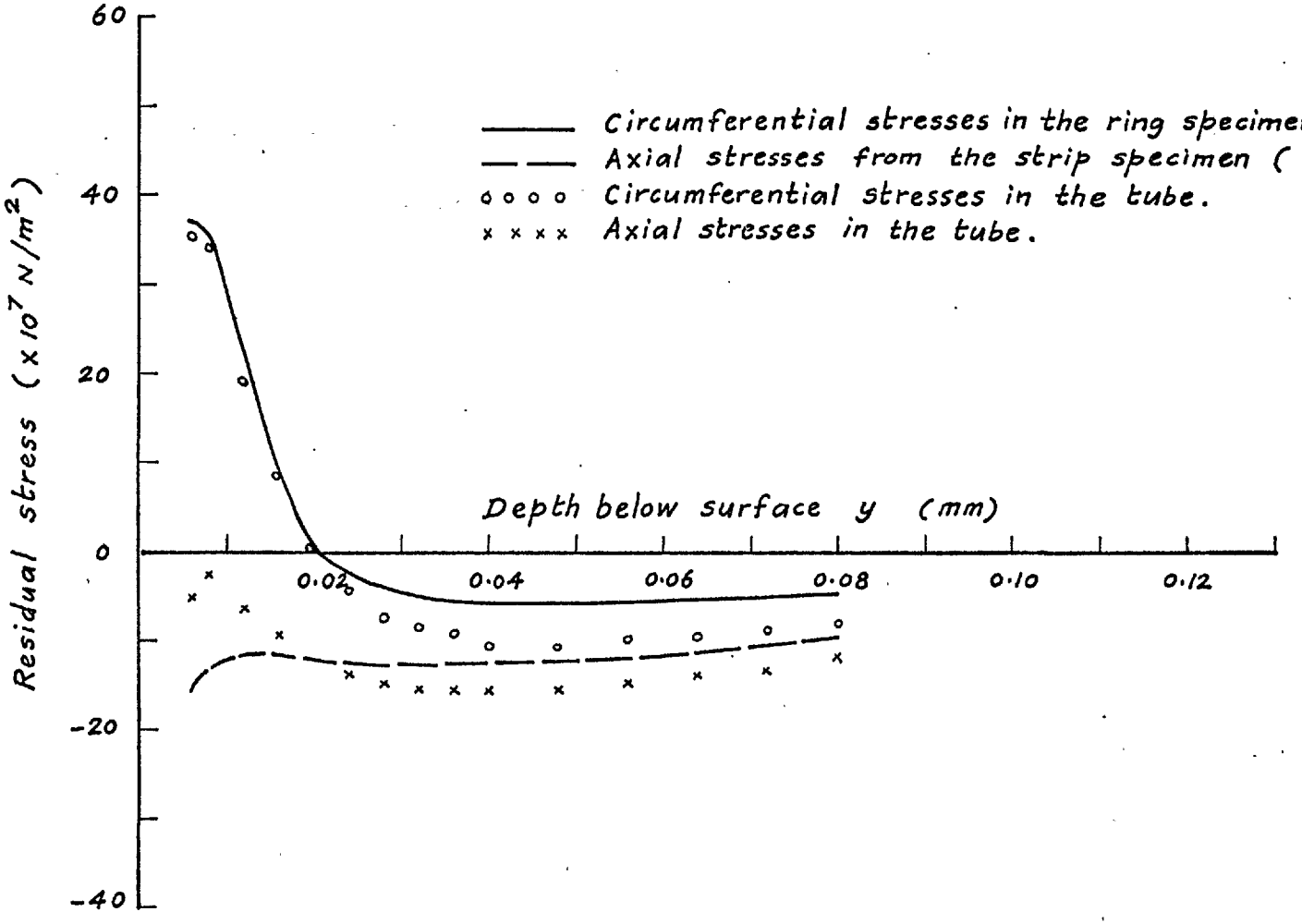

Fig. 5.18. Axial and circumferential stresses in a turned tube.

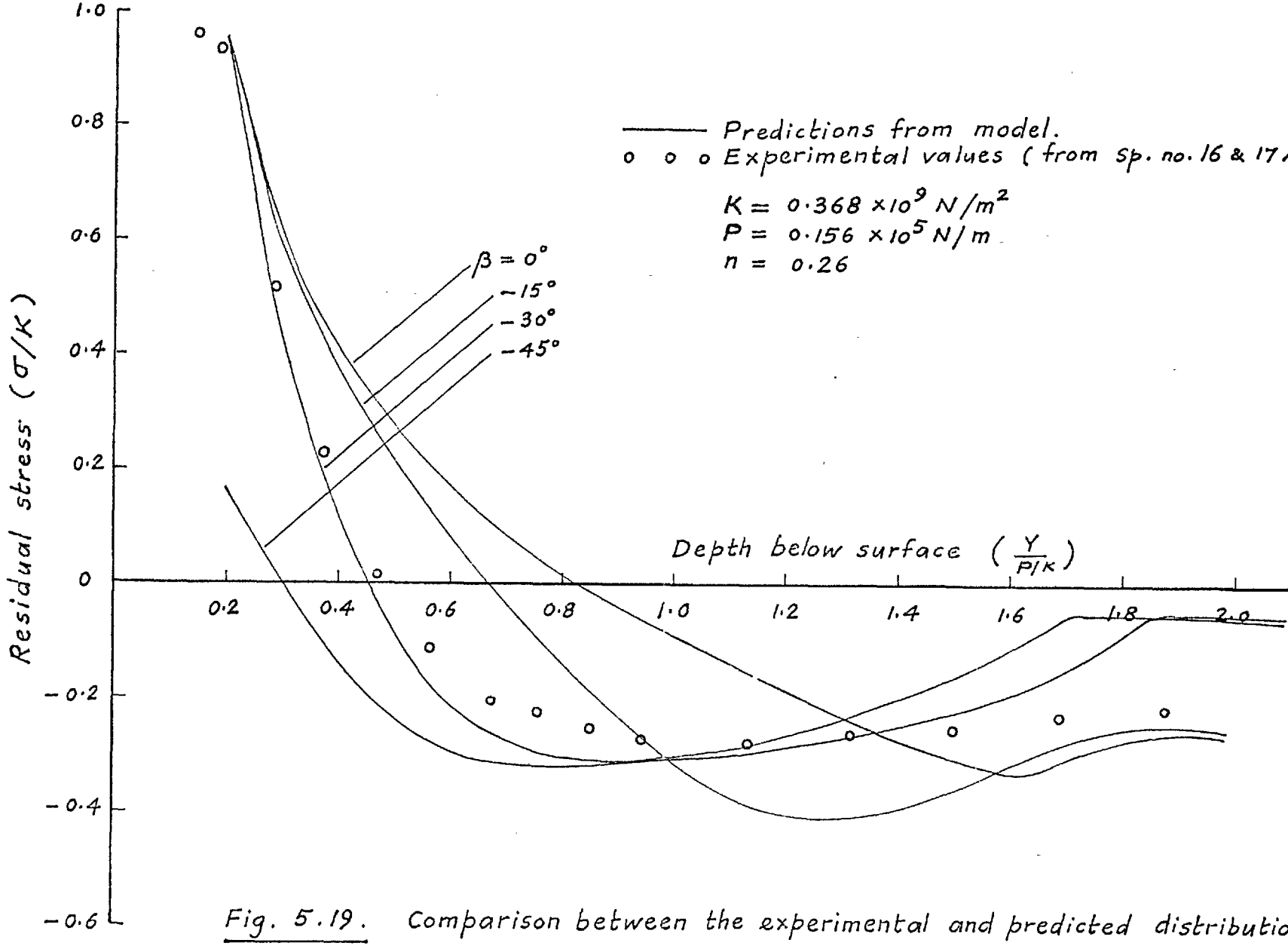

Fig. 5.19. Comparison between the experimental and predicted distributions.

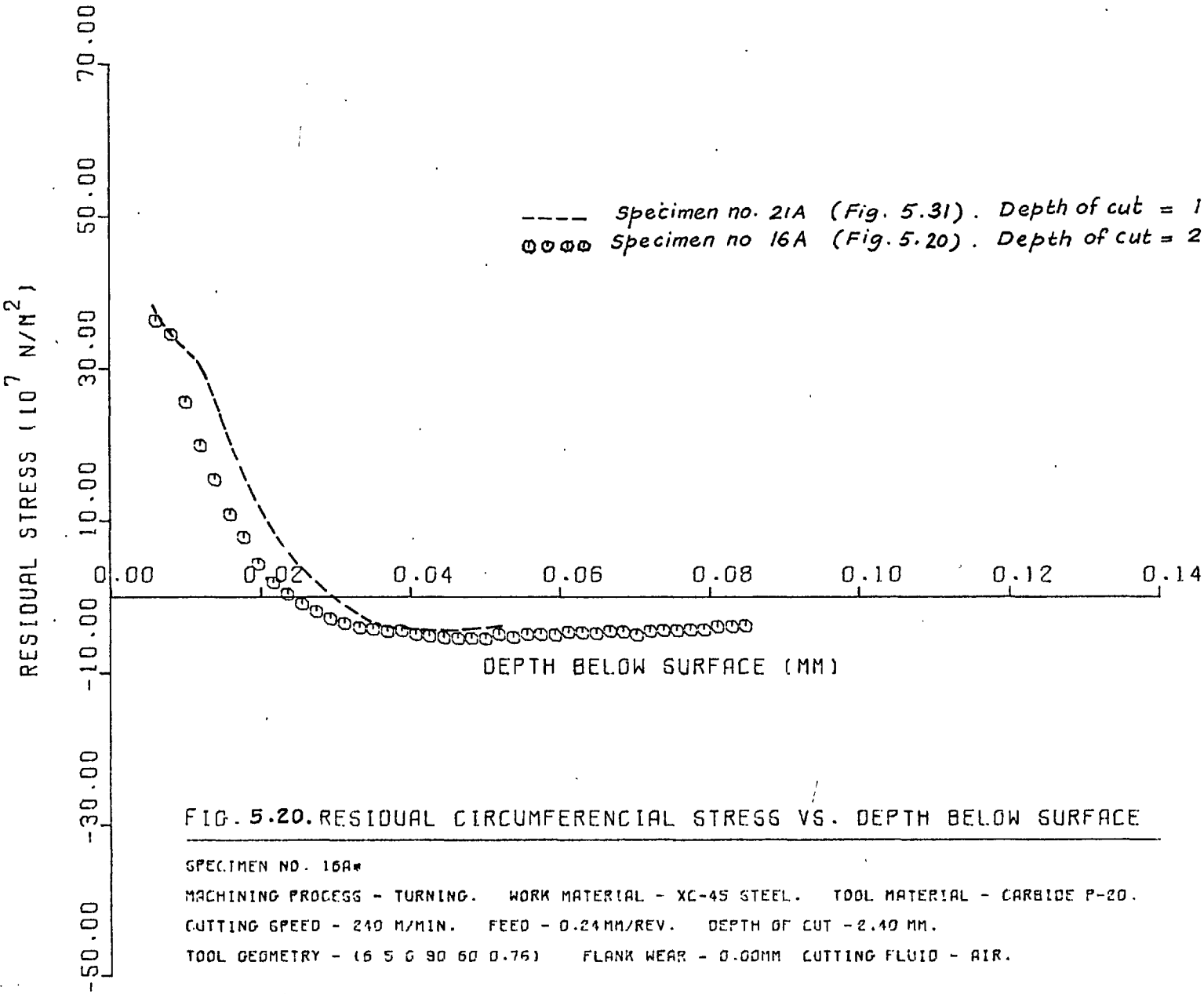

FIG. 5.20. RESIDUAL CIRCUMFERENCIAL STRESS VS. DEPTH BELOW SURFACE

SPECIMEN NO. 16A*

MACHINING PROCESS - TURNING. WORK MATERIAL - XC-45 STEEL. TOOL MATERIAL - CARBIDE P-20.

CUTTING SPEED - 240 M/MIN. FEED - 0.24MM/REV. DEPTH OF CUT - 2.40 MM.

TOOL GEOMETRY - (6 5 6 90 60 0.76) FLANK WEAR - 0.00MM CUTTING FLUID - AIR.

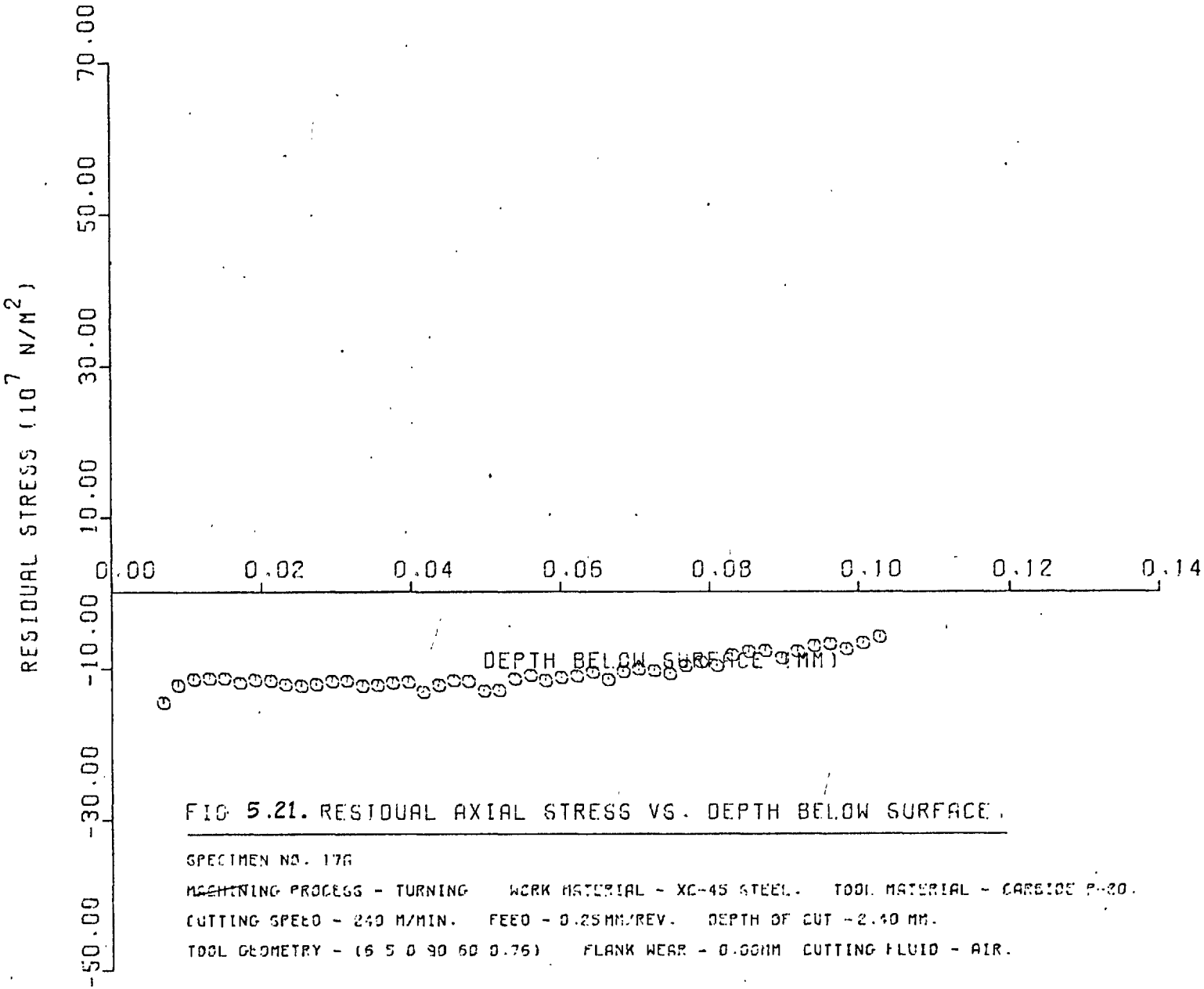

FIG 5.21. RESIDUAL AXIAL STRESS VS. DEPTH BELOW SURFACE.

SPECIMEN NO. 17G

MACHINING PROCESS - TURNING WORK MATERIAL - XC-45 STEEL. TOOL MATERIAL - CARBIDE P-20.

CUTTING SPEED - 240 M/MIN. FEED - 0.25MM/REV. DEPTH OF CUT - 2.40 MM.

TOOL GEOMETRY - (6 5 0 90 60 0.76) FLANK WEAR - 0.00MM CUTTING FLUID - AIR.

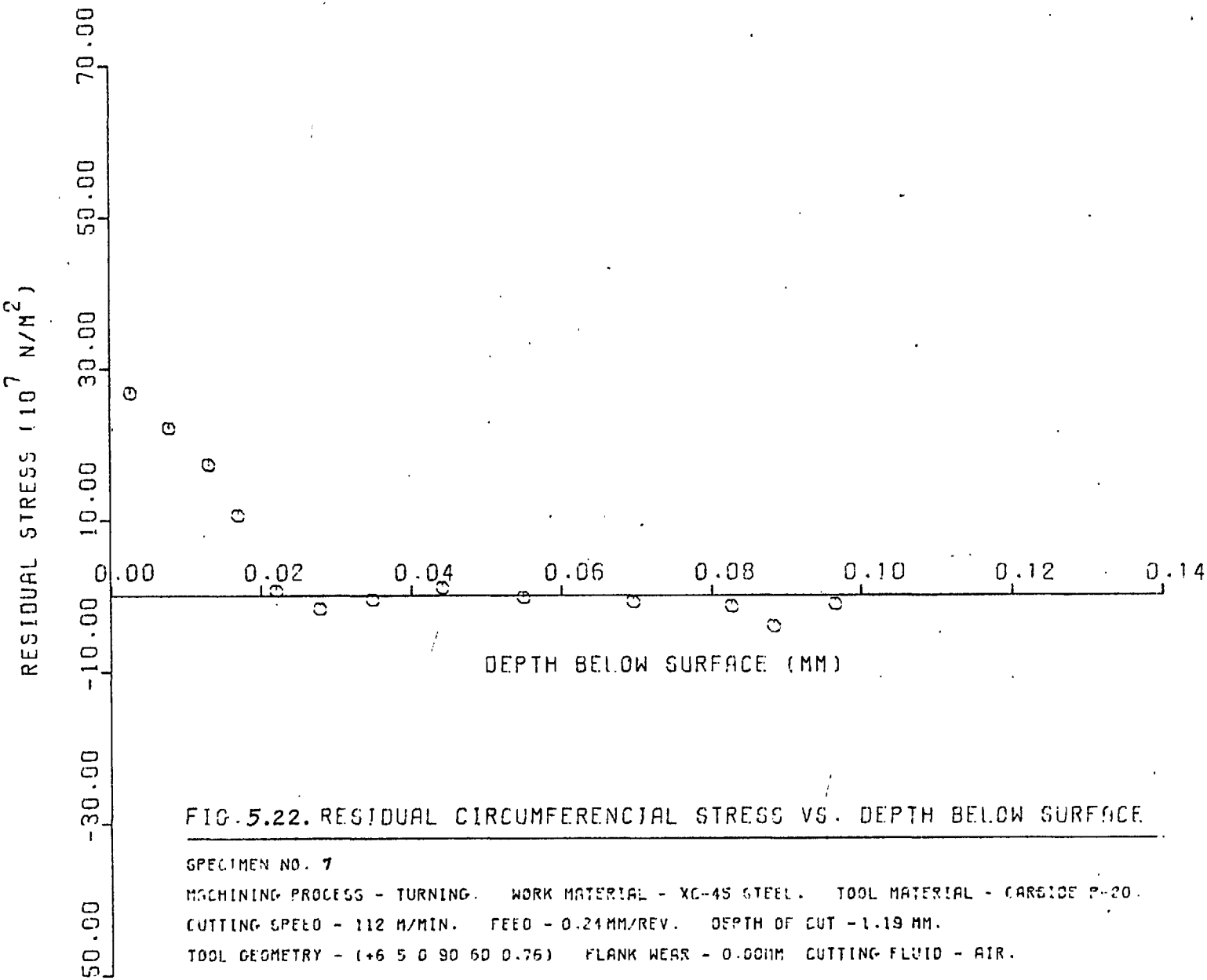

FIG. 5.22. RESIDUAL CIRCUMFERENCIAL STRESS VS. DEPTH BELOW SURFACE

SPECIMEN NO. 7

MACHINING PROCESS - TURNING. WORK MATERIAL - XC-45 STEEL. TOOL MATERIAL - CARBIDE P-20.

CUTTING SPEED - 112 M/MIN. FEED - 0.24 MM/REV. DEPTH OF CUT - 1.19 MM.

TOOL GEOMETRY - (+6 5 0 90 60 0.76) FLANK WEAR - 0.00MM CUTTING FLUID - AIR.

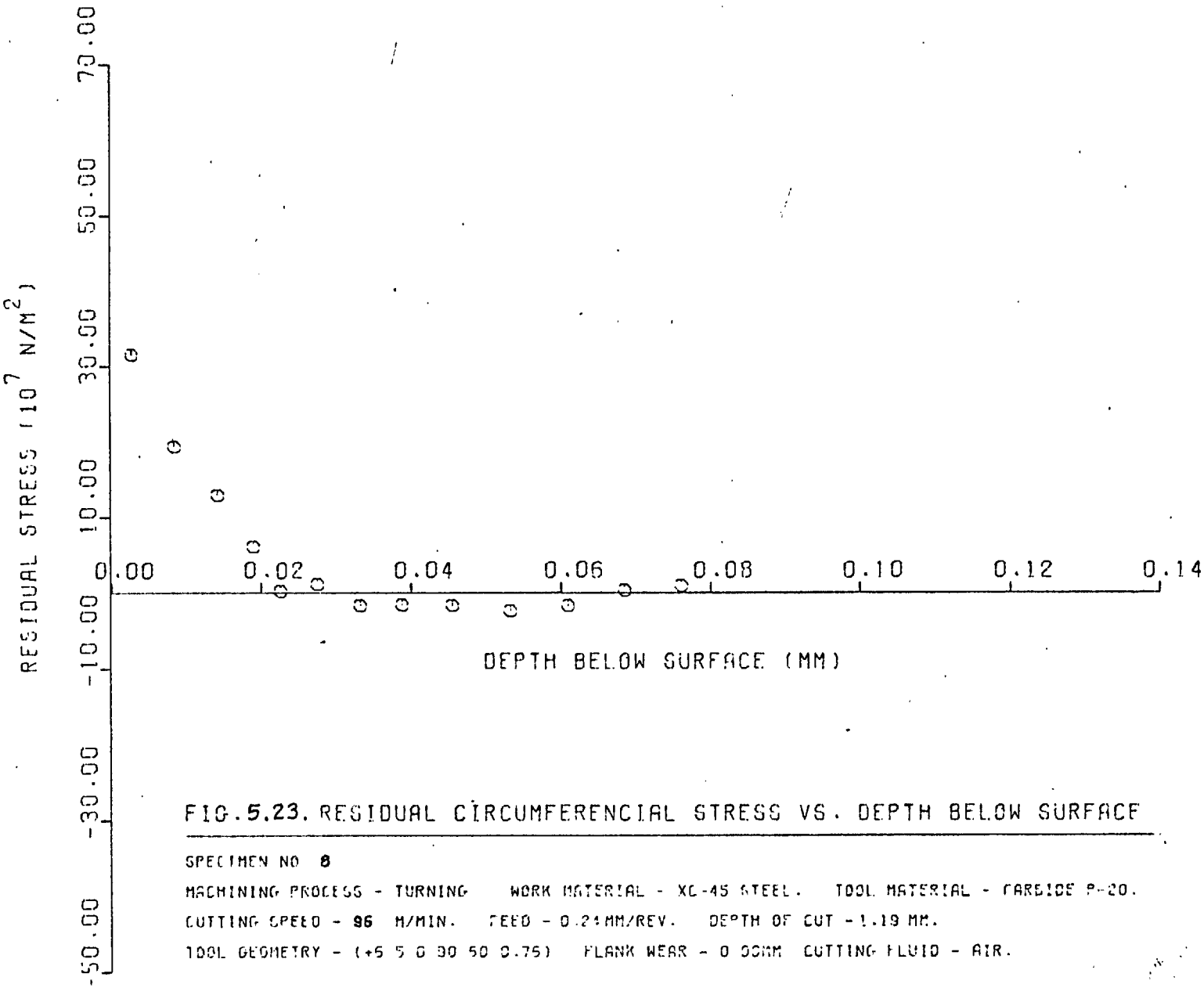

FIG. 5.23. RESIDUAL CIRCUMFERENCIAL STRESS VS. DEPTH BELOW SURFACE

SPECIMEN NO 8

MACHINING PROCESS - TURNING WORK MATERIAL - XC-45 STEEL. TOOL MATERIAL - CARBIDE P-20.

CUTTING SPEED - 96 M/MIN. FEED - 0.24MM/REV. DEPTH OF CUT - 1.19 MM.

TOOL GEOMETRY - (+5 5 0 30 50 0.75) FLANK WEAR - 0.00MM CUTTING FLUID - AIR.

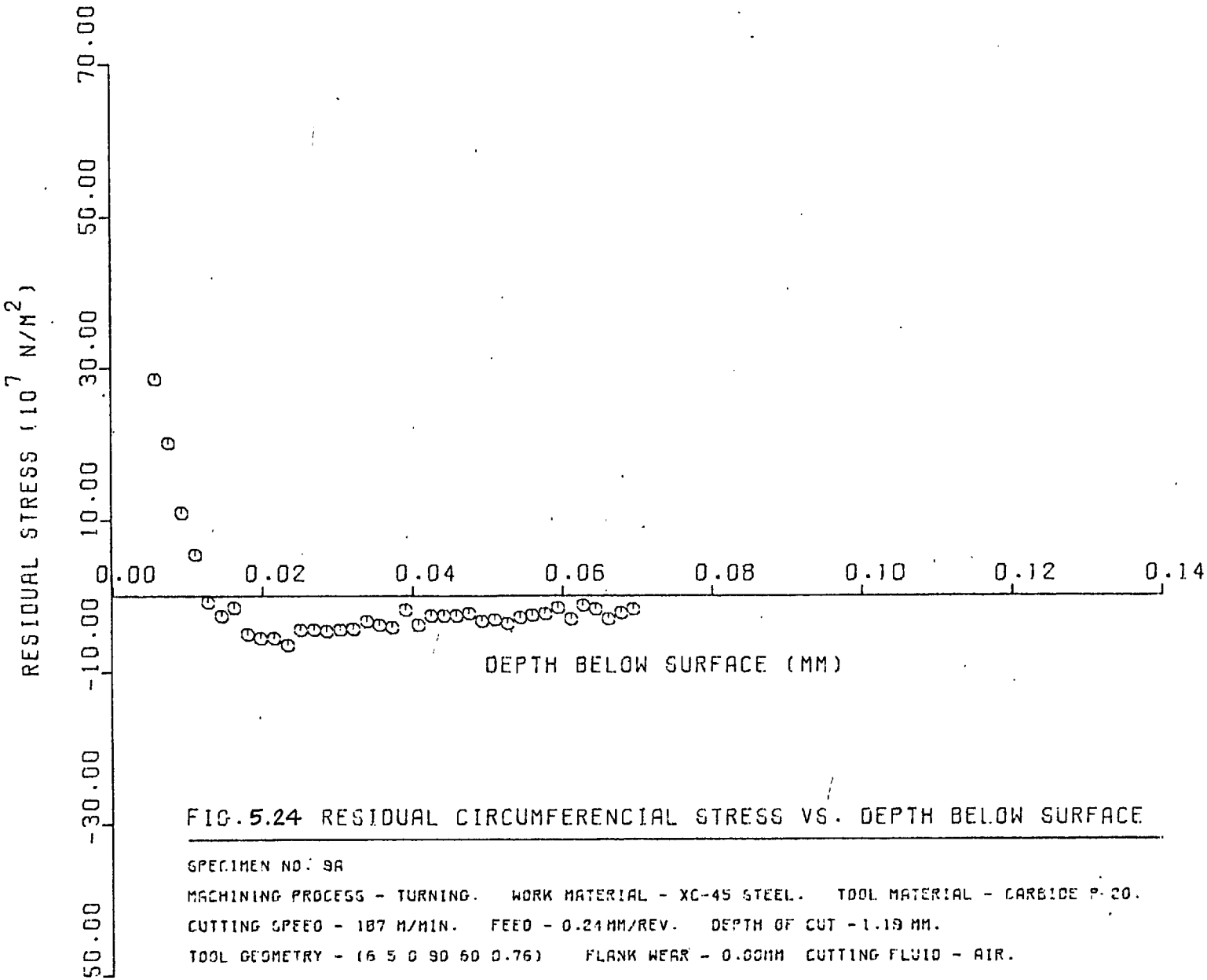

FIG. 5.24 RESIDUAL CIRCUMFERENCIAL STRESS VS. DEPTH BELOW SURFACE

SPECIMEN NO: 9A

MACHINING PROCESS - TURNING. WORK MATERIAL - XC-45 STEEL. TOOL MATERIAL - CARBIDE P-20.

CUTTING SPEED - 187 M/MIN. FEED - 0.24 MM/REV. DEPTH OF CUT - 1.19 MM.

TOOL GEOMETRY - (6 5 0 90 60 0.76) FLANK WEAR - 0.00MM CUTTING FLUID - AIR.

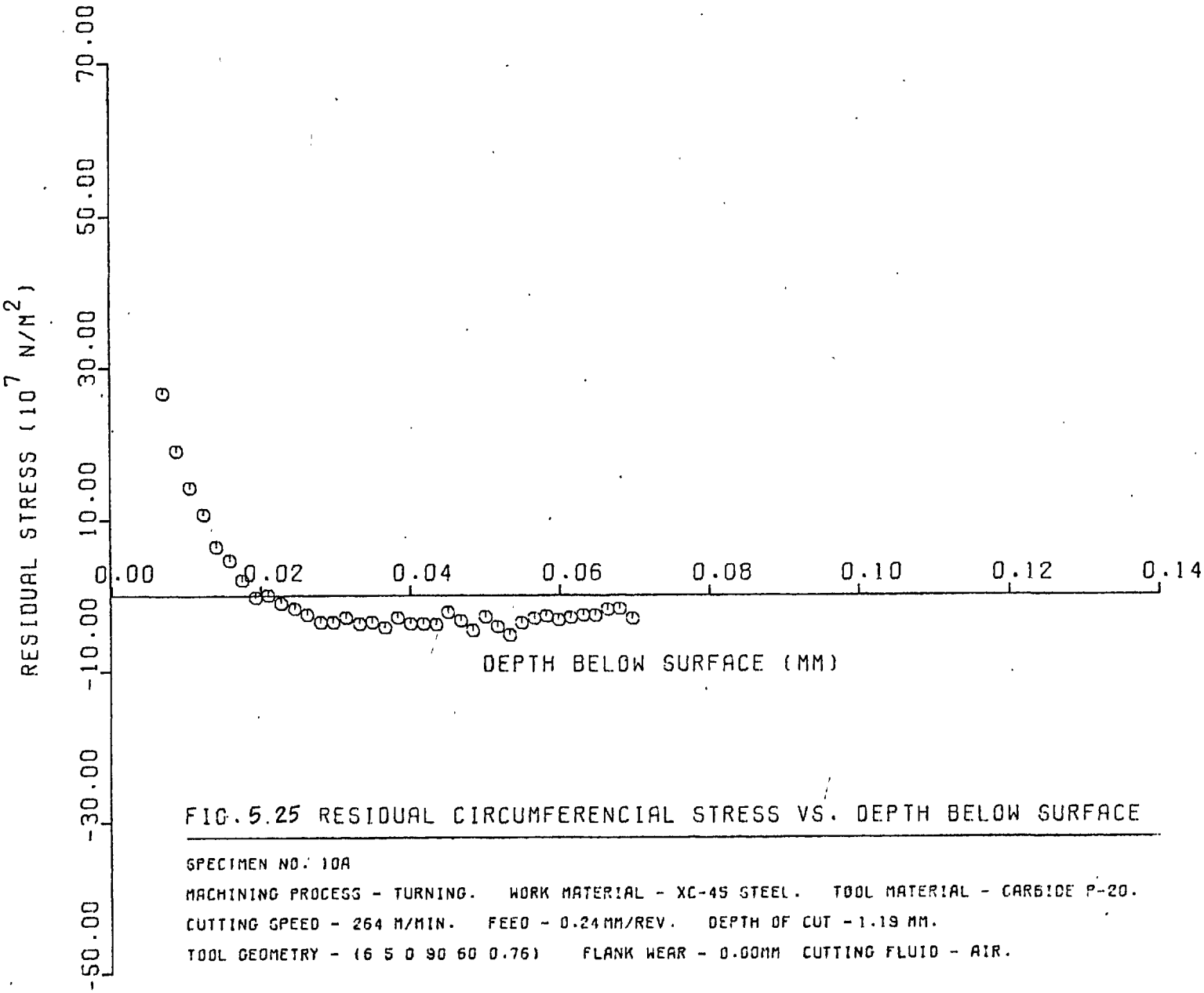

FIG. 5.25 RESIDUAL CIRCUMFERENCIAL STRESS VS. DEPTH BELOW SURFACE

SPECIMEN NO. 10A

MACHINING PROCESS - TURNING. WORK MATERIAL - XC-45 STEEL. TOOL MATERIAL - CARBIDE P-20.

CUTTING SPEED - 264 M/MIN. FEED - 0.24 MM/REV. DEPTH OF CUT - 1.19 MM.

TOOL GEOMETRY - (6 5 0 90 60 0.76) FLANK WEAR - 0.00MM CUTTING FLUID - AIR.

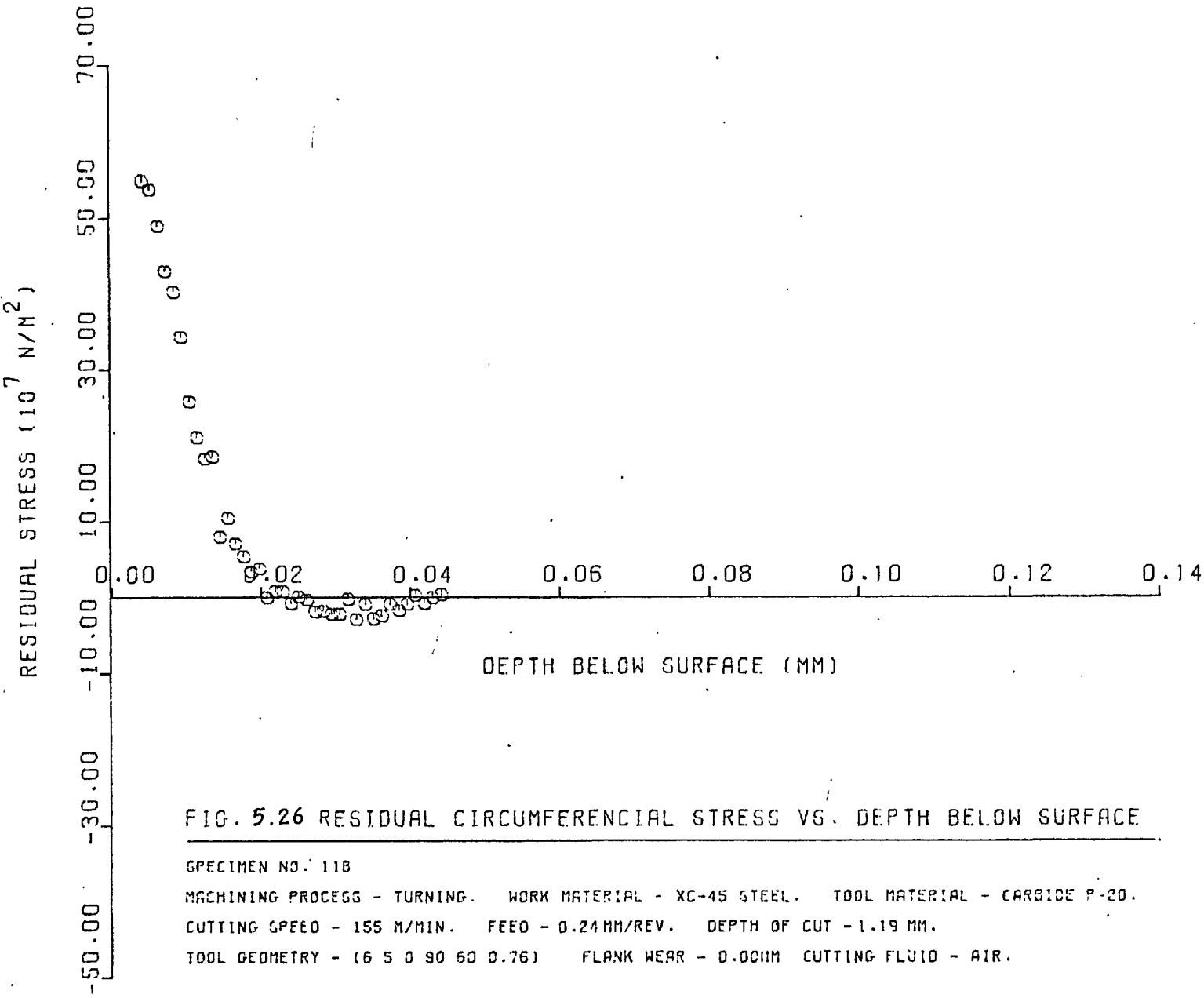

FIG. 5.26 RESIDUAL CIRCUMFERENCIAL STRESS VS. DEPTH BELOW SURFACE

SPECIMEN NO. 11B

MACHINING PROCESS - TURNING. WORK MATERIAL - XC-45 STEEL. TOOL MATERIAL - CARBIDE P-20.

CUTTING SPEED - 155 M/MIN. FEED - 0.24 MM/REV. DEPTH OF CUT - 1.19 MM.

TOOL GEOMETRY - (6 5 0 90 60 0.76) FLANK WEAR - 0.00MM CUTTING FLUID - AIR.

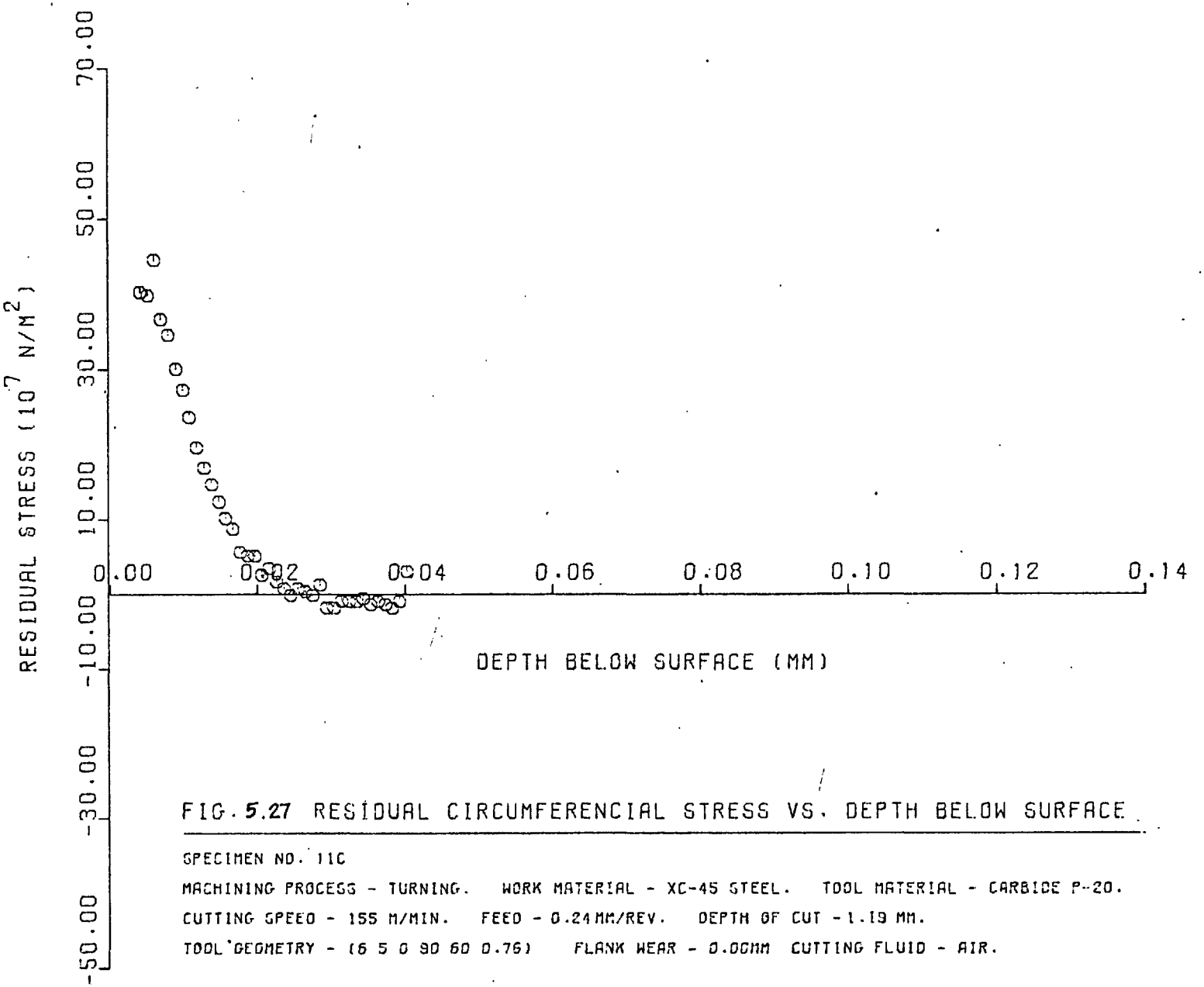

FIG. 5.27 RESIDUAL CIRCUMFERENCIAL STRESS VS. DEPTH BELOW SURFACE

SPECIMEN NO. 11C

MACHINING PROCESS - TURNING. WORK MATERIAL - XC-45 STEEL. TOOL MATERIAL - CARBIDE P-20.

CUTTING SPEED - 155 M/MIN. FEED - 0.24 MM/REV. DEPTH OF CUT - 1.19 MM.

TOOL GEOMETRY - (6 5 0 90 60 0.76) FLANK WEAR - 0.00MM CUTTING FLUID - AIR.

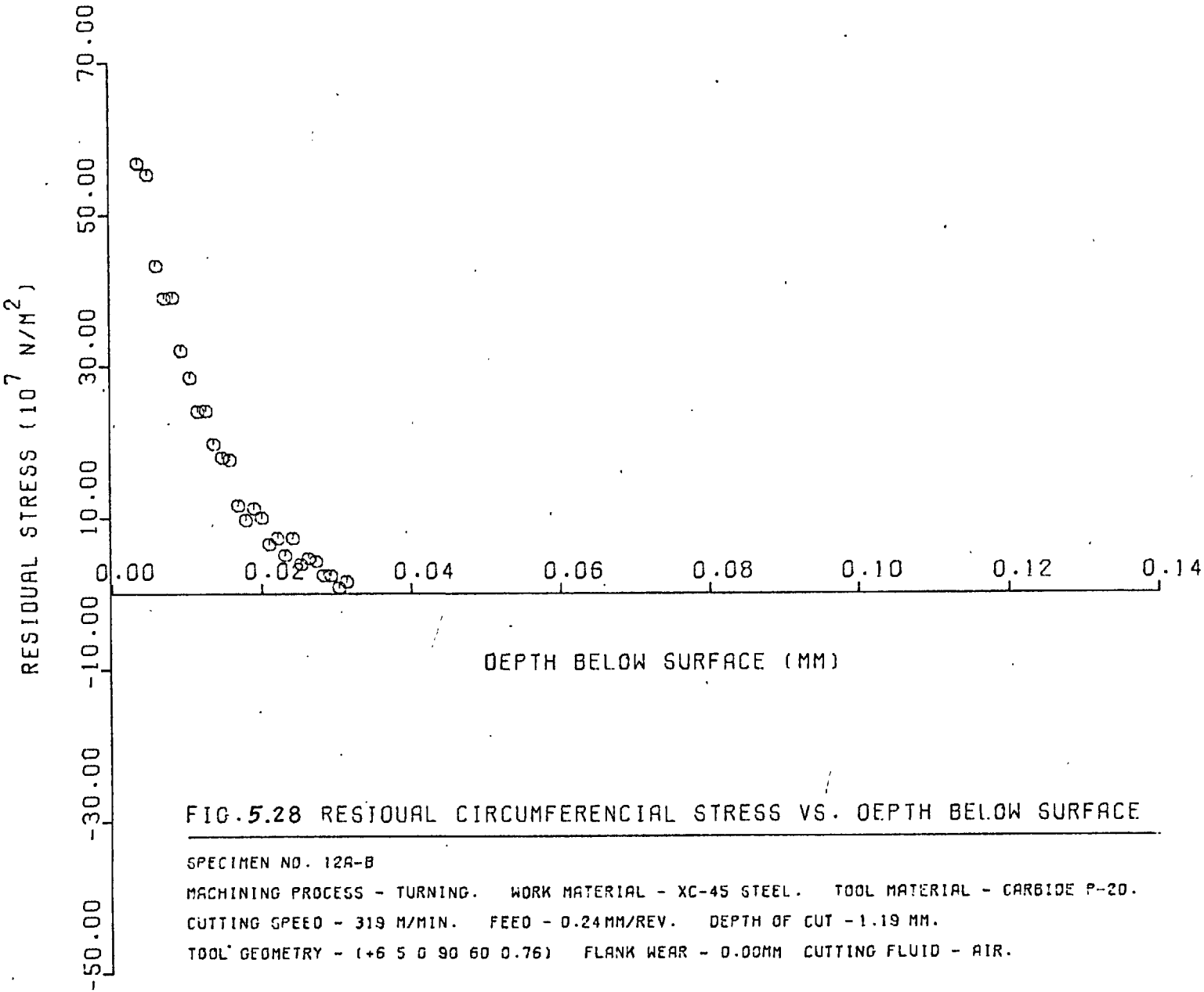

FIG. 5.28 RESIDUAL CIRCUMFERENCIAL STRESS VS. DEPTH BELOW SURFACE

SPECIMEN NO. 12A-B

MACHINING PROCESS - TURNING. WORK MATERIAL - XC-45 STEEL. TOOL MATERIAL - CARBIDE P-20.

CUTTING SPEED - 319 M/MIN. FEED - 0.24 MM/REV. DEPTH OF CUT - 1.19 MM.

TOOL GEOMETRY - (+6 5 0 90 60 0.76) FLANK WEAR - 0.00MM CUTTING FLUID - AIR.

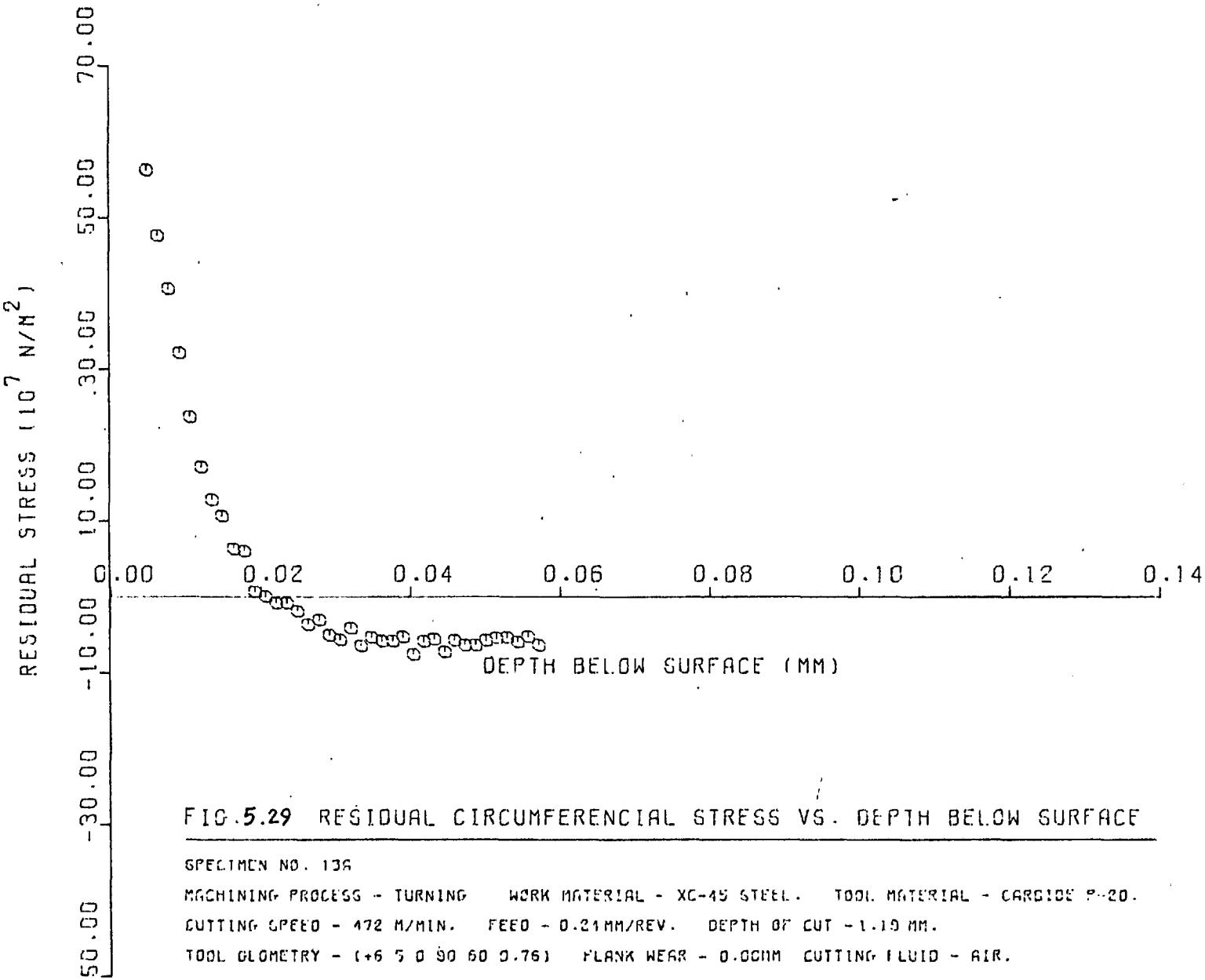

FIG.5.29 RESIDUAL CIRCUMFERENCIAL STRESS VS. DEPTH BELOW SURFACE

SPECIMEN NO. 136

MACHINING PROCESS - TURNING WORK MATERIAL - XC-45 STEEL. TOOL MATERIAL - CARBIDE P-20.

CUTTING SPEED - 472 M/MIN. FEED - 0.21MM/REV. DEPTH OF CUT - 1.19 MM.

TOOL GEOMETRY - (+6 5 8 90 60 0.76) FLANK WEAR - 0.00MM CUTTING FLUID - AIR.

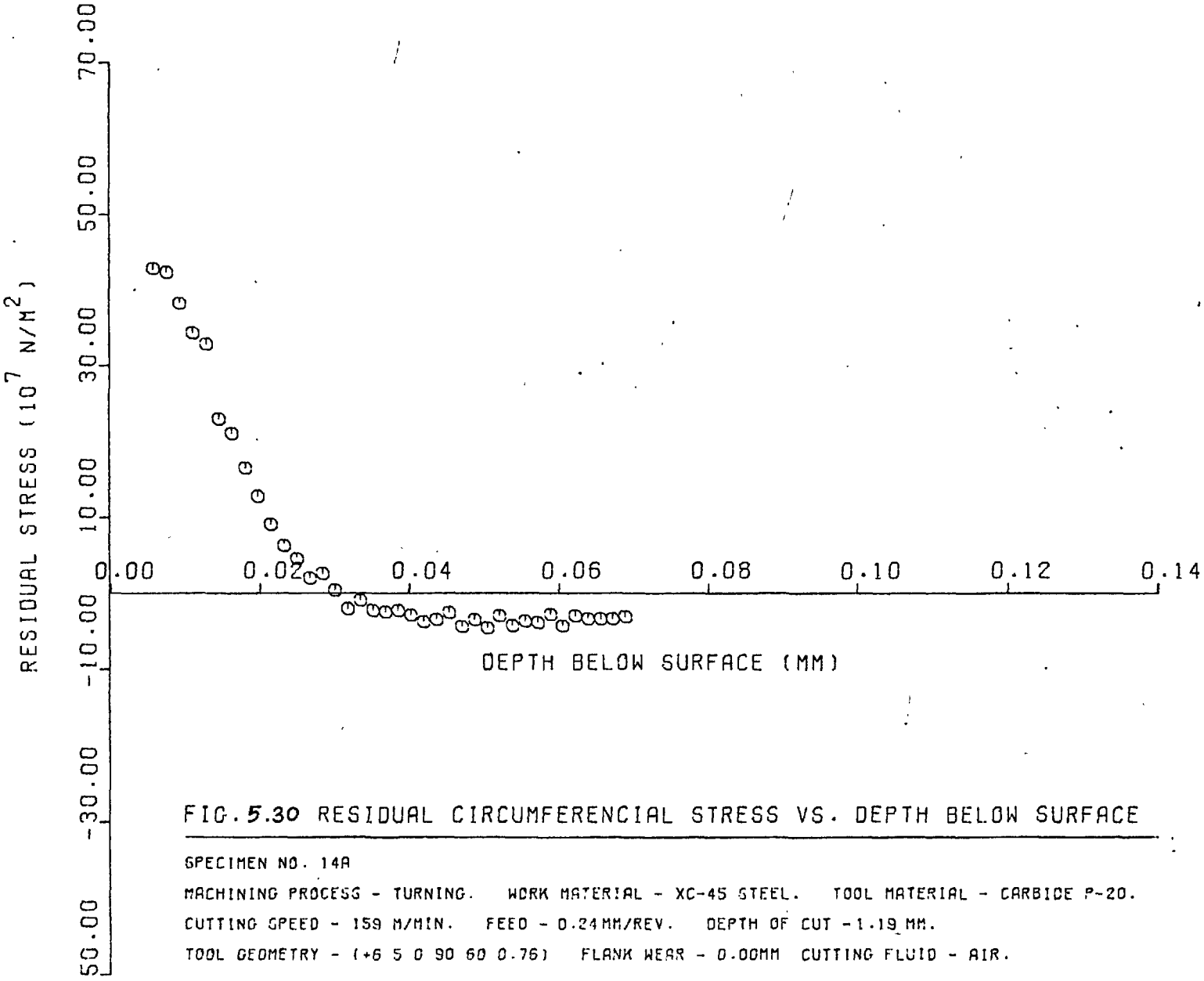

FIG. 5.30 RESIDUAL CIRCUMFERENCIAL STRESS VS. DEPTH BELOW SURFACE

SPECIMEN NO. 14A

MACHINING PROCESS - TURNING. WORK MATERIAL - XC-45 STEEL. TOOL MATERIAL - CARBIDE P-20.

CUTTING SPEED - 159 M/MIN. FEED - 0.24 MM/REV. DEPTH OF CUT - 1.19 MM.

TOOL GEOMETRY - (+6 5 0 90 60 0.76) FLANK WEAR - 0.00MM CUTTING FLUID - AIR.

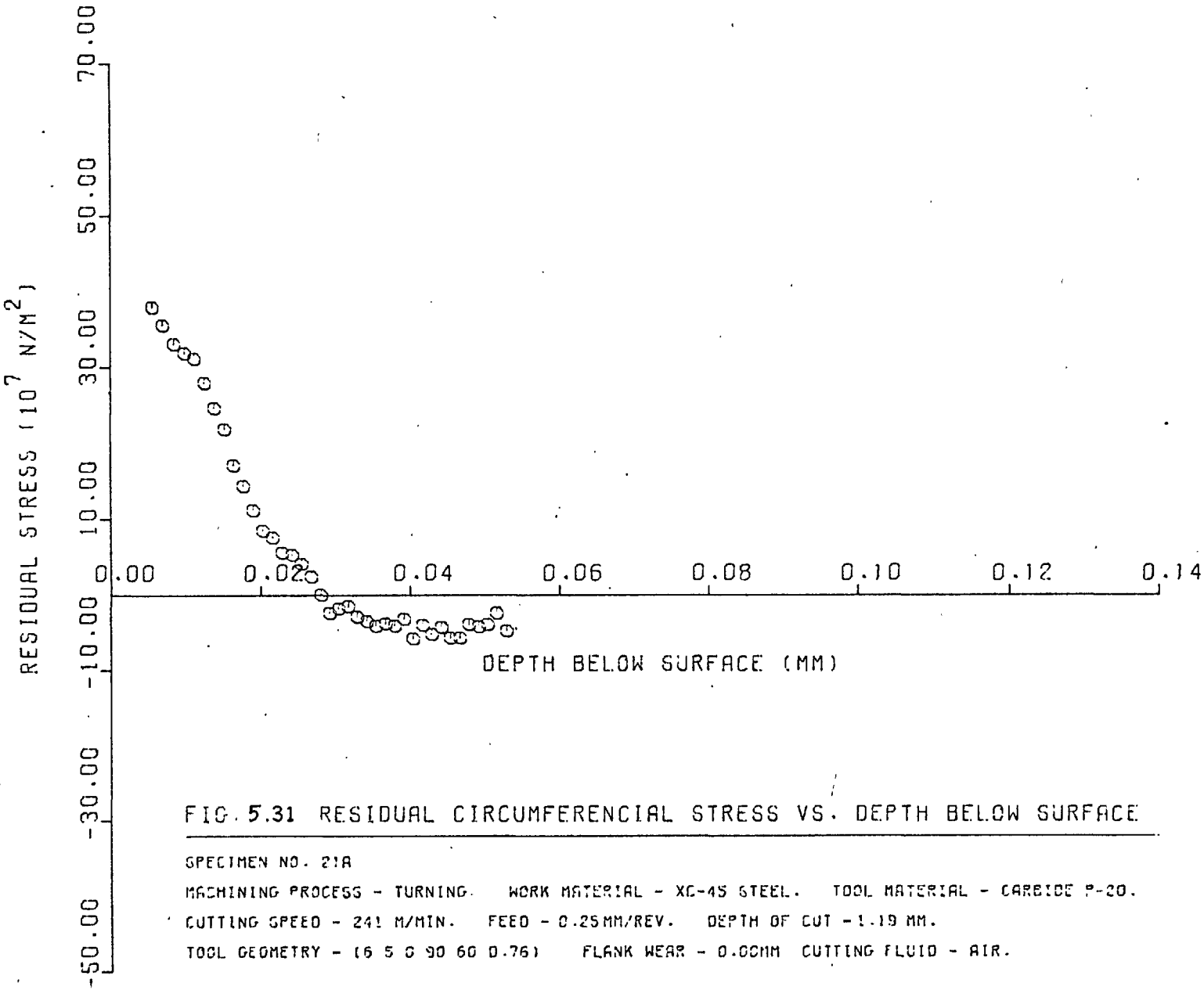

FIG. 5.31 RESIDUAL CIRCUMFERENCIAL STRESS VS. DEPTH BELOW SURFACE

SPECIMEN NO. 21A

MACHINING PROCESS - TURNING. WORK MATERIAL - XC-45 STEEL. TOOL MATERIAL - CARBIDE P-20.

CUTTING SPEED - 241 M/MIN. FEED - 0.25MM/REV. DEPTH OF CUT - 1.19 MM.

TOOL GEOMETRY - (6 5 0 90 60 0.76) FLANK WEAR - 0.00MM CUTTING FLUID - AIR.

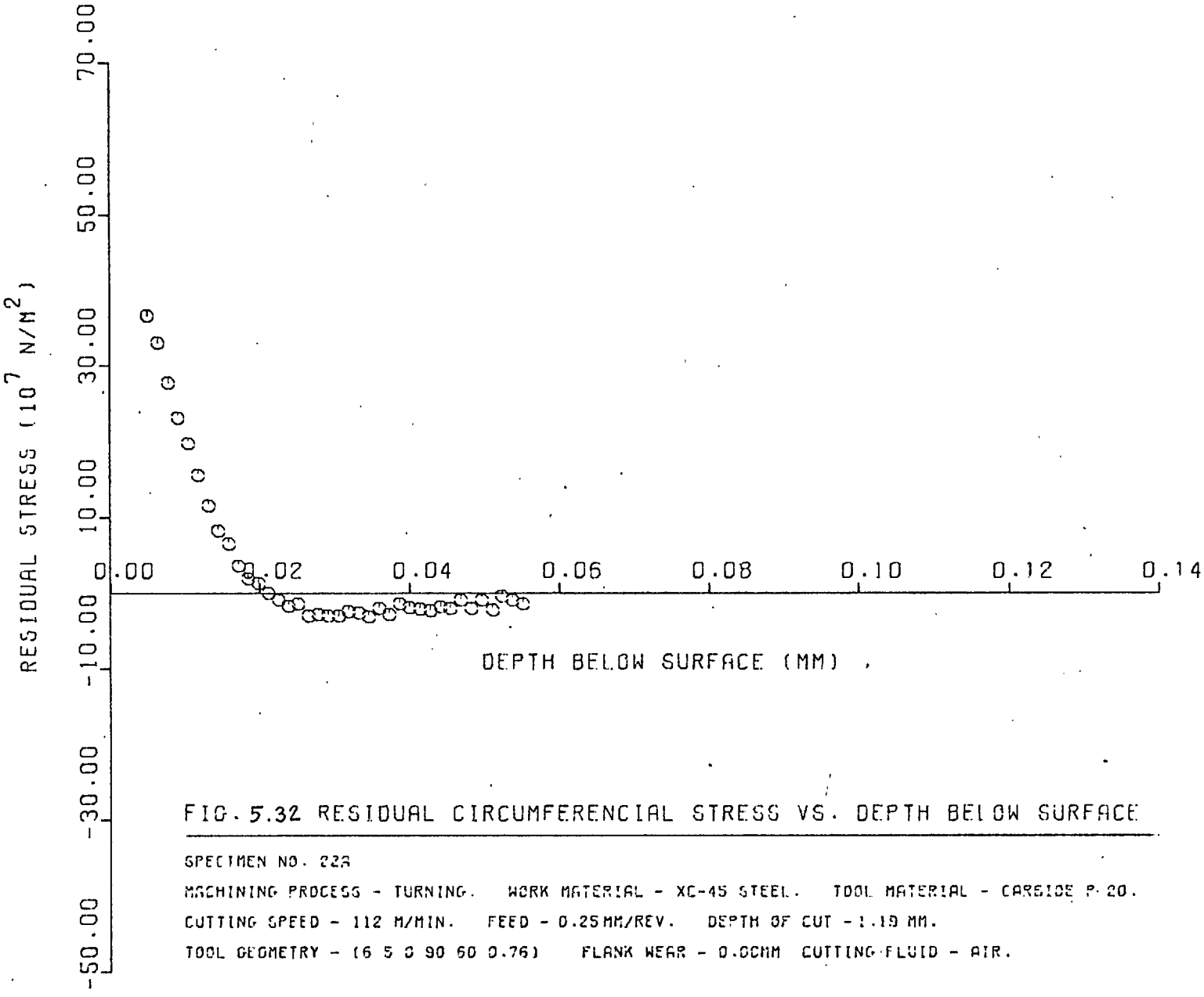

FIG. 5.32 RESIDUAL CIRCUMFERENCIAL STRESS VS. DEPTH BELOW SURFACE

SPECIMEN NO. 228

MACHINING PROCESS - TURNING. WORK MATERIAL - XC-45 STEEL. TOOL MATERIAL - CARBIDE P-20.

CUTTING SPEED - 112 M/MIN. FEED - 0.25MM/REV. DEPTH OF CUT - 1.19 MM.

TOOL GEOMETRY - (6 5 8 90 60 0.76) FLANK WEAR - 0.00MM CUTTING FLUID - AIR.

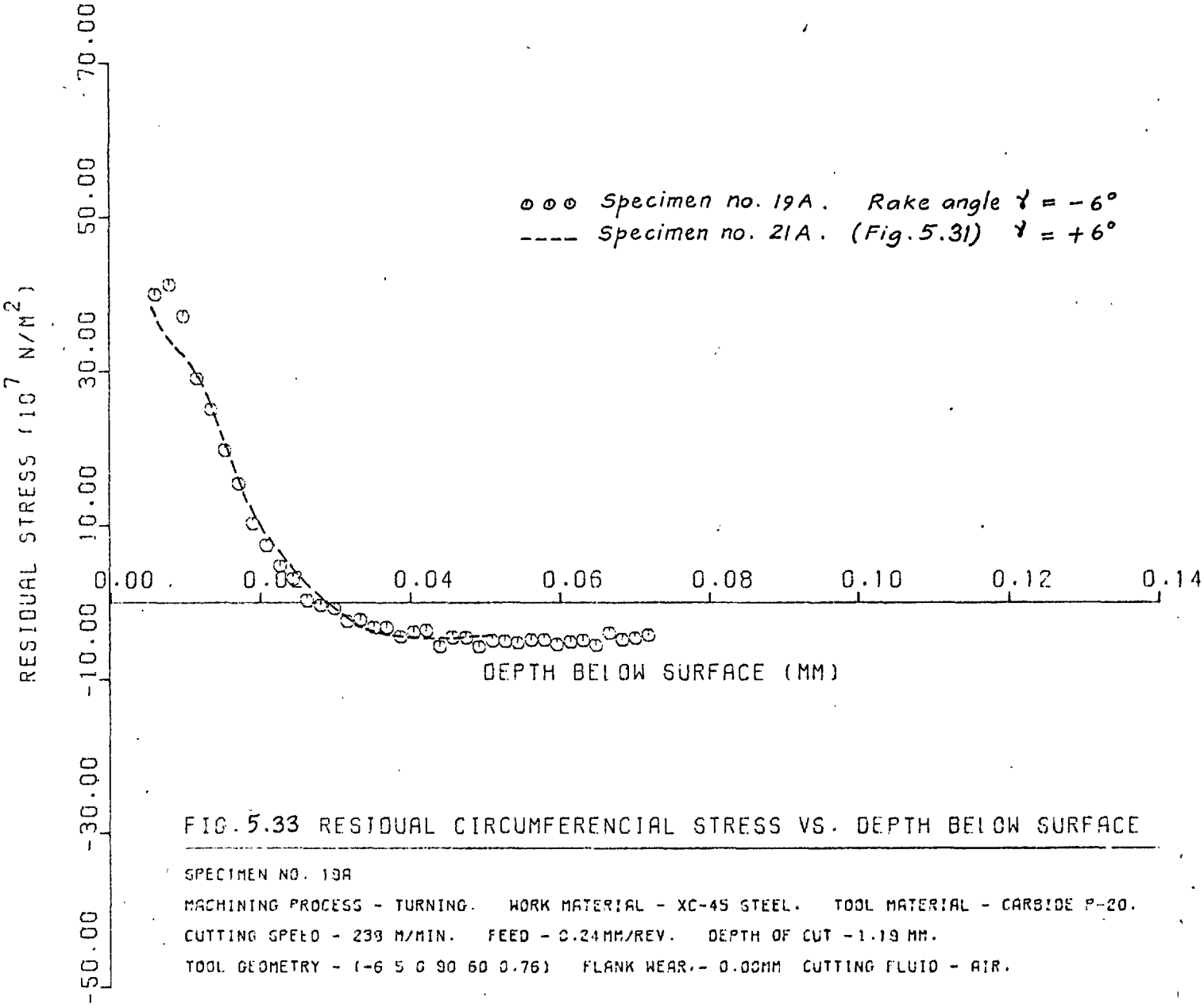

FIG. 5.33 RESIDUAL CIRCUMFERENCIAL STRESS VS. DEPTH BELOW SURFACE

SPECIMEN NO. 19A

MACHINING PROCESS - TURNING. WORK MATERIAL - XC-45 STEEL. TOOL MATERIAL - CARBIDE P-20.

CUTTING SPEED - 238 M/MIN. FEED - 0.24MM/REV. DEPTH OF CUT - 1.19 MM.

TOOL GEOMETRY - (-6 5 6 90 60 0.76) FLANK WEAR - 0.00MM CUTTING FLUID - AIR.

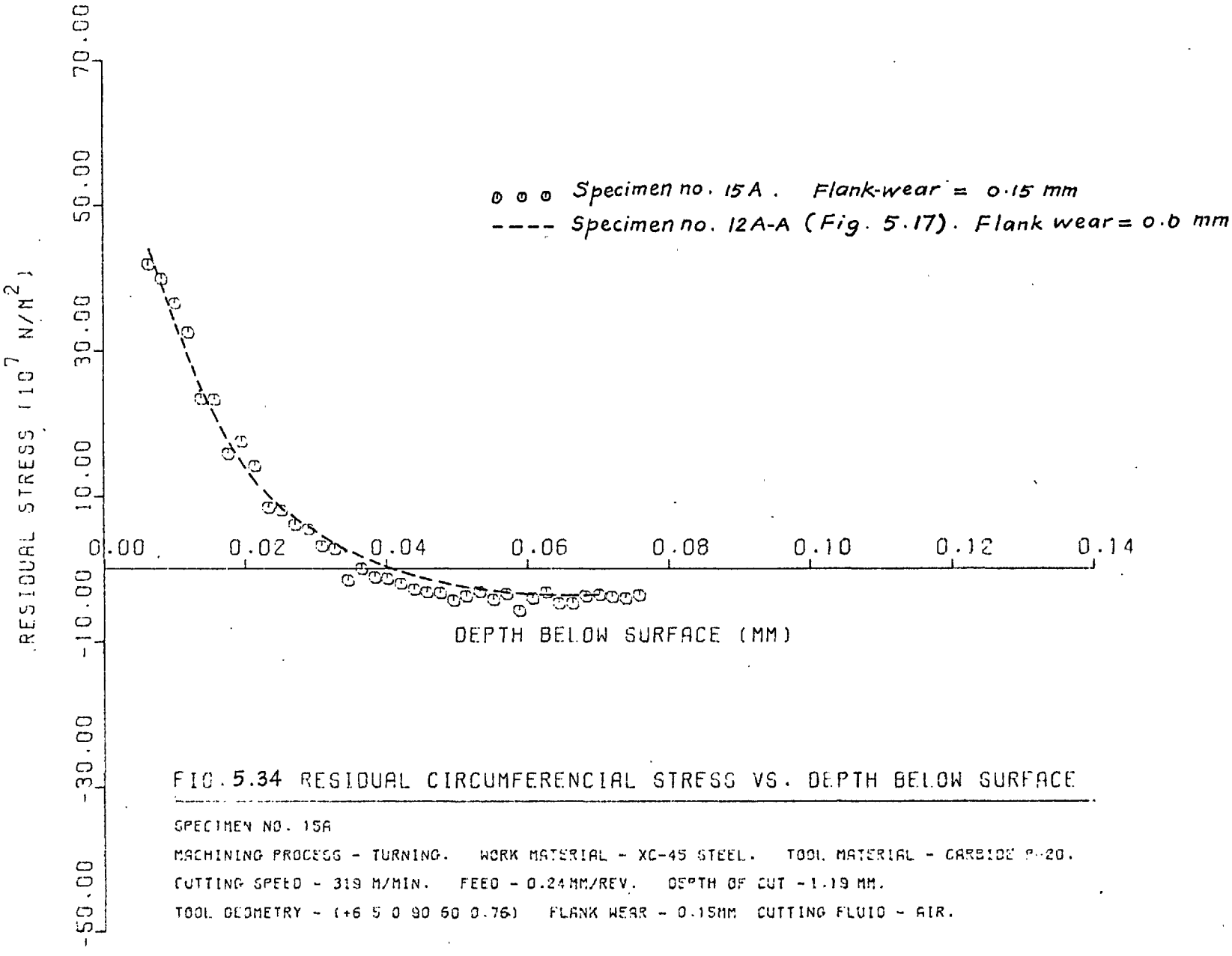

FIG. 5.34 RESIDUAL CIRCUMFERENCIAL STRESS VS. DEPTH BELOW SURFACE

SPECIMEN NO. 15A

MACHINING PROCESS - TURNING. WORK MATERIAL - XC-45 STEEL. TOOL MATERIAL - CARBIDE P-20.

CUTTING SPEED - 319 M/MIN. FEED - 0.24 MM/REV. DEPTH OF CUT - 1.19 MM.

TOOL GEOMETRY - (+6 5 0 90 60 0.76) FLANK WEAR - 0.15MM CUTTING FLUID - AIR.

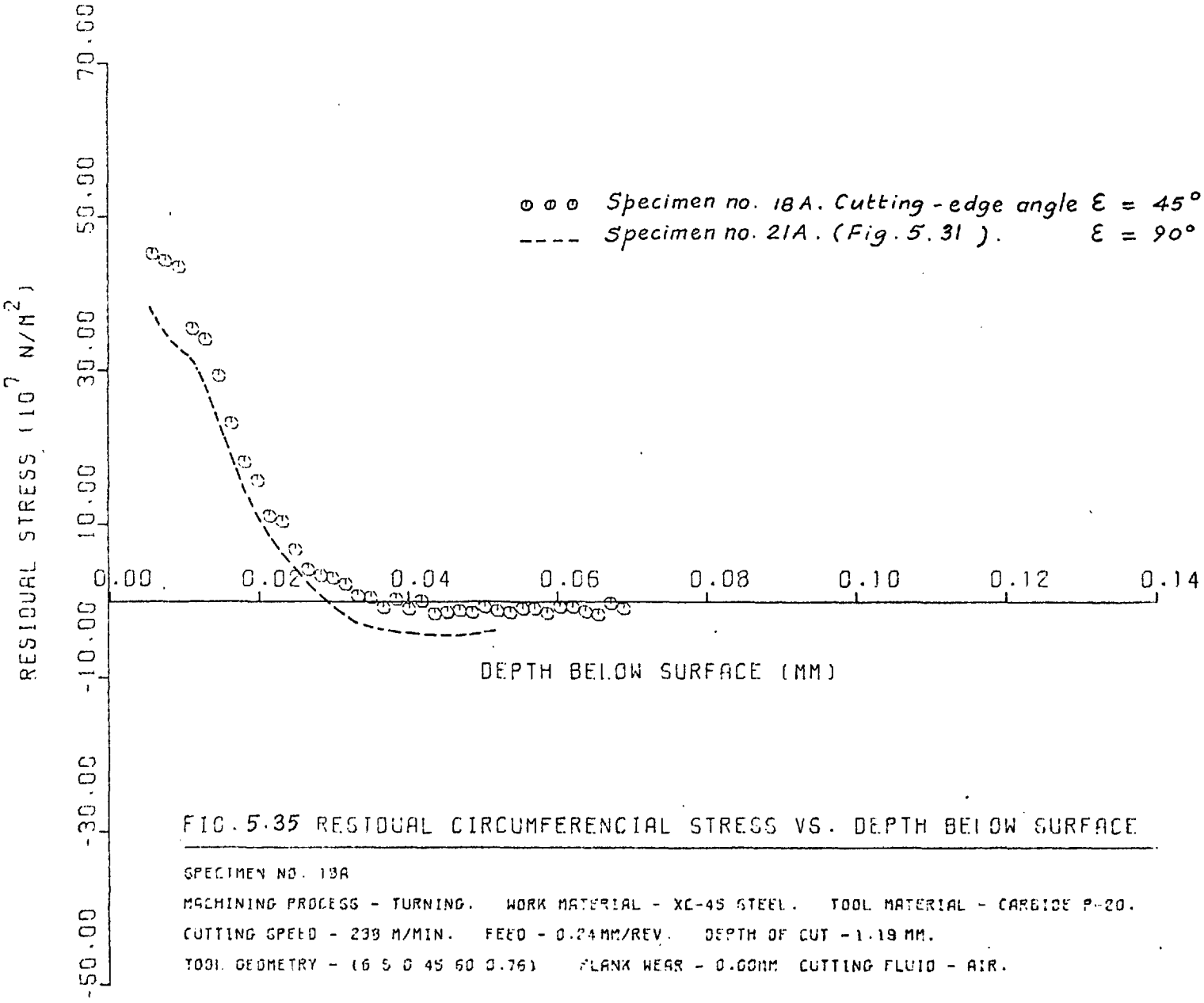

FIG. 5.35 RESIDUAL CIRCUMFERENCIAL STRESS VS. DEPTH BELOW SURFACE

SPECIMEN NO. 18A

MACHINING PROCESS - TURNING. WORK MATERIAL - XC-45 STEEL. TOOL MATERIAL - CARBIDE P-20.

CUTTING SPEED - 239 M/MIN. FEED - 0.24 MM/REV. DEPTH OF CUT - 1.19 MM.

TOOL GEOMETRY - (6 5 0 45 60 0.76) FLANK WEAR - 0.00MM CUTTING FLUID - AIR.

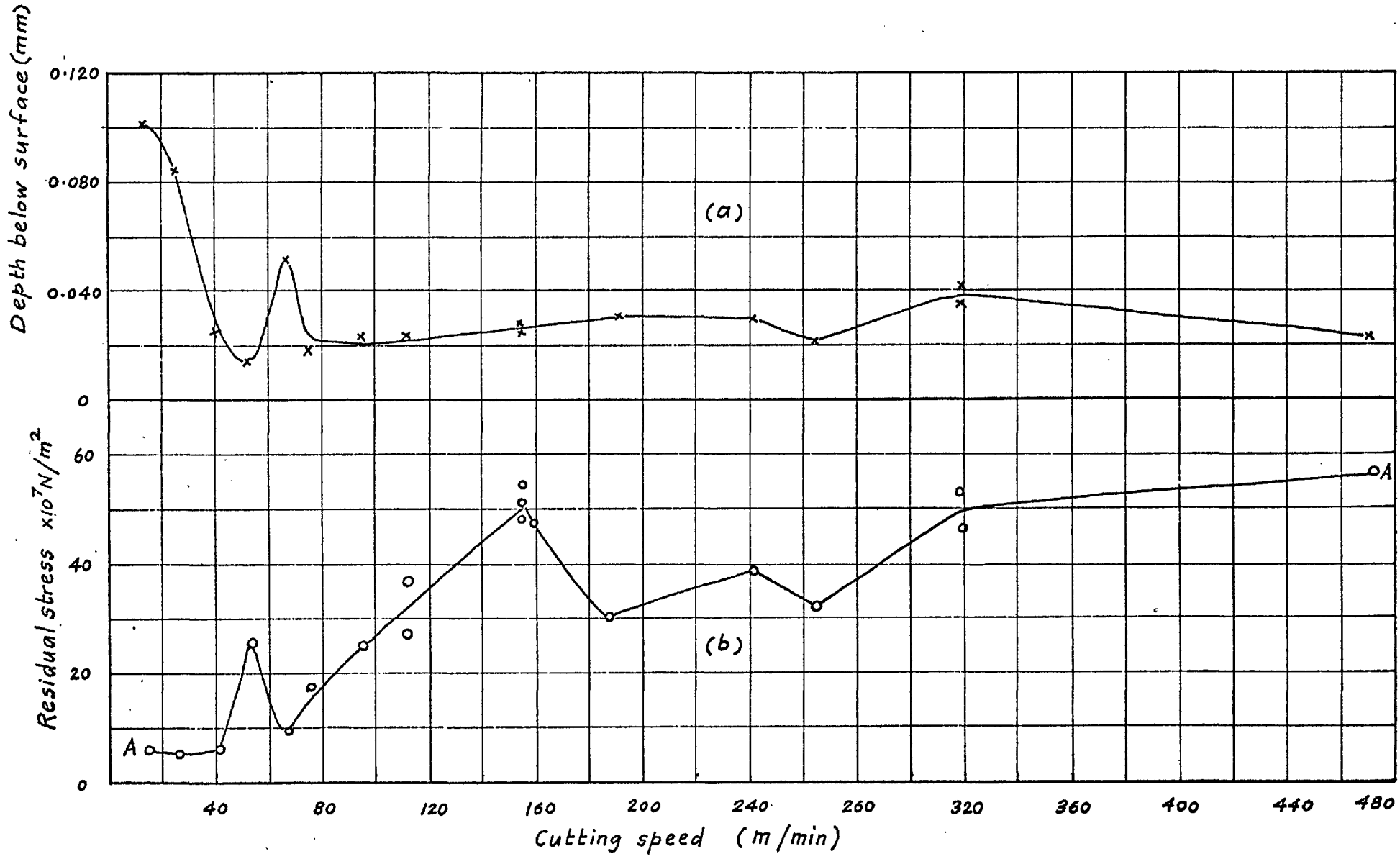

Fig. 5.36. Effect of cutting speed.

(a) o stress at 0·005 mm from surface.

(b) x Depth of tensile layer.

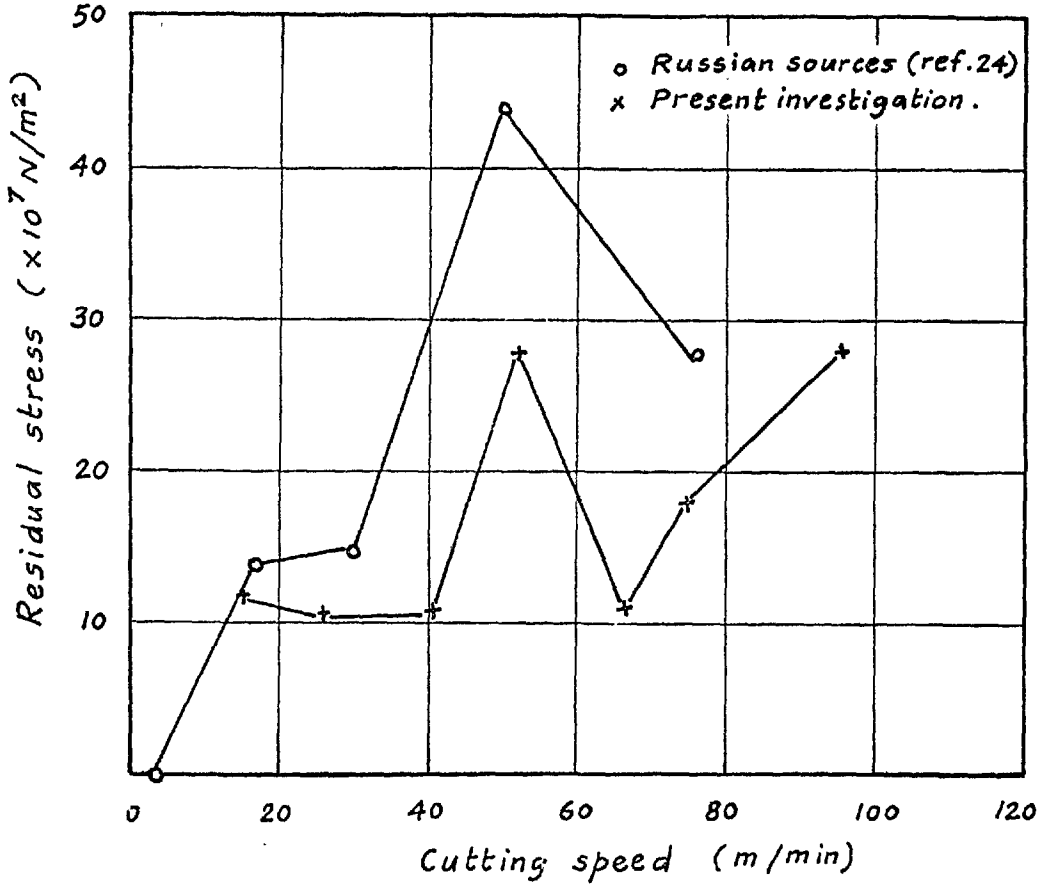

Fig. 5.37. Variation of the peak tensile stress with cutting speed in the range in which significant changes in the b.u.e occur.

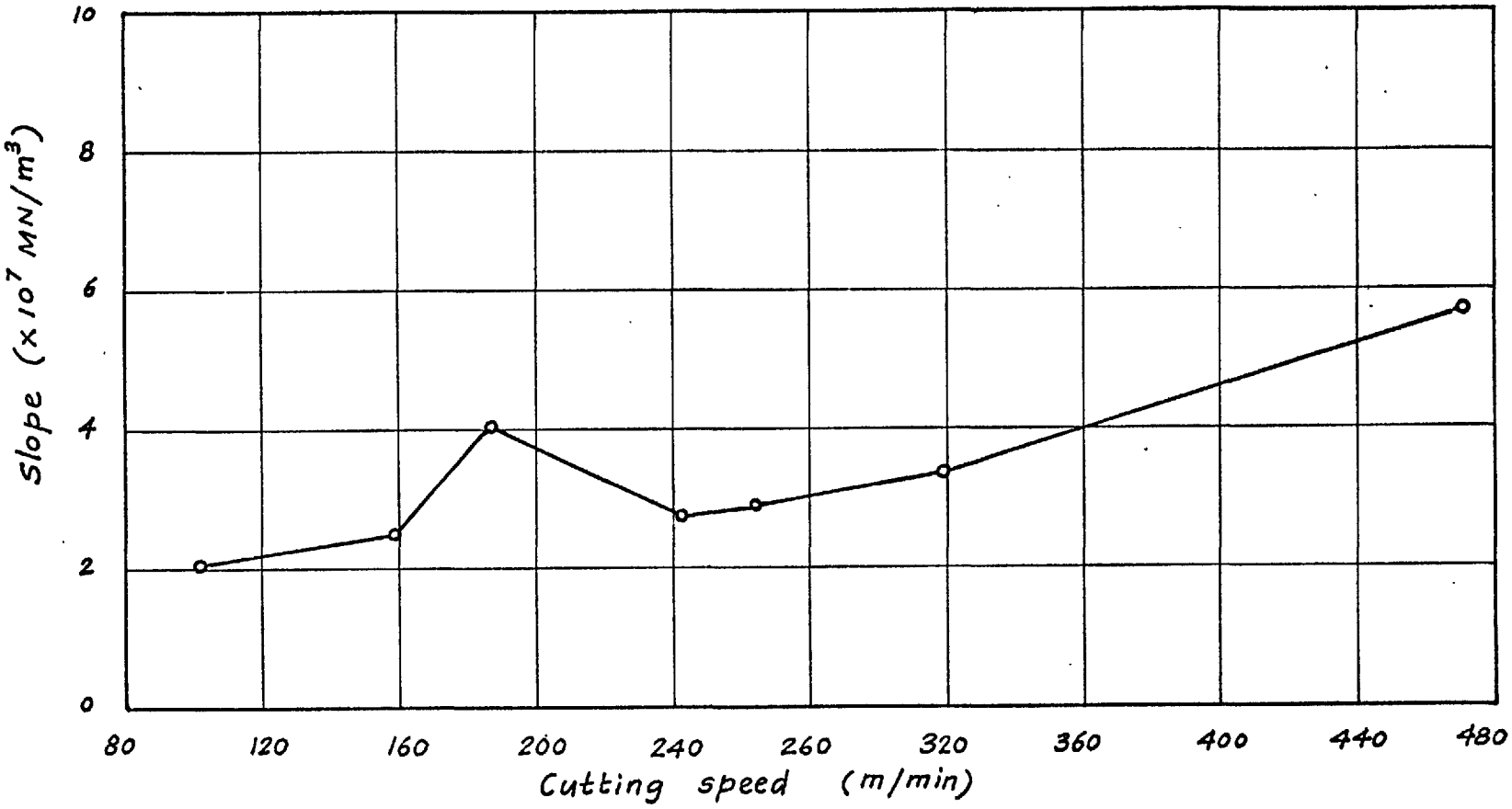

Fig. 5.38. Variation of the average slope of the tensile portion of the residual-stress distribution with cutting speed.

Appendix 3.1

Stress and strain fields within a semi-infinite solid under a line load

The equilibrium of a wedge of semi-angle λ, acted upon by a line load P per unit length along its apex, is considered (Fig.1)*, after the analysis given by Sokolovskii[108]. Exponential work-hardening behaviour $\bar{\sigma} = k(\bar{\epsilon})^n$ is assumed for the material.

For plane strain, $\tau_{\theta z} = \tau_{rz} = 0$ and σ_r, σ_θ, σ_z, $\tau_{r\theta}$ are functions only of r and θ. Equations of equilibrium for plane strain may be written in cylindrical coordinates as

$$\frac{\partial \sigma_r}{\partial r} + \frac{1}{r}\frac{\partial \tau_{r\theta}}{\partial \theta} + \frac{\sigma_r - \sigma_\theta}{r} = 0$$

$$\frac{\partial \tau_{r\theta}}{\partial r} + \frac{1}{r}\frac{\partial \sigma_\theta}{\partial r} + \frac{2\tau_{r\theta}}{r} = 0 \qquad (1)$$

The stress distribution is assumed to be of the form

$$\sigma_r = \sigma_r(r, \theta)\ ,\ \sigma_\theta = 0 = \tau_{r\theta} \qquad (2)$$

The condition of equilibrium then reduces to

$$\frac{\partial \sigma_r}{\partial r} + \frac{\sigma_r}{r} = 0 \quad \text{or} \quad \frac{\partial}{\partial r}(r\,\sigma_r) = 0 \qquad (3)$$

* p. 175

Writing the stress-strain relationship as $S_s = KE_s^n$, where

$$S_s = \sqrt{\frac{1}{6}\left\{(\sigma_\theta - \sigma_z)^2 + (\sigma_z - \sigma_r)^2 + (\sigma_r - \sigma_\theta)^2\right\} + \tau_{r\theta}^2} \quad \text{and}$$

$$E_s = \sqrt{\frac{1}{6}\left\{(\epsilon_\theta - \epsilon_z)^2 + (\epsilon_z - \epsilon_r)^2 + (\epsilon_r - \epsilon_\theta)^2\right\} + \gamma_{r\theta}^2} \qquad (4)$$

it follows that $S_s = \frac{1}{2}|\sigma_r|$ and $E_s = |\epsilon_r|$ for this stress-state. Hence the stress component σ_r can be represented explicitly in terms of θ and r :

$$S_s = \propto P\, t(\theta)/r, \quad \sigma_r = -C\, 2 \propto P\, t(\theta)/r, \quad C = \pm 1 \qquad (5)$$

E_s and ϵ_r can be written as

$$E_s = \left(\frac{S_s}{K}\right)^{\frac{1}{n}} = \left(\frac{\propto P}{K r}\right)^{\frac{1}{n}} g(\theta),$$

$$\epsilon_r = -\epsilon_\theta = -C\left(\frac{\propto P}{K r}\right)^{\frac{1}{n}} g(\theta) \quad \text{where} \quad t = g^n \qquad (6)$$

The parameter $\propto$ is introduced as a scaling factor, determined as explained later. This allows a further condition $t(0) = 0$ to be imposed without loss of generality.

The equation for compatibility under plane-strain conditions is given by

$$r \frac{\partial}{\partial r} \left(r \frac{\partial \epsilon_\theta}{\partial r} \right) + \frac{\partial^2 \epsilon_r}{\partial \theta^2} + r \frac{\partial}{\partial r} (\epsilon_\theta - \epsilon_r) = 2 \frac{\partial^2}{\partial r . \partial \theta} (r \gamma_{r\theta}) \tag{7}$$

Upon substituting for ϵ_r and ϵ_θ from equation (6), equation (7) yields

$$\frac{d^2 g}{d\theta^2} + \frac{2n - 1}{n^2} g = 0 \tag{8}$$

Sokolovskii assumed the following form for the solution of this differential equation, C' and δ being the constants of integration

$$g = C' (1 + \delta\theta), \qquad n = \tfrac{1}{2}$$

$$g = C' \cos (\ell\theta + \delta), \quad n > \tfrac{1}{2}$$

and $$g = C' \cosh (m\theta + \delta), \quad n < \tfrac{1}{2}$$

where $\ell^2 = (2n - 1)/n^2$ and $m^2 = (1 - 2n)/n^2$ (9)

The constant C' is eliminated using the condition $t(0) = 1$ to give

$$t(\theta) = (1 + \delta\theta)^{\frac{1}{2}}, \qquad n = \tfrac{1}{2}$$

$$t = \left\{ \frac{\cos (\ell\theta + \delta)}{\cos \delta} \right\}^n, \quad n > \tfrac{1}{2}$$

$$t = \left\{ \frac{\cosh (m\theta + \delta)}{\cosh \delta} \right\}^n, \quad n < \tfrac{1}{2} \tag{10}$$

The boundary conditions, $\sigma_\theta = \tau_{r\theta} = 0$ when $\theta = \pm \lambda$,

are satisfied since σ_θ and $\tau_{r\theta}$ are assumed to be identically zero.

Considering the equilibrium of the external load

$$P \cos\beta = -\int_{-\lambda}^{+\lambda} \sigma_r \cos\theta \, r \, d\theta$$

$$P \sin\beta = -\int_{-\lambda}^{+\lambda} \sigma_r \sin\theta \, r \, d\theta \qquad (11)$$

Substituting for σ_r from equation (5), the equations (11) must be solved to evaluate the constants α and δ.

For $n < \frac{1}{2}$ (which is the case for most engineering alloys), equations (11) take the following form, when Sokolovskii's solution (equations (10)) is used:

$$\sin\beta = -\int_{-\pi/2}^{\pi/2} 2C\alpha \left\{\frac{\cosh(m\theta + \delta)}{\cosh\delta}\right\}^n \sin\theta \, d\theta$$

$$\cos\beta = -\int_{-\pi/2}^{\pi/2} 2C\alpha \left\{\frac{\cosh(m\theta + \delta)}{\cosh\delta}\right\}^n \cos\theta \, d\theta \qquad (12)$$

λ taking the value $\pi/2$ for the semi-infinite solid.

By division,

$$\tan\beta = \frac{-\int_{-\pi/2}^{\pi/2} C\cosh^n(m\theta + \delta) \sin\theta \, d\theta}{\int_{-\pi/2}^{\pi/2} C\cosh^n(m\theta + \delta) \cos\theta \, d\theta} \qquad (13)$$

from which δ may be determined.

Analytic solution for δ could not be found and hence numerical integration was performed for various values of δ to obtain the δ vs. β relationship.

Thus, for real values of δ, the entire range for $|\beta|$ from 0 to $\pi/2$ could not be covered.

However, assuming the solution of the differential equation (8) to be of the general form

$$g = C\,(1 + \delta\theta), \qquad n = \frac{1}{2}$$

$$g = C \cos(\ell\theta + \delta), \qquad n > \frac{1}{2}$$

$$g = A \cosh m\theta + B \sinh m\theta, \qquad n < \frac{1}{2}$$

For $n < \frac{1}{2}$, the condition $g(0) = 1$ results in $A = 1$ and hence

$$g = \cosh m\theta + B \sinh m\theta$$

$$= \left(\frac{B+1}{2}\right)\left\{e^{m\theta} - \frac{(B-1)}{(B+1)}\, e^{-m\theta}\right\}$$

$$= \frac{1}{(1-\delta)}\,(e^{m\theta} - \delta\, e^{-m\theta}) \quad \text{where} \quad \delta = \frac{B-1}{B+1}$$

Corresponding to equation (13), the following one results.

$$\tan\beta = \frac{\displaystyle\int_{-\pi/2}^{\pi/2} (e^{m\theta} - \delta e^{-m\theta})^n \sin\theta\, d\theta}{\displaystyle\int_{-\pi/2}^{\pi/2} (e^{m\theta} - \delta e^{-m\theta})^n \cos\theta\, d\theta} \qquad (14)$$

Equation (14) enables values of $|\beta|$ from 0 to $\pi/2$ to be covered by taking real values for δ. Graphs of $\delta(\beta)$ are shown in Fig.3.4 and 3.5. It can be seen from these that the relationship $\delta = m\beta$, taken by Okushima and Kakino[89], is not strictly valid.

Once the value of δ is known for a given value of β, α follows from equation (12):

$$\alpha = -\frac{\sin\beta}{\int_{-\pi/2}^{\pi/2} 2C\left\{\frac{1}{(1-\delta)}\left(e^{m\theta} - \delta e^{-m\theta}\right)\right\}^{n} \sin\theta \, d\theta}$$

Fig.3.6 shows graphs of $\alpha(\beta)$.

The stress and strain distributions are then given by the equations (5) and (6) respectively.

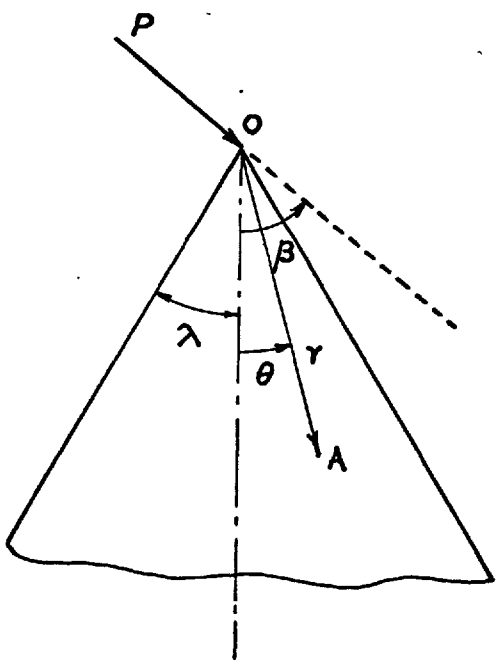

Fig. 1. The case of a wedge subjected to a line load P. (Appendix 3.1.)

Appendix 3.2

Computer programme for determining residual-stress distributions from the analytical model.

The interpretation of the main FORTRAN variables is given in Table 1.* The flow chart in Fig.1† gives the basic steps in the main programme (MAIN). Details regarding the control of step size (Δx) and the limits for x (x_i and x_f), and other features can be seen from the listing of the programme. When $n \geqslant \frac{1}{2}$, the value of α is calculated by the subroutine ALF. Subroutines STRAIN, ALF, XI and YLD are self explanatory.

When $n < \frac{1}{2}$, α is obtained from a separate programme ALFA and supplied to MAIN through data. A listing of ALFA is also included.

* p. 177
† p. 178

Table 1

Names of the main variables in the programme RESID.

XK,XMEW	- Strength coefficient K, and strain-hardening index n.
F	- Ploughing force P.
E,XNEW	- Young's modulus E, and Poisson's ratio ν.
BETA,AL,LD	- β, α and δ respectively.
YLD	- Current yield stress.
YINIT	- Initial yield stress (intersection of $\sigma = E$ and $\sigma = K\epsilon^n$)
Y	- Depth below surface.
X	- Distance along the direction of cutting.
DY,DX	- Increments in Y and X respectively.
ST,SN	- Components of stress and strain respectively.
SD	- Deviatoric-stress components.
SM	- Mean stress σ_m.
EFST	- Effective stress $\bar{\sigma}$.
DSN	- Components of strain increment.
DSND	- Components of deviatoric-strain increment.
DSD	- Components of deviatoric-stress increment.
EP	- Effective plastic strain.
DEP	- Effective plastic-strain increment.
HRDI	- Nondimensional hardness index.
DT(I)	- Location for storing the I^{th} value of depth for which residual stresses are computed.
S(I,J)	- Vector for storing residual-stress components (J = 1,2,3,4) for the depth DT(I).

Other variables are explained in the programme.

Fig.1. Flow chart for Programme MAIN.

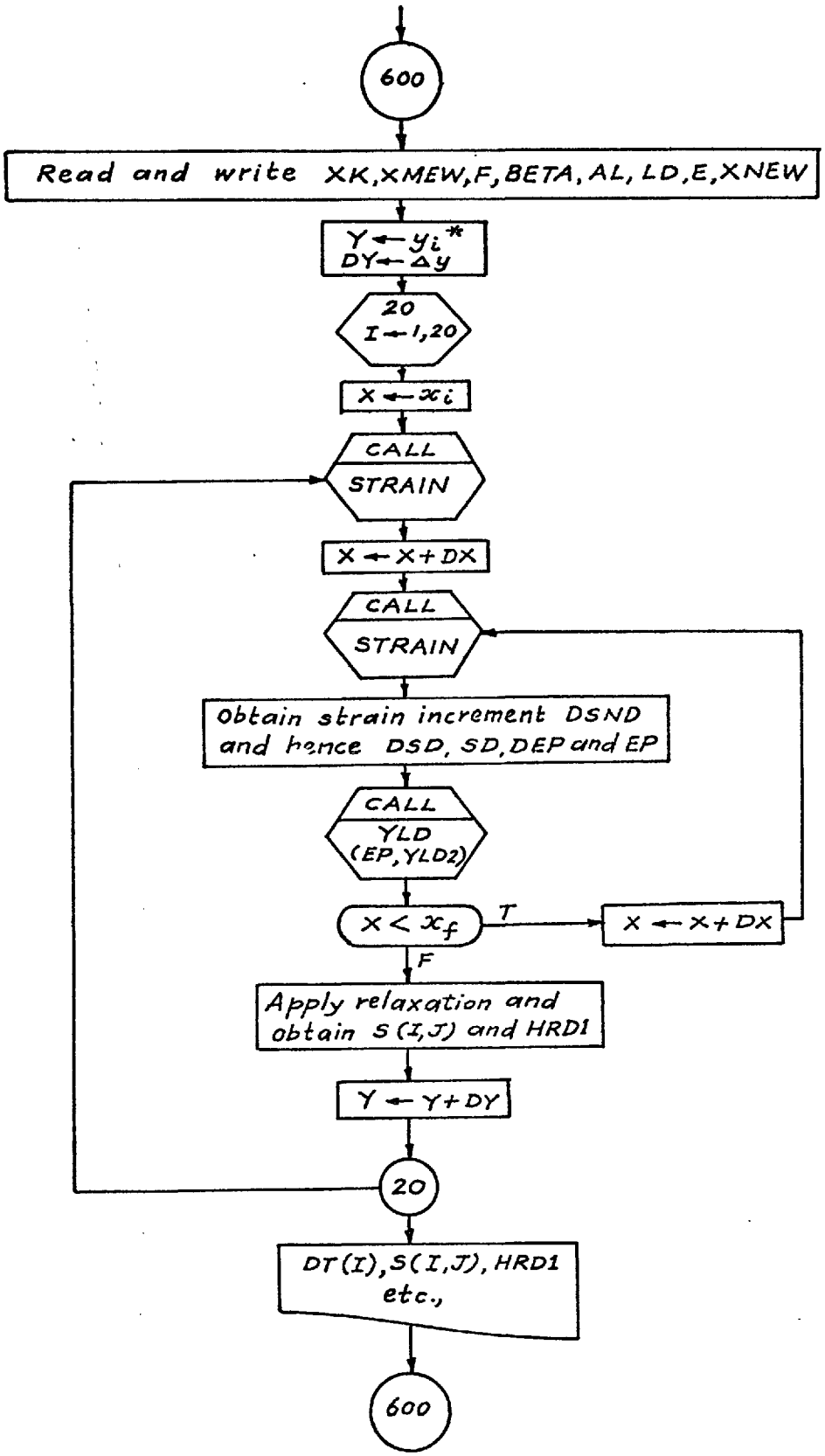

* y_i and Δy are any desired numerical values.

```
$IBFTC MAIN
C       PROGRAM FOR DETERMINING RESIDUAL STRESS DISTRIBUTION DUE TO
C       THE PASSAGE OF A STRAIN FIELD OVER A SEMI-INFINITE BODY.
        REAL LD
        DIMENSION S(30,4),ST(4),SN(4),SN1(4),SD(4),DSD(4),SD1(4),DSN(4),
       2DSND(4),RD(4),RSD(4),STD(4),FX(10),DT(30),SPX(30),SPZ(30),HRD1(30)
        COMMON/D/XK,XMEW,F,DEL,E,XNEW
        COMMON/SUN/X,Y,AL,SN,ST
600     READ(5,44)XK,XMEW,F,BETA,E,XNEW
44      FORMAT(E10.0,F10.3,E10.1,F10.3,E10.0,F10.2)
        XKS=XK
        FS=F
        PI=355./113.
        BLK=E/(1.-2.*XNEW)/3.
        G=E/2./(1.+XNEW)
        READ(5,601)NCASE
601     FORMAT(I2)
        DO 67 NI=1,NCASE
        READ(5,301)BETA,AL,LD
301     FORMAT(3F10.5)
        DO 900 IM=1,1
        XK=XKS*FLOAT(IM)
        F=FS*FLOAT(IM)
        NT=0
        IF(XMEW.LT.0.5)GO TO 400
        DEL=-BETA
        CALL ALF(AL)
        GO TO 401
400     DEL=LD
401     WRITE(6,45)XK,XMEW,F,BETA,E,XNEW,DEL,AL,LD
45      FORMAT(//1X,6(2X,E15.5)/1X,3(2X,E15.5))
        Y=0.020E-3
        DY=0.010E-3
C       LOOPS FOR DIFFERENT DEPTHS BELOW SURFACE.
        DO 20 I=1,20
C       IP,INP,ICP,INC,IPL AND L66 ARE USED FOR COUNTING THE NUMBER OF
C       ITERATIONS IN THE VARIUS LOOPS.
        IP=0
        INP=0
        ICP=0
        INC=0
        IPC=0
        L66=0
C       STORE VALUES OF DEPTHS BELOW SURFACE IN ARRAY DT
        DT(I)=Y*1.0E3
C       COMPUTATION OF RESIDUAL STRESS FOR A GIVEN DEPTH BELOW SURFACE.
        YLD=(E**XMEW/XK)**(1./(XMEW-1.))
C       YLD2=SQUARE OF THE CURRENT YIELD STRESS.
        YLD2=YLD*YLD
        EP=0.
        YINIT=YLD
        WRITE(6,100)YLD
100      FORMAT(10X,16HINITIAL YIELD = ,E13.5)
        X=-1.5E-3
69      CALL STRAIN
        INC=INC+1
        IPC=IPC+1
C       DEVIATORIC STRESS COMPONENTS
        SM=ST(3)
```

```
      DO 3 K=1,3
3     SD(K)=ST(K)-SM
      SD(4)=ST(4)
      EFST=3.*(SD(1)*SD(1)+SD(4)*SD(4))
      IF(EFST.GT.YLD2.AND.INC.EQ.1)GOTO 181
      IF(EFST.GE.YLD2)GO TO 79
      IF(X.GT.1.5E-3)GO TO 99
      X=X+0.010E-3
      GO TO 69
181   X=X-0.010E-3
      INC=1
      GO TO 69
79    X=X-0.010E-3
      CALL STRAIN
      SM=ST(3)
      DO 171 K=1,3
171   SD(K)=ST(K)-SM
      SD(4)=ST(4)
70    DO 71 L=1,4
71    SN1(L)=SN(L)
      X=X+0.002E-3
      DX=0.002E-3
      GO TO 66
300   DX=DX/2.
      X=X-DX
66    CALL STRAIN
      DO 6 L=1,4
      DSN(L)=SN(L)-SN1(L)
      ADSN=ABS(DSN(L))
      IF(ADSN.GT.1.0)GO TO 50
      IF(ADSN.GT.0.0012)GO TO 72
6     CONTINUE
      GO TO 73
72    DX1=(DX/ADSN)*0.001
      X=X-DX+DX1
      DX=DX1
      L66=L66+1
      GO TO 66
73    DSNM=(DSN(1)+DSN(2)+DSN(3))/3.
C     COMPONENTS OF STRAIN INCREMENT.
      DO 7 L=1,3
7     DSND(L)=DSN(L)-DSNM
      DSND(4)=DSN(4)
      INC=INC+1
      IPC=IPC+1
C     COMPUTING COMPONENTS OF DEVIATORIC STRESS INCREMENT ASSUMING
C     HOOKE'S LAW.
      DO 8 L=1,3
8     DSD(L)=2.*G*DSND(L)
      DSD(4)=G*DSND(4)
      DSM=3.*BLK*DSNM
C     DEVIATORIC STRESS COMPONENTS AND MEAN STRESS AFTER STRAIN INCREMEN
      DO 9 L=1,4
9     SD1(L)=SD(L)+DSD(L)
      SM1=SM+DSM
      EFST1=1.5*(SD1(1)*SD1(1)+SD1(2)*SD1(2)+SD1(3)*SD1(3)+2.*SD1(4)*SD1
     1(4))
      EFRT1=SQRT(EFST1)
      IF(EFST1.LE.YLD2)GO TO 18
```

```
      EFST=1.5*(SD(1)*SD(1)+SD(2)*SD(2)+SD(3)*SD(3)+2.*SD(4)*SD(4))
      EFRT=SQRT(EFST)
      IF(EFST.GE.YLD2)GO TO 12
      F1=1.5*(DSD(1)*DSD(1)+DSD(2)*DSD(2)+DSD(3)*DSD(3)+2.*DSD(4)*
     1DSD(4))
      GAM=F1+EFST-EFST1
      R=(GAM+SQRT(GAM*GAM+4.*(YLD2-EFST)*F1))/(2.*F1)
C     STORE IN DSND(I) THE FRACTION OF DEVIATORIC STRAIN INCREMENT
C     RESPONSIBLE FOR STRESSING BEYOND YLD.
      DO 11 L=1,4
      DSD(L)=R*DSD(L)
      SD(L)=SD(L)+DSD(L)
11    DSND(L)=(1.-R)*DSND(L)
      EFST=1.5*(SD(1)*SD(1)+SD(2)*SD(2)+SD(3)*SD(3)+2.*SD(4)*SD(4))
      EFRT=SQRT(EFST)
      DSM=R*DSM
      SM=SM+DSM
      DSNM=(1.-R)*DSNM
      GO TO 10
C     STRESS INCREMENTS USING PRANDTL-REUSS EQUATIONS.
12    R=0.
10    DW=0.
      DO 14 L=1,4
      DDW=DSND(L)*SD(L)
14    DW=DW+DDW
      RHD=((YLD/XK)**(1./XMEW))/(XMEW*YLD)-1./E
      HD=1./RHD
      DWD=4.5*DW*G/YLD2/(HD+3.*G)
      DO 15 L=1,3
15    DSD(L)=2.*G*(DSND(L)-DWD*SD(L))
      DSD(4)=2.*G*(DSND(4)/2.-DWD*SD(4))
      DSM=3.*BLK*DSNM
C     COMPONENTS OF PLASTIC STRAIN INCREMENT AND EFFECTIVE PLASTIC
C     STRAIN INCREMENT.
      DEP=DW/YLD/(1.+HD/3./G)
      IF(DEP.LT.0.)GO TO 101
      GO TO 102
101   ADEP=ABS(DEP)
      ICP=1
      IF(ADEP.LT.0.5E-9)GO TO 110
      INC=INC-1
      GO TO 300
110   INP=INP+1
102   EP=EP+DEP
      IP=IP+ICP
      ICP=0
      CALL YIELD(EP,YLD2)
      YLD=SQRT(YLD2)
      HRD1(I)=YLD/XK
C     NEW DEVIATORIC STRESS COMPONENTS AND MEAN STRESS.
      DO 16 L=1,4
16    SD(L)=SD(L)+DSD(L)
      SM=SM+DSM
      EFST=1.5*(SD(1)*SD(1)+SD(2)*SD(2)+SD(3)*SD(3)+2.*SD(4)*SD(4))
      YLD2=EFST
      YLD=SQRT(EFST)
      GO TO 4
18    DO 19 L=1,4
19    SD(L)=SD1(L)
```

```
      SM=SM1
4     IF(X.LT.1.5E-3)GO TO 70
      GO TO 81
99    WRITE(6,80)INC,EFST
80    FORMAT(1X,16HNO PLASTIC FLOW.,4X,I4,4X,E14.5)
      NT=I
      HRD1(I)=YINIT
81    CONTINUE
      DO 21 L=1,3
21    S(I,L)=SD(L)+SM
      S(I,4)=SD(4)
      IF(NT.EQ.I)GO TO 716
      WRITE(6,200)Y
200   FORMAT(1HX,20HDEPTH BELOW SURFACE=,E12.3)
      WRITE(6,22)I,(S(I,M),M=1,4)
22    FORMAT(16X,I2,4(2X,E15.4))
      Y=Y+DY
C     RESTORING EQUILIBRIUM BY RELAXATION.
      S(I,1)=S(I,1)-XNEW*S(I,2)/(1.-XNEW)
      S(I,3)=S(I,3)-XNEW*S(I,2)/(1.-XNEW)
      S(I,2)=0.
      WRITE(6,22)I,(S(I,M),M=1,4)
      WRITE(6,52)INC,IP,INP,IPC,L66
52    FORMAT(1HX,20HNO. OF STRAIN STEPS=,I4,4X,24HSTEPS WITH DEP.NEGETIV
     1E=,I4,4X,19HNEG. STEPS ALLOWED=,I4,4X,13HNO. OF ITER.=,I4,4X,I4)
      GO TO 20
50    WRITE(6,53)INC,DSN(L)
53    FORMAT(1HX,29HSTRAIN INCREMENT IS TOO LARGE,5X,I4,5X,E15.5)
      S(I,1)=1.0E20
      WRITE(6,200)Y
      Y=Y+DY
20    CONTINUE
      NT=20
716   XKT=XK*1.0E-6
      ET=E*1.0E-6
      BT=BETA/PI*180.
      FT=F*1.0E-6
      WRITE(6,700)
700   FORMAT(1H1////////20X,5HTABLE, 7X,51HRESIDUAL STRESS VS. DEPTH BEL
     1OW SURFACE (PREDICTED))
      WRITE(6,701)XKT,XMEW,ET,XNEW,FT,BT
701   FORMAT(//20X,22HSTRENGTH COEFFICIENT =,E11.4,8HMN/M SQ.,2X,30HSTRA
     1IN-HARDENING COEFFICIENT =,F6.3/20X,22HYOUNG'S MODULUS      =, E11
     2.4,8HMN/M SQ.,15X, 17HPOISSON'S RATIO =,F6.3 /20X,22HMAGNITUDE OF
     3LOAD     =,E11.4,4HMN/M,15X,21HINCLINATION OF LOAD =,F5.1,4HDEG.//)
      WRITE(6,702)
702   FORMAT(26X,11HDEPTH BELOW,12X,13HSTRESS IN THE,10X,20HSTRESS PERPE
     1NDICULAR/30X, 7HSURFACE,9X,16HDIRECTION OF CUT,7X,23HTO THE DIRECT
     2ION OF CUT/33X, 4H(MM),15X,10H(MN/M SQ.),20X,10H(MN/M SQ.)//)
      DO 703 IT=1,NT
      SX=S(IT,1)*1.0E-6
      SZ=S(IT,3)*1.0E-6
      SPX(IT)=SX
      SPZ(IT)=SZ
      IF(SX.GT.1000.)GO TO 703
      WRITE(6,705)DT(IT),SX,SZ
705   FORMAT(32X,F5.3,18X,F7.1,23X,F7.1)
703   CONTINUE
      WRITE(6,704)
```

```
704    FORMAT(///55X,5HTABLE/55X,10H----------)
       WRITE(6,700)
       WRITE(6,701)XKT,XMEW,ET,XNEW,FT,BT
       WRITE(6,802)
802    FORMAT(20X,14HNONDIMENSIONAL,7X,14HNONDIMENSIONAL,12X,14HNONDIMENS
      1IONAL,5X,14HNONDIMENSIONAL/23X,11HDEPTH BELOW,8X,13HSTRESS IN THE,
      26X,20HSTRESS PERPENDICULAR,11X,8HHARDNESS/27X,7HSURFACE,5X,16HDIRE
      3CTION OF CUT,3X,23HTO THE DIRECTION OF CUT,13X,6HVALUES//)
       DO 800 J=1,NT
       IF(SPX(J).GT.1000.)GO TO 800
       SPX(J)=SPX(J)/XKT
       SPZ(J)=SPZ(J)/XKT
       DT(J)=DT(J)*1.0E-3/F*XK
       WRITE(6,805)DT(J),SPX(J),SPZ(J),HRD1(J)
805    FORMAT(26X,F8.3,14X,F7.3,19X,F7.3,12X,F7.3)
800    CONTINUE
       WRITE(6,704)
       WRITE(6,706)
706    FORMAT(1H1)
900    CONTINUE
67     CONTINUE
       GO TO 600
       END
```

```
$IBFTC ALF
      SUBROUTINE ALF(AL)
      DIMENSION R(20)
      COMMON/D/XK,XMEW,F,DEL,E,XNEW
      HPI=355./226.
      K=1
      N2=100
4     N=N2/2
      IF(N*2.NE.N2)STOP
      H=355./113./FLOAT(N2)
      TH=-HPI
      ZI=XI(TH,XMEW,DEL)*COS(TH)
      TH=TH+H
      ZI1=XI(TH,XMEW,DEL)*COS(TH)
      S=ZI+4.*ZI1
      N1=N-1
      DO 2 I=1,N1
      TH=-HPI+H*FLOAT(2*I)
      ZI=XI(TH,XMEW,DEL)*COS(TH)
      TH=-HPI+H*FLOAT(2*I+1)
      ZI1=XI(TH,XMEW,DEL)*COS(TH)
2     S=2.*ZI+4.*ZI1+S
      TH=HPI
      ZI=XI(TH,XMEW,DEL)*COS(TH)
      S=H*(ZI+S)/3.
      R(K)=S
      WRITE(6,25)S,N2
25    FORMAT(1H0,20X,7H*S,N2/*,F10.5,I10)
      K=K+1
      N2=N2*2
      IF(K.GE.3)GO TO 3
      GO TO 4
3     RD=(R(K-1)-R(K-2))/R(K-1)
      RD=ABS(RD)
      IF(RD.LE.0.001)GO TO 8
      GO TO 4
8     AL=COS(DEL)/2./S
      WRITE(6,24)AL
24     FORMAT(1H0,20X,10H*ALPHA = *,F10.5)
      WRITE(6,27)XK,XMEW,F,DEL,E,XNEW
27    FORMAT(1H0,20X,22H*K,MEW,F,DELTA,E,NEW/*,6E12.3/)
      RETURN
      END
```

```
$IBFTC STRN
      SUBROUTINE STRAIN
      DIMENSION SN(4),S(4)
      COMMON/D/XK,XMEW,F,DEL,E,XNEW
      COMMON/SUN/X,Y,AL,SN,S
      IF(X.LT.1.485E-3)GO TO 20
      DO 21 I=1,4
      S(I)=0.
21    SN(I)=0.
      GO TO 25
20    XC=XK
      RAD2=X*X+Y*Y
      RAD=SQRT(RAD2)
      ANGLE=ATAN(X/Y)
24    ZI=XI(ANGLE,XMEW,DEL)
      STR=-2.*AL*ZI/RAD*F
      XK1=1.
      IF(STR.LT.0.)XK1=-1.
      SNR=XK1*(AL*(ABS(F))*(ABS(ZI))/XC/RAD)**(1./XMEW)
      SNC=-SNR
      S(1)=STR*X*X/RAD2
      S(2)=STR*Y*Y/RAD2
      S(3)=(S(1)+S(2))/2.
      S(4)=-STR*X*Y/RAD2
      SN(2)=SNR*Y*Y/RAD2+SNC*X*X/RAD2
      SN(1)=-SN(2)
      SN(3)=0.
      SN(4)=-2.*(SNR-SNC)*X*Y/RAD2
25    RETURN
      END
```

```
$IBFTC XZI
      FUNCTION XI(TH,XMEW,DEL)
      IF(XMEW.GT.0.5)GO TO 1
      IF(XMEW.EQ.0.5)GO TO 2
      XM=SQRT((1.-2.*XMEW)/XMEW/XMEW)
      BR=(EXP(XM*TH)-DEL*EXP(-XM*TH))/(1.-DEL)
      GO TO 11
2     BR=(1.+DEL*TH)
      GO TO 11
1     XN=SQRT((2.*XMEW-1.)/XMEW/XMEW)
      T1=XN*(TH+DEL)
      BR=COS(T1)/COS(XN*DEL)
11    IF(ABS(BR).GE.0.00001)GO TO 10
      XI=0.
      GO TO 3
10    IF(BR)4,5,5
5     XI=BR**XMEW
      GO TO 3
4     XI=-(ABS(BR))**XMEW
3     RETURN
      END
```

```
$IBFTC YLD
      SUBROUTINE YIELD(EP,YLD2)
      COMMON/D/XK,XMEW,F,DEL,E,XNEW
      K=0.
      SP=XK*EP**XMEW
5     S=XK*(EP+SP/E)**XMEW
      TV=(S-SP)/S
      IF(TV-0.001)2,2,3
3     SP=S
      K=K+1
      IF(K.GE.200)GO TO 4
      GO TO 5
4     WRITE(6,6)
6     FORMAT(20X,46H*200 ITERATIONS EXCEEDED IN SUBROUTINE YIELD.*)
2     YLD2=S*S
      RETURN
      END
```

```
$DATA
   0.368E9    0.26       0.368E5  0.0        2067.0E8    0.3
 1
-0.523     0.1882     -107.0
$EOF
```

```
$IBFTC ALFA
      REAL LD
      DIMENSION R(20),R1(20)
      DATA AB1,AB2/1HI,1HR/
      NCASE=9
      DO 67 NI=1,NCASE
      READ(5,44)XK,XMEW,F,DEL,E,XNEW
44    FORMAT(E10.0,F10.3,E10.1,F10.3,E10.0,F10.2)
      WRITE(6,27)XK,XMEW,F,DEL,E,XNEW
27    FORMAT(1H0,20X,22H*K,MEW,F,DELTA,E,NEW/*,6E12.3/)
      WRITE(6,34)
34    FORMAT(1H0,15X,5HLAMDA,15X,5HRATIO,15X,4HBETA,15X,5HDELTA, 3X,4HTY
     1PE,12X,3HAL1,12X,3HAL2/)
      HPI=355./226.
      BETA=DEL
      IF(XMEW-0.5)40,40,41
40    CM=SQRT((1.-2.*XMEW)/XMEW/XMEW)
      GO TO 42
41    CM=SQRT((2.*XMEW-1.)/XMEW/XMEW)
42    DEL=+BETA
      DO 11 MK=1,3
      DEL=800.0
      IF(MK.EQ.2)DEL=-800.0
      IF(MK.EQ.3)DEL=0.
43    CONTINUE
      K=1
      N2=100
4     N=N2/2
      IF(N*2.NE.N2)STOP
      H=355./113./FLOAT(N2)
      TH=-HPI
      ZI=XI(TH,XMEW,DEL)*COS(TH)
      CI=ZI*TAN(TH)
      TH=TH+H
      ZI1=XI(TH,XMEW,DEL)*COS(TH)
      CI1=ZI1*TAN(TH)
      S=ZI+4.*ZI1
      C=CI+4.*CI1
      N1=N-1
      DO 2 I=1,N1
      TH=-HPI+H*FLOAT(2*I)
      ZI=XI(TH,XMEW,DEL)*COS(TH)
      CI=ZI*TAN(TH)
      TH=-HPI+H*FLOAT(2*I+1)
      ZI1=XI(TH,XMEW,DEL)*COS(TH)
      CI1=ZI1*TAN(TH)
      C=2.*CI+4.*CI1+C
2     S=2.*ZI+4.*ZI1+S
      TH=HPI
      ZI=XI(TH,XMEW,DEL)*COS(TH)
      CI=ZI*TAN(TH)
      S=H*(ZI+S)/3.
      C=H*(CI+C)/3.
      R(K)=S
      R1(K)=C
      WRITE(6,25)S,C,N2
25    FORMAT(1H0,20X,9H*S,C,N2/*,2F10.5,I10)
      K=K+1
      N2=N2*2
```

```
      IF(K.GE.3)GO TO 3
      GO TO 4
3     RD=(R(K-1)-R(K-2))/R(K-1)
      RD1=(R1(K-1)-R1(K-2))/R1(K-1)
      RD=ABS(RD)
      RD1=ABS(RD1)
      IF(N2.GE.1600)GO TO 8
      IF(RD.LE.0.001.AND.RD1.LE.0.001)GO TO 8
      GO TO 4
8     RATIO=C/S
      LD=DEL
      IF(ABS(LD).LT.0.00001)GO TO 90
      DELTA=-0.5*ALOG(ABS(LD))
90    BET=ATAN(RATIO)
      IF(LD)19,20,20
20    TYPE=AB1
      GO TO 31
19    TYPE=AB2
31    AL1=COS(BET)/2./S
      AL2=SIN(BET)/2./C
      WRITE(6,30)LD,RATIO,BET,DELTA,TYPE,AL1,AL2
30    FORMAT(1HX,F20.5,F20.5,F19.5,F20.5,6X,A1,2F15.5)
      IF(ABS(DEL).LE.0.100)GO TO 11
      DEL=DEL*0.5
      GO TO 43
11    CONTINUE
67    CONTINUE
      STOP
      END


$IBFTC CXI
      FUNCTION XI(TH,XMEW,DEL)
      IF(XMEW.GT.0.5)GO TO 1
      IF(XMEW.EQ.0.5)GO TO 2
      XM=SQRT((1.-2.*XMEW)/XMEW/XMEW)
      BR=(EXP(XM*TH)-DEL*EXP(-XM*TH))/(1.-DEL)
      GO TO 11
2     BR=(1.+DEL*TH)
      GO TO 11
1     XM=SQRT((2.*XMEW-1.)/XMEW/XMEW)
      T1=(XM*TH+DEL)
      BR=COS(T1)/COS(DEL)
11    IF(ABS(BR).GE.0.00001)GO TO 10
      XI=0.
      GO TO 3
10    IF(BR)4,5,5
5     XI=BR**XMEW
      GO TO 3
4     XI=-(ABS(BR))**XMEW
3     RETURN
      END

$DATA
     .716E9   0.050        .383E5   0.5        2067.0E8    0.3
$EOF
```

Appendix 4.1

Programme for computing residual stresses from experimental data.

Fig.1* gives a flow-chart for the main programme RESID. The various subroutines called by RESID, have the following functions.

CRATE reads the input data with an echo check and calculates the thickness of metal removed and the corresponding deflection at the end of each minute of polishing.

CORECT makes correction for redistribution due to layer removal.

SLIT computes relief due to slitting.

RPLOT is for obtaining the Calcomp plots of the distributions.

A listing of the programme follows from p. 191.

* p. 190

Fig.1 Flow chart for programme RESID.

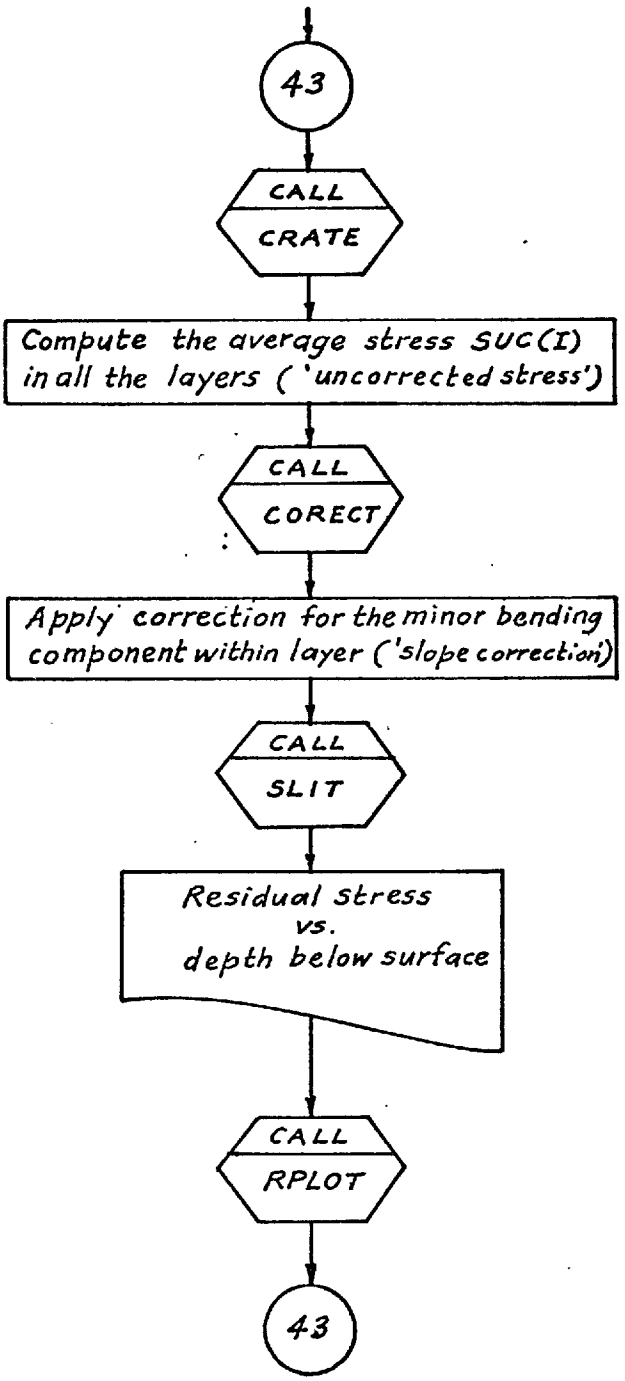

```
      PROGRAM RESID(INPUT,OUTPUT,TAPE5=INPUT,TAPE6=OUTPUT,TAPE25,TAPE27)
C     COMPUTATION OF RESIDUAL STRESSES FROM EXPERIMENTAL DATA
      DIMENSION  A(90), B(90),RR(90), SUC(90), SCOR(90), SD(90), SBNG(90
     1),DEL(90),YY(90),EL(90),GEO(2),FLUID(2)
      COMMON R,DEL,A,BO,S,N,E,DR,ST
      COMMON/CR/SPNO,SFPM,FEED,DEPTH,WEAR,FLUID,GEO/RP/YY,SUC/CR/IST,DS
      READ(5,70)NPROB
70    FORMAT(I2)
      IREG=1
      ICAL=1
      CALL START
      CALL PLOT(1.0,1.0,-3)
43    CALL CRATE
      DO 34 I=1,N
      B(I)=BO-A(I)
34    CONTINUE
      AK2=A(1)
      DO 33 I=2,N
      AK1=A(I)
      A(I)=A(I)-AK2
      AK2=AK1
33    CONTINUE
      A(N+1)=0.
      NN=N+1
      I= 1
      R=R-BO/2.0
       RO= R
C     DELR IS THE CHANGE IN RADIUS DUE TO THE REMOVAL OF LAYER
711   DEL(I)=DEL(I)/3600./180.*3.141
      DELR=-DEL(I)*R*R/(S+DEL(I)*R)
712   R=R+DELR
C     RR(I) IS THE RADIUS AFTER THE REMOVAL OF THE 'I'TH LAYER
C     THE RADIUS RR(I) IS REFFERRED TO THE CURRENT CENTRAL PLANE
      RR(I) = R
      P=B(I)
      AD=RR(I)*ALOG((2.*RR(I)+B(I))/(2.*RR(I)-B(I)))
      IF (I.GT.1) GO TO 706
      EK=1.-1./(1.-RR(I)/RO)/(1.-AD/P)
      DUA=(A(I)+B(I))/2.+RO*(1.-P/AD)
      GO TO 708
706   IF (DELR.EQ.0.) GO TO 709
707   EK=1.-1./(1.-RR(I)/RR(I-1))/(1.-AD/P)
      DUA=(A(I)+B(I))/2.+RR(I-1)*(1.-P/AD)
C     SUC(I) IS THE UNCORRECTED STRESS IN THE 'I'TH LAYER
708   SUC(I)=E*B(I)*RR(I)/A(I)/EK/DUA
      GO TO 710
709   SUC(I)=0.
710   CONTINUE
200    I=I+1
      IF (I.GE. NN)  GO TO 16
      GO TO  711
C     CORRECTION OF RESIDUAL STRESSES FOR REDISTRIBUTION
C     DUE TO LAYER REMOVAL
16    SUC(1)=0.
      SUC(2)=0.
      N1=3
18    CONTINUE
      DO 20 I=1,N
      SCOR(I)=SUC(I)
```

```
20      CONTINUE
        K=1
62      XM=(RR(K)/B(K))*ALOG((RR(K)+B(K)/2.0)/(RR(K)-B(K)/2.0))-1.0
        SMALLE=XM*RR(K)/(XM+1.0)
        CALL COPECT(B,A,K,SUC,E,RR,SD,SBNG,N,RO)
        DO 60 J=1,N
        SCOR(J)=SCOR(J)-SD(J)-SBNG(J)
60      CONTINUE
        K=K+1
        IF (K.GE.NN) GO TO 61
        GO TO 62
61      CONTINUE
C       SLOPE CORRECTION
        DO 165 I=N1,N
        IF (I.EQ.N ) GO TO 133
        F=(SCOR(I)-SCOR(I+1))*A(I)/(A(I)+A(I+1))
133     SCOR(I)=SCOR(I)-F*A(I)/3./(A(I)+B(I))
165     CONTINUE
201     XM=(RO/BO)*ALOG((RO+BO/2.)/(RO-BO/2.))-1.
        SMALLE=XM*RO/(XM+1.)
202     DO 141   I=1,N
        IF(I.EQ.1)GO TO 80
        Y=Y-(A(I-1)+A(I))/2.
        GO TO 81
80      Y=(BO-A(I))/2.
81      YY(I)=BO/2.-Y
        IF(IST.EQ.0) GO TO 142
        EL(I)=ST/BO*2.* Y+DS
        GO TO 141
142     CALL SLIT(TT,Y,E,RO,BO,DR)
        EL(I)=TT
141     CONTINUE
203     WRITE(6,600)SPNO,SFPM,FEED,DEPTH,(GEO(I),I=1,2),WEAR,(FLUID(I),
       1I=1,2)
600     FORMAT(1H1//////20X,*TABLE                              RESIDUAL STRESS VS.
       1DEPTH BELOW SURFACE.*//20X,*SPECIMEN NO. *,A6/20X,*MACHINING PROC
       2SS - TURNING.   WORK MATERIAL - XC-45 STEEL.   TOOL MATERIAL - CA
       3BIDE P-20.*/20X,*CUTTING SPEED -*,F4.0,*M/MIN.   FEED - *,F4.2,*M
       4/REV.   DEPTH OF CUT - *,F4.2,*MM*/20X,*TOOL GEOMETRY *,2A10,*
       5LANK WEAR - *,F4.2,*MM   CUTTING FLUID - *,2A10///)
        WRITE(6,303)
        DO 415 I=1,N
        YY(I)=YY(I)*25.4
        SCOR(I)=SCOR(I)/145.038
        EL(I)=EL(I)/145.038
415     CONTINUE
303     FORMAT(28X,*STRESS LOCATION*,6X,*STRESS IN*6X,*RELIEF ON*,6X,
       1*STRESS IN*/30X,*BELOW SURFACE*,6X,*SLIT RING*,7X,*SLITTING*,2X,
       2*ORIGINAL RING*/39X,*(MM)*5X,*(MN/M SQ.)*,5X,*(MN/M SQ.)*,5X,
       3*(MN/M SQ.)*/)
        LL=2
        DO 414 I=N1,N
        SUC(I)=SCOR(I)+EL(I)
        LL=LL+1
        IF(LL.NE.3)GO TO 414
        WRITE(6,304)YY(I),SCOR(I),EL(I),SUC(I)
304     FORMAT(36X,F7.5,3(7X,F8.1))
        LL=0
414     CONTINUE
```

```
      WRITE(6,305)
305   FORMAT( ///58X,5HTABLE/58X,9H---------)
      CALL RPLOT(N,NPROB,IREG,ICAL)
      IF((ICAL-1).EQ.NPROB) GO TO 44
      GO TO 43
44    STOP
      END
```

```
$IBFTC CRATE
      SUBROUTINE CRATE
C     COMPUTATION FOR CURRENT THICKNESS VS. TIME VALUES
C     AND RATE OF METAL REMOVAL
      DIMENSION X(90),Y(90),DL(90),AR(90),IDL(90),GEO(2),FLUID(2)
      COMMON R,DL,AR,BO,S,K,E,DR,ST
      COMMON/CR/SPNO,SFPM,FEED,DEPTH,WEAR,FLUID,GEO,IST
C     'SPNO' IS THE IDENTIFICATION NUMBER OF THE SPECIMEN.
13    READ(5,14)SPNO
14    FORMAT(A6)
      READ(5,40)IST,GF
C     IF THE SPECIMEN IS CURVED, 'IST' IS SET TO ZERO.
C     'GF' IS THE STRAIN-GAUGE FACTOR.
40    FORMAT(I1,F10.5)
C     'SFPM' IS THE CUTTING SPEED IN FEET PER MINUTE.
C     'FEED' IS THE FEED IN INCHES PER REVOLUTION.
C     'DEPTH' IS THE DEPTH OF CUT IN INCHES.
C     'WEAR' IS THE FLANK WEAR IN INCHES.
C     'FLUID' AND 'GEO' REPRESENT RESPECTIVELY THE CUTTING FLUID USED
C     AND THE GEOMETRY OF THE CUTTING TOOL (ASME SPECIFICATION).
      READ(5,171)SFPM,FEED,DEPTH,WEAR,(FLUID(I),I=1,2),(GEO(I),I=1,2)
171   FORMAT(4F10.4/4A10)
      SFPM=SFPM/3.28
      FEED=FEED*25.4
      DEPTH=DEPTH*25.4
      WEAR=WEAR*25.4
C     G1 AND G2 ARE THE STRESSES OBTAINED FROM THE STRAIN GAUGE READINGS
C     'E' IS THE MODULUS OF ELASTICITY.
      READ(5,51)G1,G2,E
51    FORMAT(2F10.5/E16.7)
C     'BO' IS THE ORIGINAL THICKNESS, 'BF' THE FINAL THICKNESS,'W' THE
C     WIDTH, 'C' THE CHORDAL LENGTH, AND 'R' THE OUTER RADIUS OF THE
C     EXPOSED AREA OF THE SPECIMEN.
      READ(5,10)BO,BF,W,C,R
10    FORMAT(5F10.5)
C     'Y(I)' ARE THE SCALED VALUES OF CURRENT CORRESPONDING TO 'X(I)',
C     THE VALUES OF TIME FROM SWITCH-ON, FOR A TOTAL NUMBER OF 'N'
C     POINTS FROM THE U.V. CHART.
C     'YO' IS THE SCALED VALUE OF CURRENT BEFORE SWITCHING ON THE SUPPLY
      READ(5,1)N,(X(I),I=1,N)
1     FORMAT(I2/(5F10.5))
      READ(5,2)YO,(Y(I),I=1,N)
2     FORMAT(F10.5/(5F10.5))
      IF(IST.EQ.0)GO TO 46
C     'IDL(I)' IN MINUTES AND 'DL(I)' IN SECONDS OF ARC, TOGETHER
C     REPRESENT THE ANGULAR DEFLECTION, AT THE END OF THE 'I'TH MINUTE
C     FROM THE COMMENCEMENT OF POLISHING.
C     'K' IS THE TOTAL NUMBER OF DEFLECTION VALUES READ IN.
      READ(5,47)K,((IDL(I),DL(I)),I=1,K)
47    FORMAT(I2/(5(I2,F4.1,4X)))
      GO TO 48
46    READ(5,30)K,((IDL(I),DL(I)),I=1,K)
30    FORMAT(I2/(5(I1,1X,F4.1,4X)))
48    WRITE(6,15)SPNO
15    FORMAT(1H1,19X,*SPECIMEN NO.*,A6)
      WRITE(6,34)BO,BF,W,C,R
34    FORMAT(/20X,*BO,BF,W,C,R/*,4F10.5,F15.5)
      WRITE(6,19)YO,G1,G2,E
19    FORMAT(/20X,*YO=*,F6.2,5X,*G1,G2,E/*,2F10.5,E10.2)
```

```
      WRITE(6,17)
17    FORMAT(  //20X,*NO.*,16X,*X(I)*,16X,*Y(I)*/ )
      DO 18 I=1,N
      WRITE(6,16)I,X(I),Y(I)
16    FORMAT(  21X,I2,10X,F10.1,10X,F10.2)
18    CONTINUE
      WRITE(6,32)
32    FORMAT(//20X,*NO.*,4X,*A.C.R.*,3X,*NO.*,4X,*A.C.R.*,3X,*NO.*,4X,
     1*A.C.R.*,3X,*NO.*,4X,*A.C.R.*,3X,*NO.*,4X,*A.C.R.*/)
      WRITE(6,31)((I,IDL(I),DL(I)),I=1,K)
31    FORMAT((17X,5(4X,I2,3X,I2,1X,F4.1)))
      IF(IST.EQ.0)GO TO 41
      SD=-(G1+G2)/2.
      ST=-(G1-G2)/2.
      R=ABS(E*BO/2./ST)
      SB=ST+SD
      WRITE(6,42)R,SB
42    FORMAT(1H0,19X,*RAD. AFTER CUT-OFF =*,1X,F10.5,5X,*STRESS RELIEF A
     1T SURFACE UPON CUT-OFF = *,F10.1,* PSI.*)
      GO TO 43
41    R1=R+(G2-G1)/2./3.141
26    DR=(R*ARSIN(G1/2./R)-R1*ARSIN(G2/2./R1))/3.141
      DR=-DR
      R2=R+DR
      IF((ABS(R2-R1)).LT.0.00001) GO TO 28
      R1=R2
      GO TO 26
28    R=R2
      WRITE(6,27)R,DR
27    FORMAT(1H0,19X,*RAD. AFTER SLITTING=*,F10.5,5X,*CHANGE IN RAD.=*,
     1F10.5)
43    DO 33 I=1,K
      DL(I)=IDL(I)*60.0+DL(I)
33    CONTINUE
      FI=6.3
      AREA=0.0
      DELTA=0.0
      TP=0.0
      J=1
      TYO=Y(1)
      TO=X(1)
      T=30.0
      NN=N-1
      DO 3 I=1,NN
      TX=X(I+1)
11    IF(TX.GE.T) GO TO 6
      DELTA=(Y(I+1)+TYO-2.0*YO)*(X(I+1)-TO)/2.0/FI
      AREA=AREA+DELTA
      TYO=Y(I+1)
      TO=X(I+1)
      GO TO 3
6     TY=Y(I)+(Y(I+1)-Y(I))/(X(I+1)-X(I))*(T-X(I))
      DELTA=(TY+TYO-2.0*YO)*(T-TO)/2.0/FI
      AREA=AREA+DELTA
      IF((T-TP).NE.(60.)) GO TO 20
      AR(J)=AREA
      TP=T
      J=J+1
20    TO=T
```

```
      TYO=TY
      T=T+30.0
      IF((TX+30.).EQ.T) GO TO 3
      GO TO 11
3     CONTINUE
      IF(IST.EQ.0)GO TO 44
      S=C
      GO TO 45
44    S=2.0*R*ARSIN(C/2.0/R)
45    VOL=S*W*(BO-BF)
      RM=VOL/AREA
      CUR=AREA/X(N)
      WRITE(6,12)S,VOL,RM,CUR
12    FORMAT(//20X,*S,VOL,RM,CURRENT/*,F10.5,2F15.9,F6.3)
      AR1=S*W
      K=K-1
      DO 25 I=1,K
      AR(I)=AR(I)*RM/AR1
      DL(I)=DL(I)-DL(I+1)
25    CONTINUE
      RETURN
      END

$IBFTC CORRECT
      SUBROUTINE CORECT(B,A,I,SUC,E,R,SD,SBNG,N,RO)
      DIMENSION B(90),A(90),SUC(90),R(90),SD(90),SBNG(90)
      Y=(B(I)-A(I+1))/2.
      RD=R(I)
      IF(I.EQ.1) GO TO 10
      RP=R(I-1)
      DR=R(I)-R(I-1)
      GO TO 11
10    RP=RO
      DR=R(I)-RO
11    BD=RD*ALOG((2.*RD+B(I))/(2.*RD-B(I)))
      SEC=DR*B(I)/(RP*B(I)-(BD-B(I))*DR)
      DO 55 K=1,N
      IF (K.LE.I)GO TO 56
      SD(K)=A(I)/B(I)*SUC(I)
      SBNG(K)=-E*(BD/B(I)-RD/(Y+RD))*SEC
      IF (K.EQ. N )  GO TO 100
      Y=Y-(A(K)+A(K+1))/2.
      GO TO 55
56    SD(K)=0.
      SBNG(K)=0.
55    CONTINUE
  100  RETURN
      END

$IBFTC SLIT
      SUBROUTINE SLIT(TT,Y,E,RZ,BO,DR)
      RO=RZ-DR
      BOD=RZ*ALOG((2.*RZ+BO)/(2.*RZ-BO))
      SEC=DR*BO/(BO*RO-DR*(BOD-BO))
      TT=E*(BOD/BO-(RO+DR)/(Y+(RO+DR)))*SEC
70    RETURN
      END
```

```
$IBFTC RPL
      SUBROUTINE RPLOT(N,NPROB,IREG,ICAL)
C     PLOTTING OF RESIDUAL STRESSES VS. DEPTH BELOW SURFACE.
      DIMENSION YY(88),SUC(88),IBCD(7),IX(3),IY(3),IL1(10),IL2(8),IL3(8)
     1,Y(90),S(90),IL0(2),GEO(2),FLUID(2),IB(6)
      EQUIVALENCE(Y(3),YY(1)),(S(3),SUC(1))
      COMMON/CR/SPNO,SFPM,FEED,DEPTH,WEAR,FLUID,GEO/RP/Y,S/CR/IST
      DATA(IB(I),I=1,6)/55HFIG.     RESIDUAL AXIAL STRESS VS. DEPTH BELO
     1W SURFACE./
      DATA(IBCD(I),I=1,7)/64HFIG.     RESIDUAL CIRCUMFERENCIAL STRESS VS
     1. DEPTH BELOW SURFACE/
      DATA(IX(I),I=1,3)/24HDEPTH BELOW SURFACE (MM)/
      DATA(IY(I),I=1,3)/26HRESIDUAL STRESS (10  N/M )/
      DATA(IL0(I),I=1,2)/12HSPECIMEN NO./
      DATA(IL1(I),I=1,10)/91HMACHINING PROCESS - TURNING.   WORK MATERIA
     1L - XC-45 STEEL.   TOOL MATERIAL - CARBIDE P-20./
      DATA(IL2(I),I=1,8)/72HCUTTING SPEED -      M/MIN.   FEED -      MM/R
     1EV.   DEPTH OF CUT -      MM./
      DATA(IL3(I),I=1,8)/75HTOOL GEOMETRY -                          FLANK
     1WEAR -      MM  CUTTING FLUID - /
      N=N-2
      DO 20 I=1,N
20    SUC(I)=SUC(I)/10.0
      YY(N+1)=-0.05
      YY(N+2)=0.02
      SUC(N+1)=-60.0
      SUC(N+2)=20.0
      CALL PLOT(0.0,+0.5,3)
      CALL PLOT(0.0,0.0,2)
      CALL PLOT(+0.5,0.0,2)
      CALL PLOT(+0.5,8.3,3)
      CALL PLOT(0.0,8.3,2)
      CALL PLOT(0.0,7.8,2)
      CALL PLOT(11.7,7.8,3)
      CALL PLOT(11.7,8.3,2)
      CALL PLOT(11.2,8.3,2)
      CALL PLOT(11.2,0.0,3)
      CALL PLOT(11.7,0.0,2)
      CALL PLOT(11.7,+0.5,2)
      CALL AXIS(2.5,3.0,2H  ,2,7.0,0.0,0.0,0.02)
      CALL SYMBOL(5.0,2.5,0.1,IX,0.0,24)
      IF(IST.EQ.0)GO TO 11
      CALL SYMBOL(3.0,1.5,0.1,IB,0.0,55)
      CALL PLOT(8.5,1.4,3)
      GO TO 12
11    CALL SYMBOL(3.0,1.5,0.1,IBCD,0.0,64)
      CALL PLOT(9.5,1.4,3)
12    CALL PLOT(3.0,1.4,2)
      CALL SYMBOL(3.0,1.2,0.07,IL0,0.0,12)
      CALL SYMBOL(3.91,1.2,0.07,SPNO,0.0,6)
      CALL SYMBOL(3.0,1.0,0.07,IL1,0.0,91)
      CALL SYMBOL(3.0,0.8,0.07,IL2,0.0,72)
      CALL NUMBER(4.12,0.8,0.07,SFPM,0.0,-1)
      CALL NUMBER(5.50,0.8,0.07,FEED,0.0,2)
      CALL NUMBER(7.50,0.8,0.07,DEPTH,0.0,2)
      CALL SYMBOL(3.0,0.6,0.07,IL3,0.0,75)
      CALL SYMBOL(4.12,0.6,0.07,GEO,0.0,20)
      CALL NUMBER(6.57,0.6,0.07,WEAR,0.0,2)
      CALL SYMBOL(8.25,0.6,0.07,FLUID,0.0,20)
```

```
      CALL AXIS(2.5,0.5,2H  ,2,6.0,90.0,-50.0,20.0)
      CALL SYMBOL(2.0,2.5,0.1,IY,90.0,26)
      CALL SYMBOL(1.9,4.4,0.1,6H7    2,90.0,6)
      CALL LINE(YY,SUC,N,1,-1,1)
      IF(ICAL.EQ.NPROB)GO TO 6
      ICAL=ICAL+1
      IF(IREG.EQ.3)GO TO 8
      IREG=IREG+1
      CALL PLOT(0.0,9.0,-3)
      GO TO 10
8     IREG=1
      CALL PLOT(13.0,-18.0,-3)
      GO TO 10
6     CALL ENPLOT(13.0)
      ICAL=ICAL+1
10    RETURN
      END
```

```
$DATA
'
 1
22A
0    0.0
369.        0.0098     0.047      0.0
AIR.                   (6 5 0 90 60 0.76)
0.13982     0.17388
          30.0E006
0.09720     0.09500    0 .37417   1.00332    1.0623
17
0.0         8.0        9.5        15.0       26.0
38.         47.        61.        102.       300.
600.        900.       1200.      1500.      1800.
2100.       2400.
1.09
4.92        4.89       3.90       3.38       2.85
2.55        2.33       2.22       2.11       2.05
2.05        2.04       2.04       2.05       2.07
2.07        2.07
41
7 08.5      7 01.6     6 50.0     6 38.1     6 27.7
6 19.4      6 12.8     6 07.4     6 03.5     6 01.0
5 59.7      5 59.0     5 59.4     6 00.4     6 01.6
6 03.3      6 05.3     6 07.6     6 09.8     6 12.6
6 15.3      6 18.1     6 20.9     6 23.5     6 26.2
6 29.1      6 31.6     6 34.4     6 36.7     6 39.2
6 41.8      6 44.5     6 47.0     6 49.6     6 51.8
6 54.4      6 56.6     6 59.3     7 01.3     7 03.5
7 05.9
'
```

Appendix 4.2

Analysis of the accuracy of stress determination

To begin with, accuracy of the measurement of specimen thickness and that of deflection are considered.

(a) Thickness of the specimen

The following table gives a set of measured values of thickness (for specimen 22A) over the area of layer removal, in units of 0.001 in.

Table 1

Circumferential position	Axial position			
	1	2	3	4
1	96.40	97.17	97.15	97.24
2	96.44	97.54	97.47	97.18
3	96.46	97.23	97.28	97.11
4	96.46	97.43	97.39	97.21
5	96.44	97.5[illegible]	97.58	97.30
6	96.57	97.55	97.60	97.44
7	96.65	97.40	97.48	97.44

Estimate of standard deviation = 40.6×10^{-5} in.

95% confidence limits for the mean thickness (average of 28 readings), using t-distribution:

$$|\delta b| = \pm 15.8 \times 10^{-5} \text{ in.}$$

Hence, the maximum relative error in estimating the average thickness

$$\frac{|\delta_b|}{b} = 0.0016$$

(b) Thickness of layer removed

Measurement of thickness of the specimen after layer removal, corresponding to the same positions as in Table 1, yielded the following data for the average thickness at each of the 4 axial positions.

Table 2

	Axial position			
	1	2	3	4
Before removal	98.48	98.73	98.54	98.43
After removal	96.41	96.65	96.39	96.28
Thickness of layer	2.07	2.08	2.15	2.15

From the 4 values for thickness of layer,

$$\text{Mean} = 2.10 \times 10^{-3} \text{ in.}$$
$$\text{Estimate of s.d.} = 5.8 \times 10^{-5} \text{ in.}$$

Using t-distribution, 95% confidence limits for the average layer thickness

$$|\delta a| = \pm 9.3 \times 10^{-5} \text{ in.}$$

Hence the estimated maximum relative error in the measurement of thickness

$$|\delta a|/a = 0.0044$$

(c) Deflection

The following set of readings was taken by the autocollimator, the target being the front silvered mirror attached to the specimen mounted as during layer removal.

Table 3

Se. No.	Reading
1	4' 45.7"
2	4' 45.9"
3	4' 45.9"
4	4' 45.9"
5	4' 46.0"
6	4' 45.9"
7	4' 45.8"
8	4' 45.7"
9	4' 45.8"
10	4' 46.0"

Mean = 4' 45.86"

Estimate of s.d. = 0.107"

95% confidence limits within which a single deflection reading will lie (for normal distribution)

$= \pm 0.21$ seconds of arc or $\pm 1.0 \times 10^{-6}$ radians.

(d) Circumferential length (S) of the exposed region

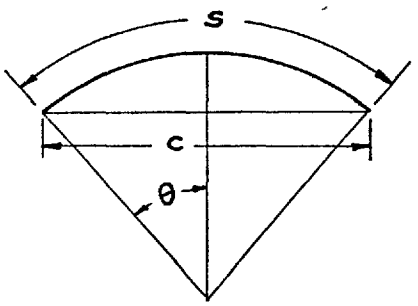

The Measuring Machine (MU-214B) was used to measure c. S was calculated from the relation (Fig.1):

$$S = 2R \sin^{-1}\left(\frac{c}{2R}\right)$$

The most probable error in S is given by

$$|\delta S| = \sqrt{\left(\frac{\partial S}{\partial R} \cdot \delta R\right)^2 + \left(\frac{\partial S}{\partial c} \cdot \delta c\right)^2}$$

Taking typical values,

$R = 1.069$ in. $\quad \delta R$ (max) $= 0.0005$ in.

$c = 1.00332$ in. $\quad \delta c$ (max) $= 0.0005$ in.

$$\frac{|\delta S|}{S} = 0.0005$$

(e) Stress released due to slitting

For the purpose of estimating the order of accuracy in the calculated value, simple-bending expressions may be used:

$$\frac{\sigma}{y} = \frac{M}{I} = E\left(\frac{1}{R_o} - \frac{1}{R_1}\right) = \frac{E\,(R_1 - R_o)}{R_m^{\,2}}$$

where $R_m^{\,2} = R_o\, R_1$

Since $(R_1 - R_o) \simeq \Delta g/2\pi$, where Δg is the change in the spacing between scribed lines upon slitting (appendix 4.3),

$$\sigma = \frac{E\, y\, \Delta g}{2\pi R_m^{\,2}}$$

The most probable error in σ

$$|\delta\sigma| = \sqrt{\left\{\frac{\partial\sigma}{\partial(\Delta g)}\ \delta(\Delta g)\right\}^2 + \left\{\frac{\partial\sigma}{\partial R_m}\ \delta R_m\right\}^2}$$

The following typical values have been used.

$E = 30 \times 10^6$ psi $\qquad y = 0.051$ in.

$\Delta g = 0.0134$ in. $\qquad \delta(\Delta g) = 0.00006$ in.

$R_m = 1.069$ in. $\qquad \delta R_m = 0.0005$ in.

$\therefore\ |\delta\sigma| = 12$ psi $\simeq 0.08$ MN/m^2

(f) Average stress in a layer (by layer removal)

From equation (3) of appendix 4.3, the average stress in a layer

$$\sigma = \frac{E\, b^2\, \Delta\theta}{6Sa}$$

The most probable error in σ is given by

$$|\delta\sigma| = \sqrt{\left(\frac{\partial\sigma}{\partial a}\cdot\delta a\right)^2 + \left(\frac{\partial\sigma}{\partial b}\cdot\delta b\right)^2 + \left(\frac{\partial\sigma}{\partial(\Delta\theta)}\cdot\delta(\Delta\theta)\right)^2 + \left(\frac{\partial\sigma}{\partial S}\cdot\delta S\right)^2}$$

$$\text{or}\quad \frac{|\delta\sigma|}{\sigma} = \sqrt{\left(\frac{\delta a}{a}\right)^2 + \left(\frac{2\delta b}{b}\right)^2 + \left(\frac{\delta(\Delta\theta)}{\Delta\theta}\right)^2 + \left(\frac{\delta S}{S}\right)^2}$$

Taking typical values (specimen 11A),

$a = 0.00005$ in.

$b = 0.10097$ in.

$\Delta\theta = 0.000065$ radians.

$R_m = 1.067$ in.

$S = 0.9670$ in.

$\sigma = 68500$ psi.

From the sections (a) - (d),

$$\frac{|\delta a|}{a} = 0.0044$$

$$\frac{2|\delta b|}{b} = 0.0032$$

$$\frac{|\delta(\Delta\theta)|}{\theta} = 0.0318$$

$$\text{and}\ \frac{|\delta S|}{S} = 0.0005$$

Hence $|\delta\sigma| = 2210$ psi or 15.2 MN/m^2

To compare with the 'discrete' method, a thickness of layer of 0.00020 in. is considered:

$$a = 0.00020 \text{ in.}$$

$$\Delta\theta = 0.000209 \text{ radians.}$$

$$\frac{\delta(\Delta\theta)}{\Delta\theta} = 0.00956$$

$$|\delta\sigma| = 606 \text{ psi} \quad \text{or} \quad \underline{4.2 \text{ MN/m}^2}$$

Appendix 4.3

Relationship between the change in radius and the change in slope at the free end upon layer removal

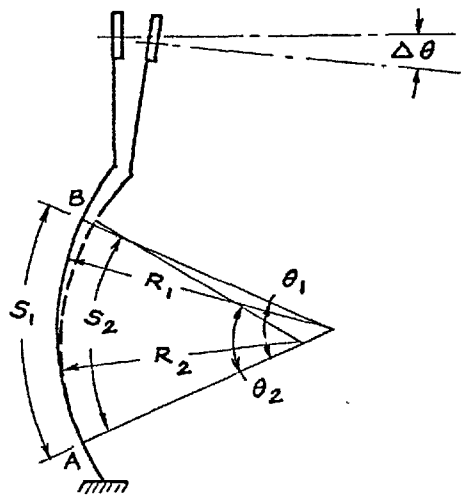

Referring to the above figure, $\Delta\theta$ is the change in slope upon the removal of a layer of thickness 'a' over an area AB, with initial circumferential length S_1. Denoting changes in the quantities by using the prefix Δ,

$$\Delta R = R_2 - R_1 = \left(\frac{S_2}{\theta_2} - \frac{S_1}{\theta_1}\right) = \left(\frac{S_1 + \Delta S}{\theta_1 + \Delta\theta} - \frac{S_1}{\theta_1}\right)$$

$$= \frac{\theta_1 \cdot \Delta S - S_1 \cdot \Delta\theta}{\theta_1 (\theta_1 + \Delta\theta)}$$

$$= \frac{R_1 \cdot \Delta S - R_1^2 \cdot \Delta\theta}{(S_1 + R_1 \cdot \Delta\theta)} \qquad (1)$$

Assuming the change in the mean circumferential length S to be negligible,

$$\Delta R = \frac{-R_1^2 \cdot \Delta\theta}{(S_1 + R_1 \Delta\theta)} \qquad (2)$$

However, ΔS may be taken into account as follws. If σ is the average stress in the layer and b the thickness of specimen,

$$\Delta S \simeq \frac{a\,\sigma\,w}{b\,w\,E} = \frac{a\,\sigma\,S_1}{b\,E}$$

$$\Delta\theta \simeq S_1\left(\frac{1}{R_2} - \frac{1}{R_1}\right) = \frac{S_1 M}{E\,I} = \frac{6\,S_1\,a\,\sigma}{E\,b^2} \qquad (3)$$

$$\therefore\ \Delta S \simeq \left(\frac{b}{6}\right)\Delta\theta \qquad (4)$$

Substituting this value for ΔS in equation (1)

$$\Delta R = \frac{(\theta_1 \Delta\theta\ b/6 - S_1 \Delta\theta)}{\theta_1\ (\theta_1 + \Delta\theta)}$$

$$= \frac{\Delta\theta\ R_1\ (b/6 - R_1)}{(S_1 + \Delta\theta\ R_1)}$$

Where $b/6 \ll R_1$ and $\Delta\theta \ll \theta_1$, ΔR may be obtained with sufficient accuracy from

$$\Delta R = \frac{\Delta\theta\ R_1^2}{S_1} \qquad (5)$$

Appendix 4.4

Change in radius due to slitting

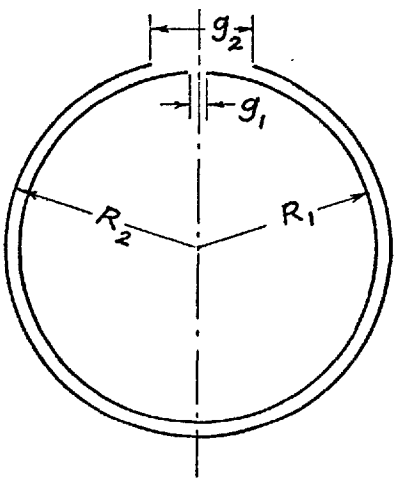

R_I and R_2 are the mean radii and g_1 and g_2 the spacing between the scribed lines, before and after slitting respectively. It is assumed that the moment released due to slitting causes a change in curvature without affecting the mean circumferential length between the scribed lines. Thus

$$2\pi R_1 - A\,(g_1) = 2\pi R_2 - A\,(g_2)$$

where $A\,(g_1)$ and $A\,(g_2)$ are respectively the arc lengths of the ring in the gaps g_1 and g_2 given by

$$A\,(g_1) = R_1 \left\{2 \sin^{-1}\left(\frac{g_1}{2R_1}\right)\right\} \text{ etc.}$$

$$R_2 - R_1 = \frac{1}{\pi}\left\{R_2 \sin^{-1}\left(\frac{g_2}{2R_2}\right) - R_1 \sin^{-1}\left(\frac{g_1}{2R_1}\right)\right\}$$

where $g_1 \ll 2R_1$ and $g_2 \ll 2R_2$

$$R_2 - R_1 \simeq \frac{1}{2\pi}\,(g_2 - g_1)$$

Appendix 5.1

Dimensional analysis

Residual-stress distribution obtained from the model may be expressed as a function of the parameters:

$$\sigma = f(y, P, k, n, E, \nu, \beta)$$

Since n, ν and β are dimensionless, σ may be expressed as

$$\sigma = C\, y^m P^n k^\ell E^p \qquad (1)$$

where m, n, ℓ and p are constant exponents and C is a dimensionless factor.

Using F and L for units of force and length respectively, in equation (1),

$$\frac{F}{L^2} = L^m \left(\frac{F}{L}\right)^n \left(\frac{F}{L^2}\right)^\ell \left(\frac{F}{L^2}\right)^p$$

Hence, $n + \ell + p = 1$

$$m - n - 2\ell - 2p = -2 \qquad (2)$$

Putting $\ell + p = q$, equation (2) gives

$$m = -n = (q - 1)$$

Substituting this result in equation (1) and rearranging,

$$\left(\frac{\sigma}{k}\right) = C \left(\frac{y}{P/k}\right)^{q-1} \left(\frac{E}{k}\right)^p$$

It follows that, by representing the residual-stress distributions in terms of the nondimensional stress (σ /k) and the nondimensional depth below surface ($\frac{y}{P/k}$), P will have no effect on the distributions.

References

1. Kahles, J.F., Bellows, G., and Field, M., "Surface Integrity Guide Lines for Machining", ASTME Technical Paper MR 69-730, 1969.
2. Forrest, P.G., "Fatigue of Metals", Pergamon Press, Oxford, 1962, p.175.
3. Rowland, E.S., "Effect of Residual Stress on Fatigue", Proceedings of the Tenth Sagamore Army Materials Research Conference, Syracuse University Press, 1964, pp.229-244.
4. Kravchenko, P.Ye., "Fatigue Resistance", Pergamon Press, Oxford, 1964.
5. Mattson, R.L., and Roberts, J.G., "Effect of Residual Stresses Induced by Strain Peening upon Fatigue Strength", Proceedings of the Symposium on Internal Stresses and Fatigue, General Motors, Elsevier, 1959, pp.337.
6. Almen, J.O., and Black, P.H., "Residual Stresses and Fatigue in Metals", McGraw-Hill Book Company, Inc., 1963, pp.226.
7. Dolan, T.J., "Residual Stress, Strain Hardening and Fatigue", Proceedings of the Symposium on Internal Stresses and Fatigue in Metals, Elsevier Publishing co., London, 1959, p.284.
8. Fielding, J., and Redfern, A.K., "Sustained Stresses and Their Effect on Stress Corrosion Cracking", AGARD Conference Proceedings No.53, Feb., 1970 Paper No.7.

9. Forsyth, P., "The Examination of Service Failures", AGARD Conference Proceedings No.53, Feb., 1970, Paper No.1.

10. Brown, R.J., "The Relative Influence of Stress and Environment on Aluminium", AGARD Conference Proceedings No.53, Feb., 1970, Paper No.3.

11. Weck, R., "Transverse Contractions and Reaction Stresses in Butt Welded Mild Steel Plates", Admiralty Ship Welding Committee Report No.R4, 1950.

12. Gurney, T.R., "Residual Stresses in a Large Circular Disc Caused by Local Heating and Cooling at Its Centre", BWRA Research Document, Report No. E/15/67, Jan., 1968.

13. Merwin, J.E., and Johnson, K.L., "An Analysis of Plastic Deformation in Rolling Contact", Proceedings of the Symposium on Fatigue in Rolling Contact, Institution of Mechanical Engineers, 1963, pp.145-154.

14. Denton, A.A., "A Study of Residual Stress Distribution in Tubes and Plates Subjected to Certain Deformation Processes", Ph.D. thesis, University of London, 1966.

15. Alexander, J.M., and Brewer, R.C., "Manufacturing Properties of Materials", D. Van Nostrand Company Ltd., London, 1963, p.436.

16. Glikman, L.A., and Stepanov, V.A., "Residual Stresses Caused by Grinding", Engineer's Digest (British Ed.), Vol.8, Aug., 1947, pp.276-277.

17. Frisch, J., and Thomsen, E.G., "Residual Grinding Stresses in Mild Steel", Trans. ASME, Vol.73, April, 1951, pp.337-346.

18. Marshal, E.R., and Shaw, M.C., "Forces in Dry Surface Grinding", Trans. ASME, Vol.74, Jan., 1952, pp.51-59.

19. Letner, H.R., "Residual Grinding Stresses in Hardened Steel", Trans. ASME, Vol.77, Oct., 1955, pp.1089-1098.

20. Letner, H.R., "Influence of Grinding Fluids upon Residual Stresses in Hardened Steel", ASME Paper 55-A-123.

21. Colwell, L.V., Sinnot, M.J., and Tobin, J.C., "The Determination of Residual Stresses in Hardened and Ground Steel", Trans. ASME, Vol.77, Oct., 1955, pp.1099-1105.

22. Kahles, J.F., and Field, M., "Surface Integrity - A New Requirement for Surfaces Generated by Material-Removal Methods", Conference on Properties and Metrology of Surfaces, Institution of Mechanical Engineers, Paper No.4, April, 1968.

23. Matalin, A.A., "Kachestvo poverkhnosti i ekspluatatsionnye svoistva detalei mashin (Surface Finish and Operating Properties of Machine Components)", Mashgiz, M.L., 1956.

24. "Ostatochnye napryazheniya v poverknostom sloe (Residual stresses in the surface layer)", Russian Translating Programme, RTS 5813,NationalLending Library, Boston Spa., Yorkshire.

25. Shaw, M.C., discussion of reference 17.

26. Field, M., "Surface Integrity in Conventional and Non-conventional Machining", Paper presented at the Seminar on Advancements in Machine Tools and Production Trends, The Pennsylvania State University, July, 1969.

27. Henriksen, E.K., "Internal Stresses in Machined Surfaces", International Association for Testing Materials, London Congress, 1937, pp.173-176.

28. Henriksen, E.K., "Residual Stresses in Machined Surfaces", Transactions of Danish Academy of Technical Sciences, No.7, 1948.

29. Henriksen, E.K., "Residual Stresses in Machined Surfaces", Trans. ASME, Vol.73, Jan., 1951, pp.69-76.

30. Henriksen, E.K., "Residual Stresses from Machining Operations", Paper No.9, ASTE Annual Collected Papers, 1957.

31. Herbert, E.G., "Work-Hardening Properties of Materials", Trans. ASME, Vol.48, 1926, p.705.

32. Digges, T.G., "Effect of Lathe Cutting Conditions on the Hardness of Carbon and Alloy Steels", Trans. ASME, Vol.54, 1932, p.286.

33. Thomassen, L., and D.M. McCutcheon, "X-ray Determination of Depth of Cold-Working by Machining", Mechanical Engineering, Vol.56, March, 1934, pp.155-157.

34. Curtiss-Wright Corporation, "Increased Production, Reduced Costs", U.S. Air Force Machinability Report, Vol.2, 1951, p.164.

35. Colwell, L.V., "Residual Stresses in Metal Cutting", Paper No.56, Proceedings of the Conference on Technology of Engineering Manufacture, London, March, 1958.

36. Vasil'ev, D.M., "X-ray Diffraction Study of the Residual-Stress Distribution in Manufactured Articles", Industrial Lab., Vol.32, No.6, June, 1966, pp.860-863.

37. Prikhod'ko, E.V., "Determination of Residual Stresses Below the Surface by Cutting Solid Cylinders", Industrial Lab., Vol.28, No.12, Aug., 1963, pp.1580-1584.

38. Birger, I.A., "Determination of Residual Stresses in Hollow and Solid Cylinders", Industrial Lab., Vol.28, No.12, Aug., 1963, pp.1584-1587.

39. Birger, I.A., "Methods of Determining Residual Stresses in Discs", Industrial Lab., Vol.28, No.7, Jan., 1963, pp.907-915.

40. Birger, I.A., "Determination of Residual Stresses in Thin-Walled Tubes", Industrial Lab., Vol.28, No.9, March, 1963, pp.1182-1188.

41. Birger, I.A., "Methods for Determining Residual Stresses in Bars and Plates", Industrial Lab., Vol.28, No.5, Dec., 1962, pp.627-634.

42. Davidenkov, N.N., "Summary of Discussion 'Classification and Detection of Residual Stresses'", Industrial Lab., Vol.26, No.7, March, 1961, pp.922-923.

43. Titov, V.K., and Lagutin, V.P., "On Errors in Determining the Residual Stresses in Hardened Gray Cast Iron by the Mechanical Method", Industrial Lab., Vol.25, No.1, Jan., 1959, pp.106-108.

44. Semko, M.F., et al, "Residual Stresses in Machined Workpieces", Russian Engineering Journal, Vol.XLVl,No.12, 1966.

45. Isaev, A.I., and Ovseenko, A.N., "The Optimum Thickness of Specimens for Determining Residual Stresses", Russian Engineering Journal, Vol.XLVll, No.8, 1967, pp.77-79.

46. Vasil'ev, D.M., "On the Method of X-ray Measurement of Macro- and Microstresses by the Method of Diffraction Photographs", Industrial Lab., Vol.25, No.1, Jan., 1959, pp.72-78.

47. Gribovskii, L., "Device for Measuring Strain During the Successive Removal of Layers by Etching for Determining Residual Stress", Industrial Lab., Vol.28, No.12, Aug., 1963, pp.1621-1623.

48. Labutin, Yu. P., "Mechanisation of Measurement and Calculation in Determining Axial Residual Stresses by the Davidenkov Method", Industrial Lab., Vol.34, No.7, July, 1968, pp.1043-1046.

49. Zherebkin, O.A., and Zherebkina, Zh.A., "Residual Stresses in Surface Layers", Russian Engineering Journal, Vol.XLVl, No.6, 1966, pp.37-38.

50. Deriagin, G.A., "Some Improvements in the Measurement of Deformations for the Determination of Residual Stresses in Thin-Walled Rings (Tubes)", Industrial Lab., Vol.24, No.2, Feb., 1958, pp.219-221.

51. Kobrin, M.M., Proshko, V.M., and Sorkin, L.S., "Residual Stress Determination by Analog Computer", Industrial Lab., Vol.32, No.3, March, 1966, pp.461-462.

52. Bronfin, M.B., and Shabonov, N.N., "A Portable Device for Removing Very Thin Layers from Metal Specimens", Industrial Lab., Vol.28, No.12, Aug., 1963, pp.1614-1616.

53. Kravchenko, B.A., "Influence of Cooling on the Nature and Intensity of Residual Stresses", Russian Engineering Journal, Vol.46, No.3, 1964, pp.60-62.

54. Mitryaev, K.F., "Investigations into Hardening and Residual Stresses in Face milling of Heat-resistant and Titanium Alloys", Russian Translating Programme, RTS 5814, National Lending Library for Science and Technology, Boston Spa, July, 1970.

55. Batrin, L.E., "Effect of Geometric Tool Parameters and Cutting Conditions on the Forces, Temperature and Residual Stresses in the Surface Layer During the Turning of Plastics", Russian Translating Programme, RTS 5815, NLL for Science and Technology, Boston Spa., Aug., 1970.

56. Matalin, A.A., "Effect of Machining Method on the Service Properties of Components", Russian Engineering Journal, Vol.XLVIII, No.11, 1968, pp.62-66.

57. Zlatin, N., et al, "Machining of New Materials", Technical Report AFML-TR-67-339, Metcut Research Associates Inc., Cincinnati, Ohio, Oct., 1967.

58. Itkin, M.E., "Work-Hardening and Stresses in Milling a Heat-Resistant Alloy", Russian Engineering Journal, Vol.XLVII, No.2, 1967, pp.71-73.

59. Christenson, A.L., and Littman, W.E., discussion of ref.19.

60. Heindlhofer, K., "Evaluation of Residual Stresses", McGraw-Hill Book Company, Inc., 1951.

61. Treuting, R.J., et al, "Residual Stress Measurement", ASM, Pittsburgh, Pa., 1951.

62. Osgood, W.R., "Residual Stresses in Metals and Metal Construction", Reinhold Publishing Corporation, NewYork, 1954.

63. Barrett, C.S., "A critical Review of the Various Methods of Residual Stress Measurement", Proc. Soc. Exp. Stress Analysis, Vol.2, No.1, 1944, pp.147-156.

64. Ford, H., "Mechanical Methods for the Measurement of Internal Stress", Symposium on Internal Stresses in metals and Alloys, Institute of Metals, 1948, pp.3-11.

65. Martin, D.L. (ed.), "Evaluation of Methods for the Measurement of Residual Stresses", Soc. of Auto. Eng. TR-147 (1957)

66. Denton, A.A., "Determination of Residual Stresses", Metallurgical Reviews, Institute of Metals, Vol.11, 1966, pp.1-23.

67. Gadd, C.W., "Residual Stress Indications in Brittle Lacquer, Proc. Soc. Exp. Stress Analysis, Vol.4, No.1, 1946, p.74.

68. Tokarcik, A.J., and Polzin, ibid., Vol.10, No.1, 1952, p.237.

69. Turley, D.M., "Deformed Layers Produced by Machining 70/30 Brass", J. Inst. Metals, Vol.96, March, 1968, pp.82-85.

70. Oppel, G.U., Proc. Soc. Exp. Stress Analysis, Vol.21, No.1, 1964, p.135.

71. Lecloux, M.R., "Evaluation of Principal Surface Stresses by Determination of Hertz's Hardness", Rev. Francaise Mecan., No.13, 1965, pp75-81.

72. Stengel, B., and Gayomann, Th., "Determination of Residual Stresses by Indentation Hardness Testing", AGARD Conference Procedings No.53, Feb., 1970, p.No.16.

73. Mathar, J., Trans, ASME, Vol.56, 1934, p.259.

74. Lake, B.R., et al, "An Investigation of Hole-Drilling Technique for Measuring Planar Residual Stresses in Rectangularly Orthotropic Materials", Experimental Mechanics, Vol.10, No.6, 1970, pp.233-239.

75. Sharpe, R.S., AGARD Conference Proceedings No.53, Feb., 1970, p.No.10.

76. "Electrochemical Technique for Residual Stress", Abstract reported in Machine Design (U.S.A.), 16th Oct., 1969, p.153.

77. Iwayanagi, J., Abuku, S., "A Contribution to the Magnetic Measurement of Stress in Plastically Deformed Carbon Steel", Proc. 11th Japan Congress on Mat. Res., 1968.

78. Oliver, R.B., "A Review of Nondestructive Methods for Evaluation of Residual Stress and Stress Corrosion", AGARD CP-53, p.No.17.

79. Barrett, C.S., and Massalski, T.B., "Structure of Metals", 3rd ed., McGraw-Hill, Inc., New York, 1966.

80. Macherauch, E., "X-ray Stress Analysis", Experimental Mechanics, Vol.6, March, 1966, pp.140-153.

81. French, D.N., and MacDonald, B.A., "Experimental Methods of X-ray Stress Analysis", Experimental Mechanics, Vol.9, Oct., 1969, pp.456-462.

82. Christenson, A.L., ed., et al., "Measurement of Stress by X-ray", SAE Report No. TR-182, 1960, pp.36.

83. Taira, S., and Yoshioka, Y., "X-ray Investigation on the Residual Stress of Metallic Materials", Bulletin of JSME, Vol.5, No.31, 1965, pp.307-314.

84. Grimaldi, R., Maneschi, S., and Pierucci, F., "Misura per diffrazione x delle tensoni residue devote a lavorazione meccanica", la melallurgia italiana, n.2-1966.

85. Sachs, G., and Espey, G., "The measurement of Residual Stresses in Metals", Iron Age, Vol.148, 1941, 18th Sept., pp.63-71, and 24th Sept., pp.36-42.

86. Denton, A.A., and Alexander, J.M., "On the Determination of Residual Stresses in Tubes", Journal of Mechanical Engineering Science, Vol.5, No.1, 1963, p.75.

87. Pomeroy, R.J., "Axial Curvature and Residual Stress Measurement in Thin Walled Tubes", International Journal of Mechanical Sciences, 1968, Vol.10, p.29.

88. Pomeroy, R.J., "Residual Stresses in Rolling Discs", Ph.D. thesis, University of Cambridge, 1968.

89. Okushima, K., and Kakino, Y., "Study on the Generating Process of Machined Surface", Bulletin of JSME, Vol.12, No.49, 1969, pp.141-148.

90. Barash, M.M., and Schoech, W.J., "A Semi-Analytical Model of the Residual Stress Zone in Orthogonal Machining", Preprint of the paper presented at the 11th International M.T.D.R. Conference, Sept., 1970.

91. Johnson, K.L., and Jefferis, J.A., "Plastic Flow and Residual Stresses in Rolling and Sliding Contact", Proceedings of the Symposium on Fatigue in Rolling Contact, Institution of Mechanical Engineers, 1963, pp.54-65.

92. Johnson K.L., "An Experimental Determination of the Contact Stresses between Plastically Deformed Cylinders and Spheres", Engineering Plasticity, Cambridge University Press, 1968, p.341.

93. Merchant, M.E., "Mechanics of Metal-Cutting Process", J. Appl. Phys., 1945, Vol.16, No.5, p.267 and No.6, p.318.

94. Lee, E.H., and Shaffer, B.W., "The Theory of Plasticity Applied to a Problem of Machining", J. Appl. Mech., Trans. ASME, Vol.73, 1951, p.405.

95. Usui, E., and Hoshi, R., "Slip-Line Fields in Metal Machining Which Involve Centred Fans", International Research in Production Engineering, ASME, New York, 1963, p.61.

96. Johnson, W., "Some Slip-Line Fields for Swaging or Expanding, Indenting, Extruding and Machining for Tools with Curved Discs", Intern. J. Mech. Sc., Vol.4, 1962, p.323.

97. Oxley, P.L.B., "Mechanics of Metal Cutting", International Research in Production Engineering, ASME, New York, 1963, p.50.

98. Zorev, N.N., "Metal Cutting Mechanics", Pergamon Press, 1966.

99. Albrecht, P., "New Developments in the Theory of Metal-Cutting Process, 1- The Ploughing Process in Metal Cutting", Paper No.59-A-243, ASME.

100. Boothroyd, G., "Fundamentals of Metal Machining", Edward Arnold (Publishers) Ltd., London, 1965.

101. Weiner, J.H., "Shear Plane Temperature Distribution in Orthogonal Cutting", Trans. ASME, Vol.77, 1955, p.1331.

102. Rapier, A.C., "A Theoretical Investigation of the Temperature Distribution in Metal-Cutting Process", Brit. J. Appl. Phys., Vol.5, 1954, p.400.

103. Loewen, E.G., and Shaw, M.C., "On The Analysis of Cutting Tool Temperatures", Trans. ASME, Vol.76, 1954, pp.217-231.

104. Zienkiewicz, O.C., "The Finite Element Method in Structural and Continuum Mechanics", McGraw-Hill Book Co., Inc., New York, 1967.

105. Zienkiewicz, O.C., Valliappan, S., and King, I.P., "Elasto-plastic Solutions of Engineering Problems, 'Initial Stress', Finite Element Approach", International Journal for Numerical Methods in Engineering, Vol.1, 1969, pp.75-100.

106. Marcal, P.V., "A Stiffness Method for Elastic-Plastic Problems", Int. J. Mech. Sci., Vol.7, 1965, pp.229-238.

107. Hill, R., "The Mathematical Theory of Plasticity", Oxford University Press, 1960.

108. Sokolovskii, V.V., "TIORIA PLASTICHNOSTI" (Theory of Plasticity), Third edition, Moscow, 1969.

109. Timoshenko, S.P., and Goodier, J.N., "Theory of Elastic Elasticity", Third edition, McGraw-Hill Book Company, Inc., London, 1970.

110. Gill, S., "A Process for the Step-by-Step Integration of Differential Equations in an Automatic Digital Computing Machine", Proc. Camb. Phil. Soc., Vol.47, 1951, p.96.

111. Yamada, Y., and Yoshimura, N., "Plastic Stress-Strain Matrix and Its Application for the Solution of Elastic-Plastic Problems by Finite Element Method", Int. J. Mech. Sci., Vol.10, 1968, pp.343-354.

112. Rao, U.R.K., "Residual Stresses due to Machining", M.Sc. thesis, University of London, 1968.

113. Winter, P.M., McDonald, W.J., "Biaxial Residual Surface Stresses from Grinding and Finish Machining 304 Stainless Steel Determined by a New Dissection Technique", Trans. ASME, Series D, Vol.91, No.1, pp.15-22.

114. Fedotev, N.P., Grilikes, S.Ya., "Electropolishing, Anodising and Electrolytic Pickling of Metals", Moscow, 1957, Translated by Behr.A., Robert Draper Ltd., Teddington, 1959.

115. Smithells, C.J., "Metals Reference Book", Vol.1, Fourth edition, Butterworths, London, 1967, p.319.

116. Doi, O., "Measurement of Principal Residual Stresses in a Plate when Their Directions are Unknown", Bulletin of JSME, Vol.8, No.30, pp.150-158, May, 1965.

117. Kalpakjian, S., "Mechanical Processing of Materials", D.Van Nostrand Co., Inc., London, 1967.

118. Fenton, R.G., and Oxley, P.L.B., "Mechanics of Orthogonal Machining: Allowing for the Effects of Strain rate and Temperature on Tool-Chip Friction", Proc. I. Mech. E., Vol.183, Part 1, No.22, 1968-69.

119. Camatini, E., "A Systematic Research on the Cold Work Produced on Carbon Steels by Machining with a lathe", Advances in Machine Tool Design and Research, Part 1, 1967, Pergamon Press, London, p.565.

120. Crookall, J.R., "The Investigation and Significance of the Built-up edge in Machining", Unpublished paper delivered to the C.I.R.P. Group 'C' - Cutting Sub-Group S1 - Machined Surfaces, 27 Jan., 1971.

121. Heginbothom, W.B., and Gogia, S.L., "Metal Cutting and the Built-up-Nose", Proc. I. Mech. E., Vol.175, No.18, 1961, pp.892-917.

122. Betz, F., "Die Beeinflubung der Schnittflachenrauheit durch die Mikrogestalt der Werkzeugschneide", Proc. CIRP Gen. Assy., Vol.18, Pisa, Italy, 1970.